Quantum dissipation of quarkonium in the quark-gluon plasma via Lindblad equation

Takahiro Miura

Department of Physics

February 1, 2021

Contents

Abstract

At modern collider facilities, such as the Relativistic Heavy Ion Collider and the Large Hadron Collider, heavy nuclei are collided at ultrarelativistic energy to create a multiparticle system. Experimental observables suggest that a new phase of nuclear matter, the quark-gluon plasma is realized in the collision center. The suppression of the yields of quarkonium states which are heavy quark-antiquark bound states is one of the observables to probe color screening and suggest the formation of the quark-gluon plasma. An understanding of the dynamical evolution of heavy quarkonium is a key factor in achieving insights into the properties of the quark-gluon plasma created in heavy ion collision experiments.

We theoretically study the dynamics of quarkonia in the quark-gluon plasma based on open quantum systems approach. We in particular focus on the dissipative effects on the relative motion of the in-medium quarkonium state, which has not yet been discussed enough. We first construct the equation of motion of the relative motion of a quarkonium in the form of the Lindblad equation. This Lindblad equation can be systematically derived from and thus related to the quantum chromodynamics, which goes beyond several phenomenological models. The Lindblad operators show the information about the interactions between a quarkonium and the surrounding quark-gluon plasma. The potential between the heavy quark pair is included in the Hamiltonian part of the Lindblad equation.

From the numerical simulations of the Lindblad equation in both U(1) and SU(3) color cases, we next discuss the relative motion of a quarkonium. We for the first time include both quantum dissipation and color degrees of freedom in SU(3) color case, which expects more realistic simulations. To implement the corresponding dynamics, we apply the stochastic unraveling called the quantum state diffusion method. In this method, the full quantum Lindbladian evolution is then cast into a nonlinear stochastic Schrödinger equation, which is numerically solved in our simulations instead of the Lindblad equation. This provides a direct link from quantum chromodynamics to the phenomenological models which are based on the nonlinear Schrödinger equations. Our simulations in one spatial dimension and at a fixed temperature show that the dissipative effects indeed allow the relative motion of the constituent quarks in a quarkonium at rest to be thermalized. This is assisted by the interplay of quantum dissipation and fluctuations. To relate the simulations to quarkonia in relativistic heavy ion collisions, we consider the time-dependent temperature of the expanding quark-gluon plasma. The dissipation turns out to be effective to the dynamics of in-medium quarkonia from the early stage, which is well within the short lifetime of the quark-gluon plasma in the experiments. This implies that the previous studies which lack dissipative effects and are based on complex potential, stochastic potential and effective theory of quarkonia are not adequate.

Acknowledgement

I would like to express sincere appreciation to Prof. Masayuki Asakawa for various supports, the discussions, and the comments at regular meetings for my study. I also would like to deeply thank Prof. Yukinao Akamatsu for the daily discussions, advice, supports for the participation in some international conferences, and encouragements. From them, I have been lead to the interesting research field. I am furthermore grateful to Prof. Alexander Rothkopf, who is one of my collaborators, for advice and comments for physics and numerical simulations via Skype and face-to-face.

Besides our collaborators, I am grateful to Prof. Masakiyo Kitazawa for giving me helpful comments on my study and my presentation. I also thank Dr. Shiori Kajimoto, who also had studied the physics of in-medium quarkonia, for meaningful discussions and comments. I also thank my colleagues in Nuclear theory group at Osaka University for warmly encouraging my study and broadening my perspectives form the discussions with them.

Chapter 1

Introduction

One of the aims in physical communities is to explore the behavior of elementary particles, which are considered as the most fundamental in all the existing substances and matter. Quark is one of the kinds of the elementary particles. The number of kinds of quarks is six, up, down, strange, charm, bottom, and top quarks. Their kinds are called flavor. These quarks and antiquarks constitute the hadrons, which are classified into mesons and baryons. Interaction in the quark systems is strong interaction and is mediated by gluon. Their dynamics is governed by quantum chromodynamics. Quarks and gluons are fundamental constituents in this theory and they have the color degrees of freedom. Depending on their conditions such as the temperature, they expect to show different aspects than in our world. Over the past few decades, the properties of nuclear matter in extreme conditions have been actively studied. In this Chapter, Sec. 1.1 provides the brief introduction of quantum chromodynamics and the expected phases of the matter in the extreme conditions. Sec. 1.2 introduce relativistic heavy ion collision experiments to explore such matter, showing some observables of quarkonia.

1.1 Quantum Chromodynamics

1.1.1 Lagrangian and Characteristics

Strong interaction is one of the most fundamental and important forces in nature and works between quarks and gluons, which constitutes a lot of kinds of hadrons. This is described by the quantum chromodynamics, which is called QCD in short. The Lagrangian is given by

$$\mathcal{L}_{\mathrm{QCD}} = \sum_f \bar{\psi}_f \left(i\gamma^\mu D_\mu - m\right) \psi_f - \frac{1}{4} F^a_{\mu\nu} F^{a\mu\nu}, \tag{1.1}$$

where $\psi_f = \psi^i_f$ denotes the quark field with three color indexes $i = 1, 2, 3$ and with mass m and γ_μ does Dirac matrices with $\mu = 0, 1, 2, 3$. The index f denotes the flavor of the quarks. In analogy to the three primary colors of light, the quark color indexes are often called red, green, and blue. The gluon field is denoted by A^a_μ and SU(3) generator by t^a with eight color indexes $a = 1, 2, \cdots 8$. The covariant derivative on quark filed D_μ and

the field strength $F^a_{\mu\nu}$ are respectively defined by

$$D_\mu = \partial_\mu - igA_\mu, \quad A_\mu \equiv A^a_\mu t^a \tag{1.2}$$

$$F^a_{\mu\nu} = \partial_\mu A^a_\nu - \partial_\nu A^a_\mu + g f^{abc} A^b_\mu A^c_\nu. \tag{1.3}$$

Here, g is the coupling constant of the interaction. From this Lagrangian Eq. (1.1), the evolution of the fields and the interaction between the fields is determined. As the photon mediates the interaction in quantum electrodynamics, the gluon mediates the interaction in QCD. However, the gluons carry colors and can interact with themselves as in the last term in Eq. (1.3). In another viewpoint, for the QCD Lagrangian to satisfy gauge invariance, gluons have self-interaction terms. The QCD Lagrangian has the gauge invariance under the local gauge transformation

$$\psi'(x) = V(x)\psi(x), \tag{1.4}$$

$$gA'_\mu(x) = V(x)(gA_\mu(x) - i\partial_\mu)V(x)^\dagger \tag{1.5}$$

with $V(x) = \mathrm{e}^{-i\theta^a(x)t^a}$, where $\theta^a(x)$ is real.

One of the characteristics of QCD is found, *asymptotic freedom*[1, 2]. Asymptotic freedom is the property that the interaction becomes weaker when a momentum transfer is larger. Thus the interaction becomes weaker in a shorter range scale. This dependence is revealed by the renormalization group equation at the one-loop level. The resultant coupling constant is dependent on the renormalization scale Q, which is often set to the processes of interest

$$\alpha_s(Q) \equiv \frac{g(Q)^2}{4\pi} = \frac{1}{4\pi b \ln\left(Q^2/\Lambda^2_{\mathrm{QCD}}\right)}, \quad b = \frac{1}{(4\pi)^2}\left(11 - \frac{2}{3}N_f\right). \tag{1.6}$$

The coupling is characterized by the scale parameter $\Lambda_{\mathrm{QCD}} \sim 250\ \mathrm{MeV}$ estimated experimentally, which characterizes typical energy scale in QCD as the coupling diverges when $Q = \Lambda_{\mathrm{QCD}}$.

Considering the light quarks such as up and down quarks in particular, whose masses are smaller than the QCD scale Λ_{QCD}. The Lagrangian with N_f flavors holds approximately chiral symmetry under the transformation $\psi'_{f,R/L} = \exp(i\theta^a_{R/L}t^a)_{ff'}\psi_{f',R/L}$ on the right-handed $\psi_{f,R}$ and left-handed quarks $\psi_{f,L}$, where t^a includes SU(N_f) generators plus the operator proportional 1 and normalized by $\mathrm{Tr}[2t^at^b] = \delta^{ab}$. In the massless limit, this symmetry completely holds. In this transformation, $\bar{\psi}\psi$ is not invariant, which implies that it is expected to serve as an order parameter of the symmetry breaking[3, 4].

QCD has another characteristic, which is called *color confinement*[5]. In the lower energy scale, the effective coupling becomes stronger and thus the interaction between quarks becomes stronger. This implies that infinite work is needed in taking infinitely away a single quark from the hadrons, without dynamical quarks. If there are dynamical quarks, at some distance between two quarks to be taken away from the hadron, the quark-antiquark pair creation occurs from the vacuum to make two pairs of quark and antiquark. A colored quark does not individually exist and such a particle is confined in the hadrons, which means the observed particles are colorless.

1.1.2 Phases in QCD matter

As stated above, quarks and gluons are confined in the hadrons in our world with low temperature and baryon density. However, from the property of the effective small coupling above the QCD energy scale, the matter composed of the deconfined quarks and gluons are expected in extreme conditions with a higher temperature[6, 7]. This matter is called the quark-gluon plasma. The lattice QCD simulations at zero baryon chemical potential, which is the non-perturbative first principle solution based on QCD, have revealed that the transition occurs at the transition temperature around $155\ \mathrm{MeV}$. They also have shown that the thermodynamical physical quantity such as energy density changes continuously and that the transition is classified to the crossover transition[8, 9, 10, 11]. With finite chemical potential, the transition between the hadron and the quark-gluon plasma phases has been predicted to be the first-order transition and the critical point has been also predicted by some model calculations[12, 13, 14, 15]. In a small chemical potential region, the lattice QCD calculations have been also performed with the Taylor expansion method[16]. In low temperature and high-density region, theoretically predicted phases are various, one of which is the color superconductivity phase where the attractive interaction between colored quarks works like Cooper pair in electric superconductivity[17, 18].

The quark-gluon plasma is expected to have existed in the early Universe with high temperature $\sim 2\times10^{12}\ \mathrm{K}$ just after the Big Bang. The color superconductivity is expected to be in the center of a neutron star with high baryon density higher than nuclear density $\sim 3\times10^{14}\ \mathrm{g/cm^3}$. These phases are schematically summarized in the diagram in Fig. 1.1.

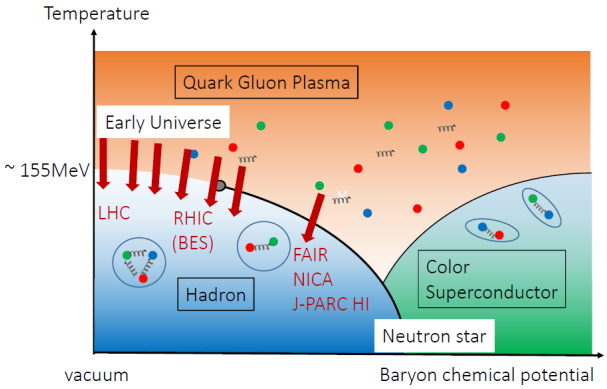

Fig. 1.1: Schematic sketch of QCD phase diagram in temperature and baryon chemical potential plane.

1.2 Relativistic Heavy Ion Collision Experiments

As stated above, the phase of the quark-gluon plasma is expected where high temperature or high baryon density is achieved. To create such an extreme condition, relativistic heavy ion collision experiments have been performed in some facilities and are planned at the new facilities. At the Alternating Gradient Synchrotron (AGS) at Brookhaven National Laboratory (BNL) and the Super Proton Synchrotron (SPS) at the European Organization for Nuclear Research (CERN), the fixed target experiments had been performed. The

beam energy or collision energy per nucleons $\sqrt{s_{\rm NN}}$ in the center of mass frame is respectively 5 GeV for gold-gold (Au-Au) collisions at AGS facility or 17 GeV for lead-lead (Pb-Pb) collisions at SPS facility. In these experiments, the clear signatures of the creation of the quark-gluon plasma were not obtained. After these fixed-target experiments, instead, the experiments where two accelerated heavy nuclei collide with each other have been performed, which can achieve higher beam energies. The heavy ion collisions can be performed and achieved at $\sqrt{s_{\rm NN}} = 200$ GeV for Au+Au collisions at RHIC and at $\sqrt{s_{\rm NN}} = 5.02$ TeV for Pb-Pb collisions at LHC. In these heavy ion collisions, we have accumulated several pieces of evidence of the production of the quark-gluon plasma and data to explore the interacting matter under extreme conditions. As a comparison of the preceding results of AGS and SPS, the multiplicity of the particle production at mid rapidity was observed to be almost flattened, which is expected to reflect the transparency of the accelerated nuclei. With agreements to the experimental situations, or in order to describe the boost invariant system in the z direction where the two heavy nuclei go and collide, we apply Bjorken description where the proper time $\tau = \sqrt{t^2 - z^2}$ and the rapidity $y = \frac{1}{2}\log\left(\frac{t+z}{t-z}\right)$ are introduced[19].

At LHC, the crossover regions near the temperature axis have been searched while the more dense regions have been searched as in beam energy scan program often called BES in short, which searches for the existence of the critical point at RHIC[20, 21]. Shortly, the colliders at a few GeV beam energy order in this research field plan to attack the much more dense region at Facility for Antiprotons and Ions Research (FIAR) at Helmholtzzentrum für Schwerionenforschung GmbH (GSI), Nuclotron-based Ion Collider Facility (NICA) at Joint Institute for Nuclear Research (JINR), and in J-PARC HI program at J-PARC.

1.2.1 Dynamical Picture of Relativistic Heavy Ion Collisions

The heavy nuclei such as Au and Pb in the relativistic heavy ion collision experiments are accelerated to near the speed of light and the theoretical description of what happens in the experiments is now based on the Bjorken description.In these high energetic setups, two Lorentz contracted nuclei collide with each other and pass through each other, leaving some parts of the kinetic energies of the incident nucleons at the colliding point. These degrees of freedom are transformed into the hot medium with low baryon density, in which gluons and quarks are created. They interact with each other and the medium becomes equilibrated quark-gluon plasma. In the RIHC experiments, quark-gluon plasma has been proved to behave like an almost perfect fluid and the hydrodynamical description can be applied to it[22, 23]. In the following, we dare to divide the dynamics in heavy ion collisions at RHIC and LHC into several stages in a standard picture as in Fig. 1.2.

1. **Equilibration**
   After colliding two Lorentz contracted heavy nuclei, the hot and low baryon-density medium is created at the colliding point. The gluons and quarks produced there then interact with each other and the matter composed of them become equilibrated from the nonequilibrium stage after some certain proper time $\tau_0 \lesssim 1$ fm, which is typically estimated by hydrodynamical simulations.

2. **Quark-gluon plasma**
   After the interactions, the medium is locally thermalized, which is what we call the

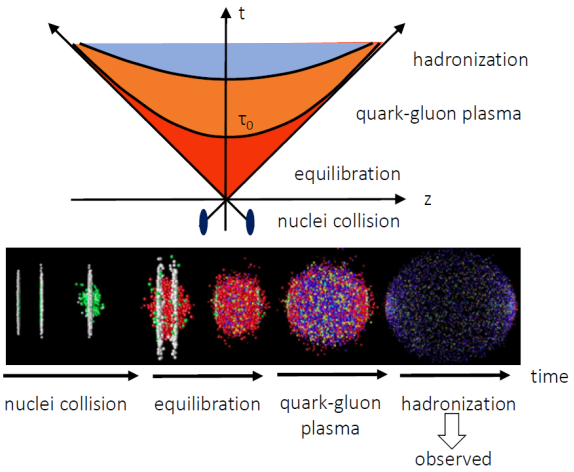

Fig. 1.2: Time evolution of the medium in a heavy ion collision. The axis t represents the evolution time and the axis z does the beam direction. The picture in the bottom is taken from Ref. [24].

quark-gluon plasma, QGP in short. In the ideal hydrodynamical expansions without the viscosity toward the longitudinal direction [1], the temperature cools according to

$$T(\tau) = T_0 \left(\frac{\tau_0}{\tau}\right)^{c_s^2}, \tag{1.7}$$

where T_0 is the temperature at $\tau = \tau_0$ with τ representing the time after the collisions and c_s represents the sound velocity, which takes $c_s^2 = \frac{1}{3}$ for a relativistic ideal noninteracting massless gas.
We here should note quarkonia, namely the bound states of heavy quark and its antiquark, which are the main object to be focused on in this thesis, are so heavier than the temperature that their thermal production can be suppressed.

3. **Hadronization**
In the space-time evolution of the quark-gluon plasma, its temperature decreases to the temperature around which the transition to the hadron phase is realized, and the medium particles experience the transition. The hadrons then interact with other hadrons and their species can change in inelastic scatterings. After these inelastic interactions, their species are fixed and the hadrons can still experience elastic scatterings. When the expansion length of the hadronic matter is larger than the mean free paths of the hadronic particles, their momenta then do not change.

4. **Observation**
Finally, these hadrons are observed via the detectors. We note that leptons and photons are also observed and that they are not affected by strong interactions and the medium evolution.

[1] In the experiments, the three dimensional expansion expects to start at the characteristic time scale estimated to $R/c_s \sim 12$ fm with Au radius R from the rarefaction wave propagation[25].

1.2.2 Observables on Quarkonium

Since the quark-gluon plasma is a matter in the deconfined phase, we have to explore the medium by the indirect hadron observables and by direct signals of photons and leptons from the quark-gluon plasma as well as the equilibration stage in the experiments. About forty years ago, quarkonium of the heavy quark bound state was proposed as a clear probe of the deconfined medium. The theoretical basis of this proposal is Debye screening phenomenon as explained later in Sec. 2.1. This behavior of quarkonium is often called quarkonium suppression, and upsilon, one of the quarkonium particles, works well in the experiments in this context. In the experiments, indeed, data on quarkonium states, whose dynamics is focused on in this thesis, have been obtained and expected to have the information of the deconfined medium[26, 27, 28, 29, 30, 31, 32, 33]. Studies on quarkonia productions and their in-medium evolutions can thus provide a window to diagnosing the properties of the quark-gluon plasma.

We here present the experimental results of quarkonium suppression. Quarkonium is detected via leptonic decay and the distribution is reconstructed by the leptonic invariant mass. Fig. 1.3 presents the dimuons invariant mass distribution which is produced in proton-proton (p-p) collisions and in Pb-Pb collisions at CMS facility. In the panel, the

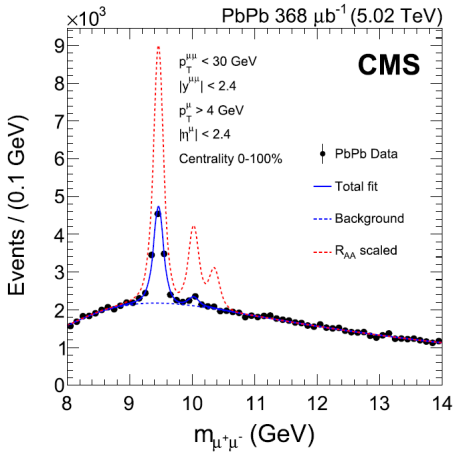

Fig. 1.3: The invariant mass distribution of muon pairs in proton-proton collisions and Pb-Pb collisions. The picture is taken from Ref. [30].

solid blue line is the fitting to the mass spectrum in Pb-Pb collisions and the dashed red represents the fitted p-p collision data, showing the separate peaks for each upsilon state $\Upsilon(1S)$, $\Upsilon(2S)$, and $\Upsilon(3S)$. Corresponding to the three states, the three peaks can be read. Comparing two collision cases, the peaks of the upsilons states are strongly suppressed, especially for the higher excited state such as $\Upsilon(2S)$ and $\Upsilon(3S)$. The higher excited states are found more suppressed in heavy ion collisions, which is often called sequential suppression in the order of the binding energy. In the experimental analysis, the double ratios of the yield in proton-proton collisions and in nucleus-nucleus (A-A) collisions

$$\frac{[\Upsilon(2S)/\Upsilon(1S)]_{AA}}{[\Upsilon(2S)/\Upsilon(1S)]_{pp}}, \quad \frac{[\Upsilon(3S)/\Upsilon(1S)]_{AA}}{[\Upsilon(3S)/\Upsilon(1S)]_{pp}} \tag{1.8}$$

is introduced, which can cancel cold nuclear matter effects coming from the presence of the nucleus and the efficiency of the detectors[31, 32, 33]. The double ratios are measured

as $0.308 \pm 0.055(\text{stat}) \pm 0.019(\text{syst})$ for $\Upsilon(2S)$ and less than 0.26 within the 95% confidence level for $\Upsilon(3S)$ in Pb-Pb collisions as Fig. 1.4 shows[32]. The experimental results

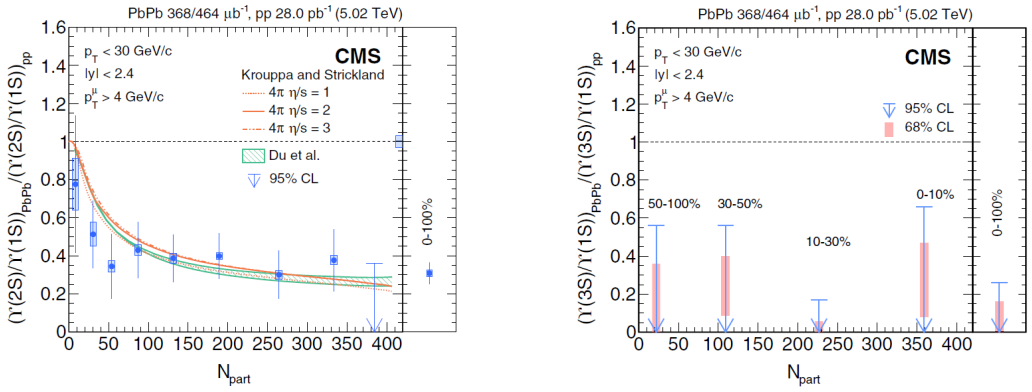

Fig. 1.4: The double ratios for $\Upsilon(2S)$ (Left) and for $\Upsilon(3S)$ (Right). The pictures are taken from Ref. [32].

on quarkonium suppression are also quantified with the nuclear modification factor

$$R_{AA} = \frac{Y_{AA}}{\langle N_{\text{coll}} \rangle Y_{pp}} . \tag{1.9}$$

Here Y_{pp} denotes the yield of the quarkonium per nucleon-nucleon collision in proton-proton collisions and Y_{AA} denotes that in nucleus-nucleus collisions. $\langle N_{\text{coll}} \rangle$ represents the number of nucleon-nucleon binary collisions. For the estimation of the number of nucleon-nucleon binary collisions, the Glauber model can be applied. Assuming that the nucleus-nucleus collision is a superposition of nucleon-nucleon collisions, the nuclear modification factor is $R_{AA} = 1$ without the medium effects. Fig. 1.5 shows that the the upsilon suppression has been observed by $R_{AA} < 1$, which indicates the medium effects.

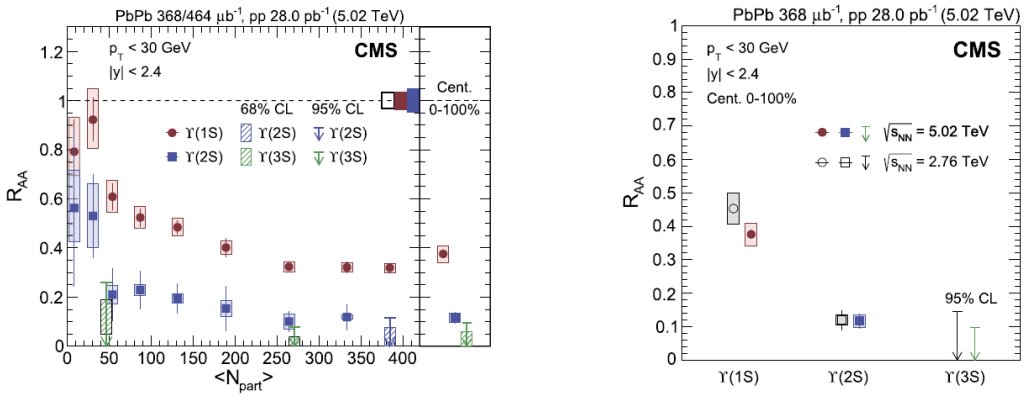

Fig. 1.5: (Left) R_{AA} for the $\Upsilon(1S)$, $\Upsilon(2S)$ and $\Upsilon(3S)$ at $\sqrt{s_{\text{NN}}} = 5.02\text{TeV}$. (Right) Comparison of R_{AA} of the upsilon states at $\sqrt{s_{\text{NN}}} = 5.02\text{TeV}$ and $\sqrt{s_{\text{NN}}} = 2.76\text{TeV}$ and sequential suppression. The pictures are taken from Ref. [30].

From the improvement of the theoretical approaches to these experiments results, it is now the era of interpreting the data by theoretical inputs and predictions as shown in the right panel in Fig. 1.4. This panel tells that the theoretical calculations with mixing the hydrodynamical evolution of the quark-gluon plasma medium and the complex potential

model on quarkonium seem to reproduce the data. These theoretical improvements on quarkonium physics are briefly summarized in Chap. 2 and also in this context in Sec. 4.2, where our motivation is stated. Thus more theoretical and experimental improvements step by step will provide more precise determinations of properties of the deconfined quark-gluon plasma medium.

The experimental results on another quarkonium state of charmonium have also been accumulated [34, 35, 36]. The suppression of upsilon yields is larger in the LHC experiments than in the RHIC experiments[37, 38]. However, the suppression of J/ψ yields is less in more central collisions at the LHC than at the RHIC as Fig. 1.6 shows. This can be

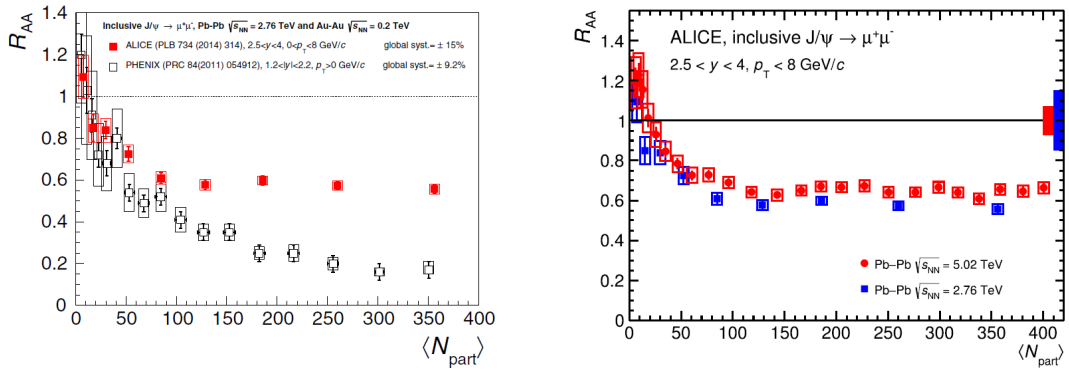

Fig. 1.6: (Left) Nuclear modification factor of J/ψ at ALICE facility and at PHENIX facility. (Right) Updated nuclear modification factor of J/ψ at ALICE facility. The left and right pictures are taken from Ref. [39] and Ref. [40].

interpreted by the phenomenon of the regeneration of J/ψ state from an initially uncorrelated charm quark-antiquark pair in the hadronization due to the larger number of the production of J/ψ particles in higher energy collisions at the LHC. Thus the suppression and the regeneration effects are important to the dynamics of the charmonium state.

Flow observables of J/ψ particle is also observed[41, 42]. Flow is a collective motion of the produced bulk matter in the collisions. The anisotropic matter leads the azimuthal distribution of the particle production, one of whose signatures is called the elliptic flow. The finite value of the elliptic flow of J/ψ suggests that J/ψ might be partially equilibrated in the medium. Although for upsilon, the finite value is zero consistent within the error bars[43], the equilibration with the surrounding medium can be important in the dynamics of the quarkonium state.

1.3 Contents of Thesis

The dynamics of quarkonia is expected to start in the early stage of the heavy ion collisions due to its larger mass than the medium temperature. As mentioned in Sec. 1.2.1, the dynamics in heavy ion collisions is composed of multiple stages. Therefore, to precisely understand the experimental results of quarkonium observables, we should take into account the whole dynamics in all the stages. In this thesis, the one stage of the quarkonium whole dynamics, in particular, quarkonium in the thermal quark-gluon plasma medium is focused on for simplification. We then discuss the real-time quantum dynamics of quarkonium in the quark-gluon plasma via the Lindblad equation with color degrees of freedom by an open quantum system framework. In this framework, we systematically incorporate

the interactions between the quarkonium system and the quark-gluon plasma environment at high temperatures. We focus on the dissipative effects on the dynamics, to which more attention has been paid, as well as the color transition effects.

This thesis is organized as follows. In Chap. 2, we overview the description of an in-medium quarkonium, which reveal not only its static property in Sec. 2.1 but also its dynamical aspects in Sec. 2.2.

In Chap. 3, we explain the general basics of open quantum systems. To be the contrast, we show the general description of closed systems in Sec. 3.1. We next explain how the open systems are described in Sec. 3.2. There, we introduce the assumptions of time scale hierarchy on open systems for the simplification of the description which are often applied in this framework. The equation of motion of the open system is called the master equation, and the special master equation, which is called the Lindblad equation, is derived in general in the regime of quantum Brownian motion. From the late evolution of the Lindblad equation, the steady-state is characterized and the detailed balance holds.

In Chap. 4, we specialize the description of a quarkonium in the quark-gluon plasma with the help of the effective theory of QCD. In Sec. 4.1, we derive the Lindblad operator of in-medium quarkonium relative motion, following the simpler derivation for the case of the single heavy quark. Its physical meanings are also discussed. The Lindblad operator can be represented in singlet-octet bases and the detailed balance relation is roughly shown to approximately hold in the late times. In Sec. 4.2, we make clear the important points of our study by relating and comparing them with several related theoretical studies. There, in the two prevalent schemes of quarkonium physics, nonrelativistic QCD and potential nonrelativistic QCD, the essential difference is the dipole approximation of quarkonium states. It is questionable that in-medium quarkonium states are in the dipole during the whole dynamics so that we expect nonrelativistic QCD to deal with a widely spread state such as an excited state.

In Chap. 5, we numerically simulate the Lindbladian quarkonium dynamics. As a way of reducing the numerical cost, we introduce the quantum state diffusion method, a method of implementing the Lindblad equation in terms of an ensemble of stochastically evolving wave functions in Sec. 5.1. Then, the stochastic Schrödinger equations to be solved in U(1) and SU(3) color cases are shown in Sec. 5.2. In Sec. 5.3, we present the numerical setups and next we present our numerical results from one-dimensional simulations for the medium with fixed temperatures in Sec. 5.4 and with the decreasing temperature in Sec. 5.5. From these simulations, we study the effect of dissipation and color transitions. These discussions are based on our papers [44, 45, 46].

Chapter 6 provides a summary and an outlook of our study.

Besides these chapters, this thesis contains some appendices. In Appendix A, we show the correlation functions of the environmental thermal gluon fields.

In Appendix B, we show that the dependence of the relative motion of a quarkonium on the center-of-mass motion and that it is marginal.

In Appendix C, we show that the dependence of the relative motion of a quarkonium on the environmental correlation length with the theoretical input of the heavy quark diffusion constant. This simulation plays a role of the first try to test whether or not the quarkonium yields in heavy ion collisions can probe the correlation length, though it is just a simulation in one dimension.

In Appendix D, we discuss the peculiar property in SU(2) case, the residual long-range quantum correlations even after the decoherence for in-medium quarkonium states. We prove this property in terms of the Lindblad equation, while it is not the case in SU(3).

Chapter 2

Quarkonium in a Medium at Finite Temperature

In the previous Chap. 1, we show several experimental results on quarkonia in heavy ion collisions. These results reflect the whole dynamics of quarkonia in the experiments and to correctly interpret the experimental data we need to theoretically understand what quarkonia experience there. In this Chap. 2, we present the theoretical tools and aspects of quarkonium physics in a thermal medium. First, we introduce the historic study on in-medium quarkonium in the context of plasma physics in Sec. 2.1. There, the suppression of the yields of quarkonia in these experiments is predicted from the Debye screening phenomenon in the deconfined medium. In addition to this discussion, in Sec. 2.2 we explain the dynamical aspects of in-medium quarkonium. The dynamical evolution of quarkonium has been considered and discussed using the real-time potential which is derived in the finite temperature field theory. The frameworks of the effective theories for the physics of heavy quarks have been also developed. From these studies, it is shown that quarkonium has a complex-valued potential.

2.1 Conventional Picture

In 1986, Matsui and Satz discussed the behavior of a quarkonium when it is in a thermal medium[47]. In the case of the heavy ion collision experiments, the surrounding thermal medium is the quark-gluon plasma. In the vacuum, the binding force between a heavy quark pair is mediated by gluon exchanges. When the quark-gluon plasma medium exits around a quarkonium, however, the exchanged gluons interact with the medium, which changes the binding force and the property of the quarkonium. The authors discussed the modification like this by the analogy of the Debye screening phenomenon in plasma physics.

In the vacuum, two heavy quarks are confined and this can be phenomenologically modeled by the vacuum Cornell potential

$$V(r) = \sigma r - \frac{\alpha}{r}, \tag{2.1}$$

in which the QCD properties of the color confinement and the asymptotic freedom are embedded in long and short distances. The potential between the heavy quark pair is in the Coulombic form in the short distance, while it is in the linearly rising form in

the large separation. In Eq. (2.1), the constant σ represents the string tension. In the deconfined matter of the quark-gluon plasma, the binding of a quarkonium is weakened by liberated surrounding color charges. The string part decreases and we expect color screening potential

$$V(r) = -\frac{\alpha}{r}\mathrm{e}^{-m_{\mathrm{D}}r}, \tag{2.2}$$

where m_{D} is Debye mass and related to Debye screening length $r_{\mathrm{D}} = m_{\mathrm{D}}^{-1}$. The screening length tells us the specific characteristic length scale over which color interactions do not reach each constituent of a quarkonium. The prediction of the suppression of quarkonium yields by Matsui and Satz is based on the argument that Debye radius r_{D} leads an upper bound and can be shorter than the binding radius of J/ψ particle. These sizes of the bound states are estimated with uncertainty principle $pr \sim 1$ by finding the minimum value of the energy of a heavy quarkonium

$$E = 2M + \frac{1}{2Mr^2} + V(r). \tag{2.3}$$

From this representaion, the operation $\frac{dE}{dr} = 0$ leads to the equation for the deconfined medium case

$$m_{\mathrm{D}}r(m_{\mathrm{D}}r + 1)\mathrm{e}^{-m_{\mathrm{D}}r} = \frac{m_{\mathrm{D}}}{M\alpha}, \tag{2.4}$$

which can have the finite value of r only in case of $M\alpha r_{\mathrm{D}} \gtrsim 1.2$. The smallest value r_{D} of screening length still allow the heavy quark pair to form a bound state. The authors chose of the parameters $\sigma \simeq 0.16\ \mathrm{GeV}^2$, $M = 1.56\ \mathrm{GeV}$, and $0.2 \lesssim \alpha \lesssim 0.5$ reflecting temperature dependence of the coupling. It is found that the binding radius $r_{J/\psi}$ can satisfy $r_{J/\psi} > r_{\mathrm{D}}$ above the transition temperature from the lattice studies and that the surrounding medium prevents J/ψ particle formation as their suggestions. This picture is based on a static potential and Hamiltonian. The suppression of quarkonium yields could be sometimes considered as a metaphor of a thermometer of the temperature of quark-gluon plasma production[48].

2.2 Recent Developments

2.2.1 Theoretical Tools

Thermal Field Theory

We here introduce and prepare the useful tools from the thermal quantum field theory[49, 50]. With the help of the thermal field theory, we can study the properties of the equilibrated system and also the dynamics out of the equilibrium, for which real-time formalism is needed. We define the following different two-point thermal averaged forward, backward, and retarded correlators of the operator $\phi(x)$ for $x^\mu = (t, \vec{x})$ such as mesonic operator $M(x)$ and the field $A^a_\mu(x)$ for a thermal medium:

$$D^{>}(x, x') \equiv \langle \phi(x)\phi(x') \rangle\,, \tag{2.5}$$
$$D^{<}(x, x') \equiv \langle \phi(x')\phi(x) \rangle = D^{>}(x', x)\,, \tag{2.6}$$

$$D^{\mathrm{R}}(x,x') \equiv i\theta(t-t')\left\langle[\phi(x),\phi(x')]\right\rangle, \tag{2.7}$$

with time-dependent Heisenberg operator $\phi(x) = \mathrm{e}^{ix^\mu p_\mu}\phi\,\mathrm{e}^{-ix^\mu p_\mu}$. The thermal average of an operator O is defined by

$$\langle O\rangle = \frac{1}{Z(\beta)}\mathrm{Tr}\left(O\mathrm{e}^{-\beta H}\right), \quad Z(\beta) = \mathrm{Tr}\left(\mathrm{e}^{-\beta H}\right) \tag{2.8}$$

with the inverse temperature β, Hamiltonian H, and the partition function Z. With these definitions, we obtain Kubo-Martin-Schwinger relation in Fourier space

$$D^{<}(\omega,\vec{q}) = \pm\mathrm{e}^{-\beta\omega}D^{>}(\omega,\vec{q}), \tag{2.9}$$

in which the upper sign is for bosons and the lower sign for fermions. From these correlators, the spectral function $\rho(\omega,\vec{x})$ is defined by

$$\rho(\omega,\vec{x}) \equiv D^{>}(\omega,\vec{x}) - D^{<}(\omega,\vec{x}) = 2\mathrm{Im}D^{\mathrm{R}}(\omega,\vec{x}). \tag{2.10}$$

These correlators can be obtained from the Euclidean correlators with imaginary-time formalism, in which the partition function is represented by

$$Z(\beta) = \int\mathcal{D}\phi\exp\left[-\int_0^\beta d\tau\int dx^3\mathcal{L}_E(\tau,\vec{x})\right] \tag{2.11}$$

with the boundary $\phi(0,\vec{0}) = \phi(\beta,\vec{0})$ for bosons or $\phi(0,\vec{0}) = -\phi(\beta,\vec{0})$ for fermions and the Fourier transfrom of the imaginary-time propagator $D_E(\tau,\vec{x}) \equiv \left\langle\phi(\tau,\vec{x})\phi(0,\vec{0})\right\rangle$ is defined through

$$D_E(iq_n,\vec{x}) = \int_0^\beta d\tau\mathrm{e}^{iq_n\tau}D_E(\tau,\vec{x}), \tag{2.12}$$

$$D_E(\tau,\vec{x}) = T\sum_n \mathrm{e}^{-iq_n\tau}D_E(iq_n,\vec{x}), \tag{2.13}$$

with discrete frequencies $q_n = \frac{2\pi n}{\beta}$ for bosons or $q_n = \frac{2\pi(n+1)}{\beta}$ for fermions. The real-time formalism is connected to the imaginary time formalism by the analytic continuation of imaginary-time to real-time $t \to -i\tau$ as

$$D_E(\tau,\vec{x}) = D^{>}(-i\tau,\vec{x}), \quad D^R(\omega,\vec{q}) = D_E(iq_n\to\omega+i\epsilon,\vec{q}). \tag{2.14}$$

Effective Theory

If a system of interest has a separated hierarchy of energy scales, we can construct and employ a powerful treatment of an effective theory. An effective theory is constructed with the separation of the scales, systematic expansions in the power counting, and symmetries. The construction is regarded as top-down from the original Lagrangian with a wider range of energy scales, that is, by integrating out the higher energy scales and deriving the Lagrangian which is effective in the lower energy scales. This construction is by e.g. matching the correlator calculated both in the original theory and in the effective theory below a certain energy cutoff Λ in a perturbative way or non-perturbative way. In lower power counting order terms, the more dominant contributions appear in the physical pro-

cesses to be considered. In the framework of the effective theories of heavy quark physics in QCD, non-relativistic QCD (NRQCD) and potential non-relativistic QCD (pNRQCD) are two prevalent schemes.

In quarkonium physics, the separation scales exist in the energy scale:

$$Mv^2 \ll Mv \ll M, \tag{2.15}$$

with the large mass M and the relative velocity inside a quarkonium v. The mass M is a hard scale for the pair creation of a quarkonium from parton hard scatterings in heavy ion collisions. The soft scale Mv may control the typical size of the bound state, considering the Coulomb bound state. The softer scale Mv^2 is related to the binding energy of the quarkonium state and its excitation. These separations allow us to construct an effective theory.

Suppose the energy cutoff scale Λ_{NRQCD} introduced with $Mv \ll \Lambda_{\mathrm{NRQCD}} \ll M$, which focuses on physical processes by quark-gluon plasma medium particles with energy or momentum below Λ_{NRQCD}. In this regime, the pair production of a heavy quark and its antiquark, which is a characteristic in the relativistic field theory, can be neglected since such high energy scales are integrated out. NRQCD is thus a non-relativistic effective description of the heavy quarks due to its large mass M and small velocity v. The NRQCD Lagrangian for heavy quarks is established as

$$\mathcal{L} = \bar{\psi}\left(iD_0 + \frac{\vec{D}^2}{2M} + c\frac{\vec{\sigma}\cdot\vec{B}}{2M}\right)\psi + (\text{antiquarks}) + \mathcal{O}\left(\frac{1}{M^2}\right)\cdots \tag{2.16}$$

in the literatures[51, 52]. The heavy quark field ψ and the anti heavy quark field is separated[53, 54], and the coefficients of each term in the Lagrangian is determined by the matching procedure. The matching is based on the requirement that the effective theory reproduces the physics of the full QCD theory below the cutoff and the matching coefficients depend on the cutoff. Also, the relevant scales of the heavy quarks and gluons are typically estimated by the power counting with v. It is $\psi \sim (Mv)^{\frac{3}{2}}$, $A_0 \sim Mv^2$, $\vec{A} \sim Mv^3$ from the equation of motion of the gauge field, assuming that the typical momentum of a heavy quark is Mv. In this counting, we may approximate $D_i \sim \partial_i$ and drop chromo-magnetic term in the sub-leading order.

When we are interested in the quarkonium binding whose physical scales $\sim Mv^2$, NRQCD has extra degrees of freedom and the integration of them can lead to another effective theory, which is called pNRQCD[51, 52]. pNRQCD focuses on a further lower energy scale with another energy cutoff scale to study the binding property of quarkonium and describes a quarkonium in the QCD medium non-relativistically for $T \ll Mv$ and $\Lambda_{\mathrm{QCD}} \ll Mv$. pNRQCD has been established by matching the calculation of heavy quark correlation functions both in NRQCD and in pNRQCD at the energy cutoff scale $\Lambda_{\mathrm{pNRQCD}}$ with $Mv^2 \ll \Lambda_{\mathrm{pNRQCD}} \ll Mv$. Within this hierarchy, quarkonia whose typical sizes are given by $(Mv)^{-1}$ can be seen as localized dipoles form the gluons. The resultant effective Lagrangian is expanded with the coupling gr and $1/M$. The degrees of freedom of the color singlet field $\mathrm{S}(\vec{R},\vec{r})$ and color octet field $\mathrm{O}(\vec{R},\vec{r})$ with the center-of-mass coordinate $\vec{R}$ and the relative coordinate $\vec{r}$:

$$\mathcal{L} = \int d^3r\,\mathrm{Tr}\left[\mathrm{S}^\dagger\left(i\partial_t - \frac{p^2}{M} - V_s(r)\right)\mathrm{S} + \mathrm{O}^\dagger\left(iD_t - \frac{p^2}{M} - V_o(r)\right)\mathrm{O}\right]$$

$$+ \mathrm{Tr}[\mathrm{O}^\dagger \vec{r}\cdot g\vec{E}\mathrm{S} + \mathrm{S}^\dagger \vec{r}\cdot g\vec{E}\mathrm{O}] + \frac{1}{2}\mathrm{Tr}[\mathrm{O}^\dagger \vec{r}\cdot g\vec{E}\mathrm{O} + \mathrm{O}^\dagger\mathrm{O}\vec{r}\cdot g\vec{E}] + \cdots . \quad (2.17)$$

This Lagrangian tells that the singlet and octet evolves in the potentials $V_s(r)$ and $V_o(r)$ which is determined by the matching procedure.

2.2.2 Dynamical Aspects of Quarkonium

Potential Definition

In the previous Sec. 2.1, we see the behavior of a quarkonium from the just static aspects in a thermal medium. Beyond the static aspects, the real-time potential is introduced, which shows that quarkonium has an imaginary part of the potential. It in turn sheds light on the dynamical aspects of the thermal medium which can affect the fate of an in-medium quarkonium state and its properties.

We here define the point-split meson operator M_Γ. The information as to what kind of meson particles is considered is encoded by Γ such as γ^μ matrix. Connecting the Dirac fields for two heavy quarks Q and $\bar{Q}$ with the Wilson line $W(\vec{x},\vec{y},t)$ and Γ, the meson operator is defined as

$$M_\Gamma(\vec{r}=\vec{x}-\vec{y},t) = \bar{Q}(\vec{x},t)\Gamma W(\vec{x},\vec{y},t)Q(\vec{y},t)\,, \quad (2.18)$$

$$W(\vec{x},\vec{y},t) = \exp\left[-ig\int_x^y dz^\mu A_\mu(z)\right]. \quad (2.19)$$

We here consider the gauge invariant meson forward correlator in the medium

$$D^>(\vec{r},t) = \langle M_\Gamma(\vec{r},t)M_\Gamma^\dagger(\vec{r},0)\rangle\,. \quad (2.20)$$

In the heavy quark mass limit, this correlator is found to be proportional to the Wilson loop. From the QCD Lagrangian, in the heavy quark mass limit where the heavy quark does not move in space, the quark propagator $G(x,y)$ satisfies

$$\left[\gamma_0(i\partial_0 - gA^0(x)\right) - M]G(x,y) = \delta^{(4)}(x-y). \quad (2.21)$$

in the leading order of the mass. In the heavy quark mass limit where the heavy quark does not move in space, the infinitely heavy quark propagator is represented by Wilson line plus phase factor e^{-iMt}. The meson correlator is thus expressed by real-time Wilson loop with $A_\mu = A_\mu^a t^a$

$$W_\square(\vec{r},t) = \mathcal{P}\exp\left[-ig\oint A^\mu dz_\mu\right] \quad (2.22)$$

where $\mathcal{P}$ represents path-ordering of the operators. In the non-perturbative calculations based on lattice QCD formalism in the Euclidean time[55], the potential $V(\vec{r})$ between the pair of a heavy quark and its antiquark with an infinite mass in the vacuum is defined through the Wilson loop in the limit of late imaginary time $\tau\to\infty$

$$V(\vec{r}) = \lim_{\tau\to\infty} V(\vec{r},\tau), \quad V(\vec{r},\tau) \equiv \frac{\partial_\tau\langle W_\square(\vec{r},\tau)\rangle^{(\mathrm{E})}}{\langle W_\square(\vec{r},\tau)\rangle^{(\mathrm{E})}}. \quad (2.23)$$

The real-time potential in Minkovskian spacetime is introduced accordingly by Wil-

son loop at finite temperatures and thus defined with meson correlator in the heavy quark mass limit

$$V(\vec{r}) = \lim_{t\to\infty} i\partial_t \log \langle W_\square(\vec{r},t)\rangle^{(\mathrm{M})} = \lim_{t\to\infty} i\partial_t \log D^{>}(r,t). \tag{2.24}$$

Perturbative Calculation

Now we calculate the static potential Eq. (2.24) using the field theoretical tools in the Euclidean time and extract static Minkovskian real-time potential by analytic continuation of Wick rotation $\tau \to it$. This evaluation was perturbatively done with hard thermal loop resummation technique at high temperature where the temperature dominates over other scales in the loop calculations[56, 57, 58]. In these studies, it is shown that the potential of a quarkonium is complex-valued and its expression is given with Debye mass m_{D} by

$$\mathrm{Re}V(r) = -C_F\alpha\left[m_{\mathrm{D}} + \frac{\exp\left(-m_{\mathrm{D}}r\right)}{r}\right], \quad \alpha = \frac{g^2}{4\pi} \tag{2.25}$$

$$\mathrm{Im}V(r) = -C_F\alpha T\phi\left(m_D r\right), \quad \phi(x) = 2\int_0^\infty dz \frac{z}{\left(z^2+1\right)^2}\left[1 - \frac{\sin(zx)}{zx}\right]. \tag{2.26}$$

The functional form of the imaginary part of the potential $\phi(x)$ is shown in Fig.2.1. The function $\phi(x)$ approaches the constant 1 for infinitely large $x > 0$. The imaginary part of

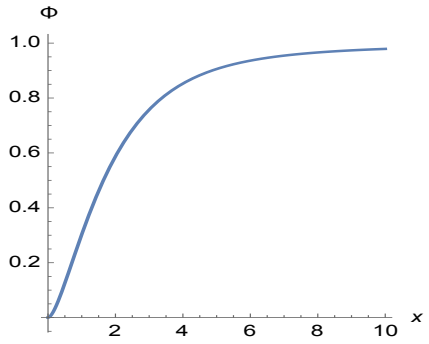

Fig. 2.1: The functional form of the imaginary part of the potential $\phi(x)$.

the potential can be interpreted as the outcomes from interactions or scatterings between the medium gluons mediating the binding of a quarkonium state. The imaginary part of the potential increases as the temperature increases, while the binding energy decreases. Therefore, quarkonium dissociation is interpreted under the different interplay between the binding energy and the thermal width at different temperatures.

Lattice Calculation

The complex potential has been also studied by lattice QCD, which allows non-perturbative simulations. At a finite temperature case, contrary to the vacuum case, it is difficult to extract the real-time potential from Eq. (2.23) because of small $\tau \sim T^{-1}$ in the temporal direction in lattice setups. Instead, the spectral decomposition of the Wilson loop is expected as a connection between the imaginary time formalism for $it \to \tau$ in lattice QCD

and the real-time potential[59]. The authors define the spectral decomposition of the Wilson loop by

$$W_{\square}(\vec{r},t) = \int d\omega e^{-i\omega t}\rho_{\square}(r,\omega) \tag{2.27}$$

and the in-medium potential by

$$V(r) = \lim_{t\to\infty} \frac{\int d\omega\omega e^{-i\omega t}\rho_{\square}(r,\omega)}{\int d\omega e^{-i\omega t}\rho_{\square}(r,\omega)}, \tag{2.28}$$

where the definition of the potential in the vacuum Eq. (2.23) is included for the spectral function of the Wilson loop $\propto \delta(\omega - V(r))$. In the lattice studies, from the discrete data on the correlation functions, its spectral decomposition has been performed with the help of the maximum entropy method[59, 60]. From the lowest lying peak in the spectral function in the small ω regions corresponding to the late-time limit, the real part of the potential $\mathrm{Re}\ V(r)$ and the imaginary part $\mathrm{Im}\ V(r)$ can be inferred from the position of the peak structure and the thermal width by the fitting of the structure. These lattice studies have shown that, at higher temperatures, the contribution of the imaginary part of the potential becomes larger while the real part transforms into the screened potential form from the vacuum potential[61, 62]. The information of the thermal width explains the lifetime of the particle, which represents the decay rate of annihilation and excitation to other states from energy and momentum exchanges with the surrounding thermal medium. We note that the thermal width does not tell which state a quarkonium state is excited to.

Towards Phenomenology

As its phenomenological applications, the survival probabilities of in-medium quarkonium states are evaluated via Schrödinger equation with this complex-valued potential[63, 64, 65]. There, the in-medium wave function does not evolve unitarily with the real binding energy. Instead, the existence of the imaginary part of the binding energy from the non-hermiticity is interpreted as the decay rate of the occupations of quarkonium states. We note that the potential defined and derived above does govern the time evolution of the mesonic correlator, not that of the wave function of a quarkonium. It does represent how fast the coherence between the wave function and the initial wave function loses. In the different prospect of the Schrödinger equation for the mesonic correlator, the spectral function can be calculated via the imaginary part of the potential in this Schrödinger equation[66, 67].

The existence of the imaginary part of the potential implies that a quarkonium even in a thermal state is not stationary but genuine dynamical from the medium effects. The question of the stability of quarkonium which is put into a thermal QCD medium from the vacuum is not answered, and quarkonium evolution is time-dependent. Thus, to understand the quarkonium stability or melting, a real-time description is needed in addition to considering the surrounding medium effects. The survival of quarkonium states is expected to be affected by how the medium modifies the binding of a quarkonium and how long it exists in the medium after it is put from the vacuum.

The non-hermiticity is compensated by the stochastic potential model[68], in which a quarkonium wave function obeys the unitary evolution. In this model, the quarkonium potential terms include the stochastic noise from the thermal fluctuations in addition to the

screening potential. This model has been revealed the decoherence to quarkonium wave function contributes its in-medium evolution[68, 69]. However, the dissipative effects are not considered during the evolution.

As another phenomenological model, Schrödinger-Langevin equation is presented and it is in the form of the nonlinear Schrödinger equation with the stochastic term[70]. Even though it includes the medium effects coming from the potential, the fluctuations, and the drag forces as in classical Langevin equation, its connection to the microscopic theoretical background remains unclear, in which context this model is one of the attempts to effectively describe a quantum system of an in-medium quarkonium.

With the motivation of dealing with the interactions between a quarkonium and the thermal quark-gluon plasma medium, the theoretical framework of the open quantum systems provides the promising way of the real-time description, which is explained in the next Sec. 3. We note that the effective theories of NRQCD and pNRQCD mentioned above are in the fields of open quantum systems. The several studies based on the open quantum system framework are successful in deriving several kinds of the equations of motions of an in-medium quarkonium, providing several viewpoints for the qualitative or quantitative explanations of the experimental data[69, 71, 72, 73, 74, 75, 76].

Chapter 3

Theory of Open Quantum Systems

In this Chap. 3, the concept and the framework of the *open* quantum systems are introduced and reviewed. In the quantum mechanics of the *closed* system, the time evolution of the wave function is described by Schrödinger equation, which is unitary evolution as seen in Sec. 3.1. However, in the situations where some irreversible processes such as energy dissipation exist, the description of Schrödinger equation generally breaks down. This stems from whether or not the system we consider is *closed*. If there is an irreversible process, the system of interest is found to be *open*, whose dynamics can be described by the *open* quantum systems approach. We in Sec. 3.2, explain how *open* systems are described, comparing the description of *closed* systems. In this approach, the dynamics can be described with the equation of motion for the density matrix for the *open* quantum system, which is called master equation. The main object in the framework of the open quantum systems is master equation. In describing the *open* systems, the procedures of deriving the master equation can be complicated and demanding and some approximations are often taken, which is shown in Sec. 3.2.1. In Sec. 3.2.2, with these assumptions in quantum Brownian motion regime, we derive the master equation which can describe energy dissipation and the relaxation to equilibrium states.

3.1 Formalism in Closed Systems

For the description of *closed* systems, Schrödinger equation for the wave function can work. In another point of view of the density matrix composed of the wave functions, the *closed* systems can be also described by von Neumann equation in the Schrödinger picture

$$\frac{d}{dt}\rho(t) = -i[H(t), \rho(t)], \quad \rho(t) = \sum_{\alpha} \omega_{\alpha} U(t, t_0) \left|\psi_{\alpha}(t_0)\right\rangle \left\langle\psi_{\alpha}(t_0)\right| U^{\dagger}(t, t_0) \tag{3.1}$$

from an initial state of the density matrix

$$\rho(t_0) = \sum_{\alpha} \omega_{\alpha} \left|\psi_{\alpha}(t_0)\right\rangle \left\langle\psi_{\alpha}(t_0)\right| \tag{3.2}$$

with some wights $\omega_{\alpha} > 0$ for each state $\psi_{\alpha}(t_0)$. Eq. (3.1) can be decomposed into the unitary evolution of the state vector $|\psi_{\alpha}\rangle$ from time t_0 to time t, which is formulated by

the Schrödinger equation with unitary operator $U(t, t_0)$

$$|\psi(t)\rangle = U(t, t_0)\,|\psi(t_0)\rangle\,, \quad U(t, t_0) = \mathcal{T}\exp\left[-i\int_{t_0}^{t} dsH(s)\right], \tag{3.3}$$

where $\mathcal{T}$ denotes time ordering.

Except for the Schrödinger picture, other equivalent pictures exist, Heisenberg picture, which is here symbolized by H, and the Interaction picture, which is here symbolized by I. First, an operator $O(t)$ in the Schrödinger picture is related to $O_{\rm H}$ in the Heisenberg picture through

$$O_{\rm H}(t) = U^{\dagger}(t, t_0)O(t)U(t, t_0). \tag{3.4}$$

In the Heisenberg picture, the density matrix is fixed to $\rho(t_0)$ at the initial time $t = t_0$. An expectation value of a physical operator, that is, an observable is calculated by

$$\langle O(t)\rangle = {\rm Tr}\{O_{\rm H}(t)\rho_{\rm H}(t_0)\} = {\rm Tr}\{O(t)\rho(t)\}, \tag{3.5}$$

which shows observables are independent of both of the pictures. The Interaction picture features the interaction between the two systems that we consider. Let us assume the Hamiltonian of the two systems plus the interaction between them is

$$H(t) = H_0 + H_{\rm int}(t), \tag{3.6}$$

where $H_{\rm int}(t)$ represents the interactions and H_0 does the isolated residual part of the two systems. The total system is *closed* and unitarily evolves with the unitary operator $U(t, t_0)$. We here define the following operators

$$U_0(t, t_0) \equiv \exp\left[-iH_0(t - t_0)\right], \quad U_{\rm I}(t, t_0) \equiv U_0^{\dagger}(t, t_0)U(t, t_0). \tag{3.7}$$

The density matrix and the operator $O_{\rm I}$ in the Interaction picture are introduced by

$$\rho_{\rm I}(t) \equiv U_{\rm I}(t, t_0)\rho(t_0)U_{\rm I}^{\dagger}(t, t_0), \tag{3.8}$$

$$O_{\rm I}(t) \equiv U_0^{\dagger}(t, t_0)O(t)U_0(t, t_0). \tag{3.9}$$

The observable O in the Interaction picture is calculated by

$$\langle O(t)\rangle = {\rm Tr}\{O_{\rm I}(t)\rho_{\rm I}(t_0)\} = {\rm Tr}\{O(t)\rho(t)\}, \tag{3.10}$$

and the von Neumann equation Eq. (3.1) is transformed into

$$\frac{d}{dt}\rho_{\rm I}(t) = -\,i[H_{\rm I}(t), \rho_{\rm I}(t)]. \tag{3.11}$$

This equation can be iteratively solved, which leads the equivalent integral form

$$\rho_{\rm I}(t) = \rho_{\rm I}(t_0) - i\int_{t_0}^{t} ds[H_{\rm I}(s), \rho_{\rm I}(s)] \tag{3.12}$$

and makes the starting point in the derivation of master equation of *open* systems as in the next Sec. 3.2.

3.2 Formalism in Open Systems

The description of *open* quantum systems is originally based on the description of *closed* quantum systems in the previous Sec. 3.1. The *open* quantum system, which is symbolized here by S, couples to the surrounding system, which is often called by the environment and symbolized here by E. The combined sets of the *open* system and the environment constitute the total *closed* system, which obeys quantum unitary evolution. On the other hand, when the *open* system S is interested in and only focused on, its dynamics is induced by the interactions between them and not unitary at all.

The situation as mentioned above can be mathematically and physically formulated as follows. We now consider a total closed system that is composed of the *open* system S of interest and the environment E. We then assume the Hilbert space $\mathcal{H}$ and the Hamiltonian of the total system H in the Interaction picture

$$\mathcal{H} = \mathcal{H}_{\mathrm{S}} \otimes \mathcal{H}_{\mathrm{E}}, \tag{3.13}$$

$$H = H_{\mathrm{S}} \otimes I_{\mathrm{E}} + I_{\mathrm{S}} \otimes H_{\mathrm{E}} + H_{\mathrm{int}}(t), \tag{3.14}$$

$$H_{\mathrm{int}}(t) = \sum_i S^i(t) \otimes E^i(t) \equiv \sum_i \left(\mathrm{e}^{iH_S t} S^i e^{-iH_S t}\right) \otimes \left(\mathrm{e}^{iH_E t} E^i \mathrm{e}^{-iH_E t}\right), \tag{3.15}$$

where the representation of the Interaction picture I are dropped. Here $\mathcal{H}_{\mathrm{S}}$ and $\mathcal{H}_{\mathrm{E}}$ respectively represent the Hilbert space of the *open* system and the environment, and the tensor product of them constitutes the Hilbert space of the total system. The self-Hamiltonians of the system and the environment are respectively denoted by H_{S} and H_{E}, and $H_{\mathrm{int}}(t)$ describes the interactions between them, which is represented by the tensor product of the *open* system part $S^i(t)$ and the environment part $E^i(t)$.

When we are just interested in some variable A of the *open* system which acts only on the Hilbert space of the *open* system, the object to be focused on is

$$\langle A \rangle = \mathrm{Tr}_{\mathrm{S}}[\rho_{\mathrm{S}} A], \tag{3.16}$$

with $\rho_{\mathrm{S}} \equiv \mathrm{Tr}_{\mathrm{E}}\, \rho$, which is called *reduced* density matrix for the *open* system. The operations of Tr_{S} and Tr_{E} denote the integration of the variables of the *open* system and the environment, respectively. Deriving the master equation of the *reduced* density matrix for the dynamics is one of the important things in the open quantum systems approach. The first procedure to tackle this is to substitute Eq. (3.12) into Eq. (3.11), which explicitly derives the master equation for the *reduced* density matrix ρ_{S}

$$\begin{aligned} \frac{d}{dt}\rho_{\mathrm{S}}(t) &= -\int_0^t ds\, \mathrm{Tr}_{\mathrm{E}}\left[H_{\mathrm{int}}(t), [H_{\mathrm{int}}(s), \rho(s)]\right] \\ &= -\int_0^t ds\, \mathrm{Tr}_{\mathrm{E}}\left[H_{\mathrm{int}}(t), [H_{\mathrm{int}}(t-s), \rho(t-s)]\right], \end{aligned} \tag{3.17}$$

where we assume $\mathrm{Tr}_{\mathrm{E}}[H_{\mathrm{int}}(t), \rho(0)] = 0$. This assumption is validated by the sets of the transformations of

$$H'_{\mathrm{int}} = H_{\mathrm{int}} - \mathrm{Tr}_{\mathrm{E}}[H_{\mathrm{int}} \rho_{\mathrm{E}}(0)], \quad H'_{\mathrm{S}} = H_{\mathrm{S}} + \mathrm{Tr}_{\mathrm{E}}[H_{\mathrm{int}} \rho_{\mathrm{E}}(0)], \tag{3.18}$$

for the initial density matrix $\rho(0) = \rho_{\mathrm{S}}(0) \otimes \rho_{\mathrm{E}}(0)$. This remains the total Hamiltonian the same as before, which allows one to take $\mathrm{Tr}_{\mathrm{E}}[H'_{\mathrm{int}}(t), \rho(0)] = 0$.

3.2.1 Sets of Approximations

For the simpler description of Eq. (3.17), some additional approximations are often imposed as in the following.

Born Approximation

Although Eq. (3.17) partially contains the density matrix of the total system $\rho(t)$, by considering Born approximation, the master equation can be expressed just in terms of $\rho_{\mathrm{S}}(t)$. Born approximation is based on the assumption that the system S and the environment E weakly interact with each other. This assumption characterizes the density matrix of the total system as

$$\rho(t) = \rho_{\mathrm{S}}(t) \otimes \rho_{\mathrm{E}}, \tag{3.19}$$

which reflects that the environment states are not affected by their interactions.

Timescale Hierarchy Assumptions

In open quantum systems approach, two kinds of the sets of timescale hierarchies are often applied. One of them is called by *quantum optical* regime and the other is called by *quantum Brownian motion* regime. In these regimes, the three timescales are involved, especially, the typical timescale τ_S of the intrinsic evolution of the system S with Hamiltonian H_{S} which is estimated by the inverse of the energy gap between the eigenstates, the typical correlation time τ_E of the environment medium E over which the environmental correlation function damps, and the relaxation time τ_R of the system S which is the timescale of the master equation and in which the reduced density matrix of the system varies appreciably. The relaxation timescale is e.g. for a single particle case, estimated by the timescale of the momentum damping. The above two regimes take the assumptions are listed in Table 3.1.

Table 3.1: Separation of timescales in quantum optical and quantum Brownian motion regimes.

Regime	Sets of timescale approximations
quantum optical	$\tau_E \ll \tau_R, \tau_S \ll \tau_R$
quantum Brownian motion	$\tau_E \ll \tau_R, \tau_E \ll \tau_S$

Markovian Approximation

Markovian approximation is applied in $\tau_E \ll \tau_R$. It provides a coarse-grained description of time evolution, dropping the memory effect of the evolution in Eq. (3.17). When the environmental correlation function decays faster than the system state varies, Eq. (3.17) reduces to the simpler form. The integrand $\rho(t-s)$ there can be replaced by $\rho(t)$ and the integrand boundary after the transformation of the integrand variable $s \to t-s$ can be changed to the infinity, since the corrections are in higher orders in the expansions of H_{int} and the environmental correlations remain finite over the shorter timescale $s \sim \tau_E$

than the timescale of interest $t \sim \tau_R$. We can then obtain the course-grained Markovian master equation

$$\frac{d}{dt}\rho_{\rm S}(t) = -\int_0^\infty ds\ {\rm Tr}_{\rm E}\left[H_{\rm int}(t), [H_{\rm int}(t-s), \rho_{\rm S}(t)\otimes\rho_{\rm E}]\right]. \tag{3.20}$$

Rotating Wave Approximation

When $\tau_S \ll \tau_R$, the applied approximation is called rotating wave approximation, which is not imposed in our discussions on in-medium quarkonium in Chap. 4. Let us define the projection $\Pi(\epsilon)$ onto the eigenstate $|\epsilon\rangle$ of H_S with the eigenvalue ϵ. Introducing the following operators

$$S^i(\omega) = \sum_{\omega=\epsilon'-\epsilon} \Pi(\epsilon) S^i \Pi(\epsilon'), \quad S^i = \sum_\omega \sum_{\omega=\epsilon'-\epsilon} S^i(\omega) \tag{3.21}$$

$$S^i_{\rm I}(\omega) = e^{iH_{\rm S}t} S^i(\omega) e^{-iH_{\rm S}t} = e^{-i\omega t} S^i(\omega), \tag{3.22}$$

the interaction Hamiltonian is given by

$$H_{\rm int}(t) = \sum_i \sum_\omega e^{-i\omega t} S^i(\omega) \otimes E^i(t). \tag{3.23}$$

in the Interaction picture. Then in Eq. (3.20), the factor $\sum_\omega \sum_{\omega'} e^{-i(\omega-\omega')t}$ appears where we note ω and ω' represents the energy difference of the two different processes. The typical intrinsic timescale of the system is $\tau_S \sim |\omega-\omega'|^{-1}$ while the relaxation time scale τ_R is assumed longer than τ_S. In the time scale τ_R considered, the rapidly oscillating factors in the time scale of τ_S drop, and the $\omega = \omega'$ part remains. This is often applied in quantum optical systems with some discrete energy levels, which leads to the simpler derivation of the master equation.

Gradient Expansions

The gradient expansion of the interaction parts is applied in $\tau_E \ll \tau_S$ and the detail is explained in the next Sec. 3.2.2 for the description of the quantum Brownian motion. In this thesis, the discussions on an in-medium quarkonium are performed in the regime of the quantum Brownian motion. The timescales for an in-medium quarkonium can be typically estimated as follows. The timescales for a bottomonium with bottom quark mass $M_b \sim 4.7$ GeV and the medium temperature $T \sim 0.4$ GeV are estimated by assuming the Coulombic bound state as

$${\tau_S}^{-1} \sim E_{\rm binding} \sim \frac{1}{2}\frac{M_b}{2}\alpha^2 \simeq \frac{1}{2}\cdot\frac{4.7\ {\rm GeV}}{2}\cdot(0.3)^2 \sim 0.1\ {\rm GeV}, \tag{3.24}$$

$${\tau_E}^{-1} \sim T \sim 0.4\ {\rm GeV}. \tag{3.25}$$

It should not be assured that the regime of quantum Brownian motion does not makes sense for an in-medium quarkonium when the resulting relaxation timescale is long. We then discuss the dynamics of in-medium quarkonia by applying Markovian approximation and the gradient expansions.

3.2.2 Quantum Brownian Motion

In addition to Born and Markovian approximations, we assume that the typical time scale of the intrinsic evolution of the system is longer than the typical environment correlation time, $\tau_E \ll \tau_S$, which can lead to the gradient expansion in the master equation.

With Eq. (3.15), Eq. (3.20) turns to

$$\frac{d}{dt}\rho_{\rm S}(t) = -\int_0^\infty ds \sum_{i,j} {\rm Tr}_{\rm E}[\rho_{\rm E}(t)E^i(t)E^j(t-s)] \times \left[S^j(t-s)\rho_{\rm S}(t)S^i(t) - S^i(t)S^j(t-s)\rho_{\rm S}(t)\right] + h.c.. \quad (3.26)$$

Since ${\rm Tr}_{\rm E}[\rho_{\rm E}(t)E^i(t)E^j(t-s)]$ takes finite for small time $s \sim \tau_E$ for $\tau_E \ll \tau_S$, we take the gradient expansions of $S^j(t-s)$ in terms of s,

$$\begin{aligned} S^j(t-s) \simeq & S^j(t) - s\dot{S}(t) + \cdots \\ = & S^j(t) - is\left[H_S, S^j(t)\right] + \mathcal{O}(s^2). \end{aligned} \quad (3.27)$$

The leading-order and next-to-leading-order terms of the gradient expansions in Eq. (3.27) shows that the stochastic effects of the random forces and the dissipative effects of the friction force in recoils of a Brownian particle during collisions in the surrounding medium as explained in Chap.4. We note that the equilibration is not achieved if the next-to-leading order term of quantum dissipation is ignored, which is what we call the recoilless limit.

Here we introduce the Fourier component of the environmental correlation function

$$\Gamma^{ij}(\omega) \equiv \int_0^\infty ds e^{is\omega}{\rm Tr}_{\rm E}[\rho_{\rm E}E^i(t)E^j(t-s)] = \int_0^\infty ds e^{is\omega}{\rm Tr}_{\rm E}[\rho_{\rm E}E^i(s)E^j(0)] \quad (3.28)$$

with the assumption of the invariance of time translation. It can be decomposed into the two parts of the hermitian part $D^{ij}(\omega)$ and the anti hermitian part $i\mathcal{V}^{ij}(\omega)$

$$D^{ij}(\omega) = \Gamma^{ij}(\omega) + \Gamma^{ji*}(\omega), \quad \mathcal{V}^{ij}(\omega) = \frac{1}{2i}[\Gamma^{ij}(\omega) - \Gamma^{ji*}(\omega)]. \quad (3.29)$$

The values $D^{ij}(\omega = 0)$ and $\mathcal{V}^{ij}(\omega = 0)$ can be expressed by the real-valued spectral density function

$$\sigma^{ij}(\omega) \equiv \int_{-\infty}^\infty ds\, e^{is\omega}{\rm Tr}_{\rm E}\left[\rho_{\rm E}[E^i(s), E^j(0)]\right] = (1 - {\rm e}^{\beta\omega})D^{ij}(\omega) \quad (3.30)$$

with the help of Kubo-Martin-Schwinger relation $D^{ij}(\omega) = {\rm e}^{\beta\omega}D^{ji}(-\omega)$. With the spectral function, we can define the following complex numbers

$$D^{ij} \equiv D^{ij}(\omega = 0) = T\left.\frac{d\sigma^{ij}}{d\omega}\right|_{\omega=0}, \quad \mathcal{V}^{ij} \equiv \mathcal{V}^{ij}(\omega = 0) = \int_{-\infty}^\infty \frac{d\omega}{2\pi}\frac{\sigma^{ij}(\omega)}{\omega}, \quad (3.31)$$

$$\eta^{ij} \equiv -i\left.\frac{d\Gamma^{ij}(\omega)}{d\omega}\right|_{\omega=0} = -\frac{1}{2}\int_{-\infty}^\infty \frac{d\omega}{2\pi}\frac{1}{\omega}\frac{d}{d\omega}\left[\frac{\sigma^{ij}(\omega)}{1 - {\rm e}^{-\beta\omega}}\right] - \frac{i}{4}\left.\frac{d\sigma^{ij}}{d\omega}\right|_{\omega=0}. \quad (3.32)$$

With these quantities, Eq. (3.26) is then transformed into

$$\frac{d}{dt}\rho_S(t) = \sum_{i,j} \begin{bmatrix} D^{ij}\left(S^j(t)\rho_S(t)S^i(t) - \frac{1}{2}\left\{S^i(t)S^j(t), \rho_S(t)\right\}\right) \\ -i\mathcal{V}^{ij}\left(S^i(t)S^j(t)\rho_S(t) - \rho_S(t)S^i(t)S^j(t)\right) \\ -\eta^{ij}\left(\dot{S}^j(t)\rho_S(t)S^i(t) - S^i(t)\dot{S}^j(t)\rho_S(t)\right) \\ -\eta^{ij*}\left(S^i(t)\rho_S(t)\dot{S}^j(t) - \rho_S(t)\dot{S}^j(t)S^i(t)\right) \end{bmatrix}, \tag{3.33}$$

up to the next-to-leading order gradient expansion. Let us here assume that the matrix D^{ij} is positive semidefinite and that $(D^{-1})_{ij}$ exists, which derives the simpler form

$$\frac{d}{dt}\rho_S(t) = -i\left[\Delta H_S(t), \rho_S(t)\right] + \sum_{i,j} D_{ij}\left[\tilde{S}^j(t)\rho_S(t)\tilde{S}^{i\dagger} - \frac{1}{2}\left\{\tilde{S}^{i\dagger}(t)\tilde{S}^j(t), \rho_S(t)\right\}\right], \tag{3.34}$$

$$\Delta H_S(t) \equiv \sum_{i,j}\mathcal{V}^{ij}S^i(t)S^j(t) + \frac{i}{2}\sum_{i,j}\left(\eta_{ij}S^i(t)\dot{S}^j(t) - \eta^*_{ij}\dot{S}^j(t)S^i(t)\right), \tag{3.35}$$

$$\tilde{S}^i(t) \equiv S^i(t) - \sum_{j,k}(D^{-1})_{ij}\eta^{jk}\dot{S}^k(t). \tag{3.36}$$

In the regime of quantum Brownian motion with weak coupling, the real part of η^{ij}, $\mathrm{Re}\,\eta^{ij}$, can be often approximated to be negligible with the cutoff frequency of spectral function and the assumption of the time scale hierarchies [77, 78]. Thus in this regime, η^{ij} is approximately proportional to the imaginary part of η^{ij}, $\mathrm{Im}\,\eta^{ij}$, and Eq. (3.36) thus reads

$$\tilde{S}^i(t) = S^i(t) + \frac{i}{4T}\dot{S}^i(t). \tag{3.37}$$

When the matrix D is positive semidefinite, Eq. (3.34) can be cast into an equivalent form with the diagonalized matrix D' with non-negative eigenvalues, which is obtained by some unitary transformation U that satisfies the relations to the new operators L^i

$$D'_{ij} = U_{ik}D_{kl}U^\dagger_{lj}, \quad \tilde{S}^i = U_{ij}L^j. \tag{3.38}$$

With these new operators, after some algebra, Eq. (3.34) can be transformed into the diagonalized form

$$\frac{d}{dt}\rho_S(t) = -i\left[\Delta H_S(t), \rho_S(t)\right] + \sum_k D'_{kk}\left[L^k(t)\rho_S(t)L^{k\dagger} - \frac{1}{2}\left\{L^{k\dagger}(t)L^k(t), \rho_S(t)\right\}\right], \tag{3.39}$$

which is in what we call Lindblad master equation form[79]. The Lindblad master equation, which is composed of the Lindblad operators L_k, satisfies the condition in which it is Markovian, trace-preserving, and positive during the evolution of the reduced density matrix. Since we can probabilistically interpret the dynamics of the open system as a mixed state, the Lindblad master equation is thus useful and reasonable in this regard.

If the description is moved into the Schrödinger picture, we employ the relation be-

tween the Schrödinger picture S and the Interaction picture I,

$$\frac{d}{dt}\rho_S(t) = -i\left[H_S, \rho_S(t)\right] + \mathrm{e}^{-iH_s t}\left(\frac{d}{dt}\rho_S^{\mathrm{I}}(t)\right)\mathrm{e}^{-iH_s t}. \tag{3.40}$$

Chapter 4

Lindblad Equation for Quarkonium in the Quark-Gluon Plasma

In this Chap. 4, the Lindblad equation for a quarkonium in the quark-gluon plasma is derived and focused on in the open quantum systems framework explained in the previous Chap. 3. We start the discussions on an in-medium quarkonium by taking, as a starting point, the non-relativistic QCD effective description and the corresponding Hamiltonian of the composed total system of a quarkonium and the quark-gluon plasma[51, 52]. Based on the open quantum systems framework with the non-relativistic QCD, we derive the Lindblad equation for a quarkonium in the quark-gluon plasma. To interpret the physical meanings encoded in its Lindblad operator, we first, for simplicity, consider the case for a single heavy quark in a thermal medium[80], which is partially related to the Caldeira Leggett model[81]. We then extend it to a two-particle system in a thermal medium, that is, a quarkonium in the quark-gluon plasma of interest in our case. We also derive and interpret the corresponding Lindblad operator by the analogy to the single heavy quark case or the Caldeira Leggett model. From the Lindblad operator, we trace out the center of mass motion to focus in particular on the relative motion of a quarkonium in color singlet-octet bases with the simple assumption as explained later.

4.1 Derivation of Lindblad Operator

The non-relativistic QCD theory is one of the effective descriptions of heavy quarks in the non-relativistic regime. In this description, the creation and annihilation of a heavy quark pair can be neglected and the description of the heavy quarks reduces to the quantum mechanical limit. Since the framework of open systems is constructed by the Hamiltonian formalism, the corresponding Hamiltonian is needed for heavy quark systems in the thermal quark-gluon plasma medium. Though this procedure of taking the Hamiltonian[68, 82, 83], we begin with

$$H_Q = \frac{p_Q^2}{2M} \otimes I_{\rm QGP} + I_Q \otimes H_{\rm QGP} + \int d^3x \left[\delta\left(\vec{x} - \vec{x}_Q\right) t_Q^a\right] \otimes g A_0^a(\vec{x}), \tag{4.1}$$

$$H_{QQ_c} = \left(\frac{p_Q^2}{2M} + \frac{p_{Q_c}^2}{2M}\right) \otimes I_{\rm QGP} + I_{QQ_c} \otimes H_{\rm QGP} + \int d^3x \left[\delta\left(\vec{x} - \vec{x}_Q\right) t_Q^a - \delta\left(\vec{x} - \vec{x}_{Q_c}\right) t_{Q_c}^{a*}\right] \otimes g A_0^a(\vec{x}), \tag{4.2}$$

where $H_{\rm QGP}$ denotes the Hamiltonian for the thermal quark-gluon plasma sector and the matrices t^a_Q and $t^{a*}_{Q_c}$ are in the color SU(N_c) algebra with Q and Q_c representing a heavy quark and its antiquark. We note that $\vec{x}_Q$, $\vec{x}_{Q_c}$, and A_0 are operators.

4.1.1 Single Quark Case

In this section, from the non-relativistic Hamiltonian (4.1), we start to derive the Lindblad equation, and relate it to the Caldeira Leggett model, which is one of the prototypes of a quantum Brownian particle. The indexes i in Eq. (3.31) and Eq. (3.32) thus hereafter turn to be the continuous variable of the position $\vec{x}$ and the discrete indexes of heavy quark colors a. Following the discussions in Sec. 3.2.2, the ingredients for the master equation are defined and obtained,

$$S^a(x) = \delta\left(\vec{x}-\vec{x}_Q\right) t^a_Q, \tag{4.3}$$

$$\dot{S}^a(x) = \left[-\frac{i}{2M}\nabla^2_x\delta\left(\vec{x}-\vec{x}_Q\right) - \frac{1}{M}\vec{\nabla}_x\delta\left(\vec{x}-\vec{x}_Q\right)\cdot\vec{p}_Q\right] t^a_Q \tag{4.4}$$

$$D_{ab}(\vec{x}-\vec{y}) = T\frac{d}{d\omega}\sigma_{ab}(\omega,\vec{x}-\vec{y})\Big|_{\omega=0} = D(\vec{x}-\vec{y})\delta_{ab}, \tag{4.5}$$

$$\mathcal{V}_{ab}(\vec{x}-\vec{y}) = -\frac{1}{2}\int_{-\infty}^{\infty}\frac{d\omega}{2\pi}\frac{\sigma_{ab}(\omega,\vec{x}-\vec{y})}{\omega} \equiv \mathcal{V}(\vec{x}-\vec{y})\delta_{ab}, \tag{4.6}$$

$$\sigma_{ab}(\omega,\vec{x}-\vec{y}) = \int_{-\infty}^{\infty} dt e^{i\omega t}\,\mathrm{Tr}_{\rm QGP}\left(\rho_{\rm QGP}\left[gA^a_0(t,\vec{x}), gA^b_0(0,\vec{y})\right]\right), \tag{4.7}$$

$$\eta_{ab}(\vec{x}-\vec{y}) = -\frac{i}{4T}D_{ab}(\vec{x}-\vec{y}), \tag{4.8}$$

whose analytic expressions in momentum space for soft external momentum scale are listed in Appendix A. Then the Lindblad equation for a single heavy quark in a thermal medium is derived form Eq. (3.39) after some algebra,

$$\frac{d}{dt}\rho_Q(t) = -i\left[H_Q,\rho_Q\right] + \sum_a\int_k\left[2L^a(\vec{k})\rho_Q L^{a\dagger}(\vec{k}) - \left\{L^{a\dagger}(\vec{k})L^a(\vec{k}),\rho_Q\right\}\right], \tag{4.9}$$

$$\begin{aligned} L^a(\vec{k}) =& \sqrt{\frac{D(\vec{k})}{2}}e^{i\vec{k}\cdot\vec{x}_Q/2}\left(1-\frac{\vec{k}\cdot\vec{p}_Q}{4MT}\right)e^{i\vec{k}\cdot\vec{x}_Q/2}t^a_Q \\ =& \sqrt{\frac{D(\vec{k})}{2}}e^{i\vec{k}\cdot\vec{x}_Q}\left(1-\frac{\vec{k}\cdot\vec{p}_Q}{4MT}+\frac{\vec{k}^2}{8MT}\right)t^a_Q, \end{aligned} \tag{4.10}$$

where we note ΔH_Q in Eq. (3.39) is constant and dropped and $\int_k$ denotes $\int\frac{d^3k}{(2\pi)^3}$ in short. This Lindblad operator was also derived in the influence functional formalism[68, 82]. The numerical simulations of a single heavy quark case with this Lindblad operator was done[80], which is quite similar to our discussions for an in-medium quarkonium.

The information of the interactions is embedded in the non-unitary part of the Lindblad master equation, in particular, in the Lindblad operator. When considering the momentum eigenstates, the operator $e^{i\vec{k}\cdot\vec{x}_Q}t^a_Q$ acting on such states represents the momentum transfer of the quark by $\vec{k}$ and changes the heavy quark color state. It is expected that the coefficient $D(\vec{k})$ represents how frequently these processes occur and the next-to-leading-

order term modifies the rate.

Here we estimate the transition rate between the process and its inverse process $\vec{p} \rightleftarrows \vec{p}+\vec{k}$ as

$$\frac{\Gamma_{\vec{p}\to\vec{p}+\vec{k}}}{\Gamma_{\vec{p}+\vec{k}\to\vec{p}}} = \frac{\left[1-\frac{\vec{k}\cdot\vec{p}}{4MT}-\frac{\vec{k}^2}{8MT}\right]^2}{\left[1+\frac{\vec{k}\cdot\vec{p}}{4MT}+\frac{\vec{k}^2}{8MT}\right]^2}. \tag{4.11}$$

With the approximation by the Taylor-expansions in small x of

$$\frac{(1+x)^2}{(1-x)^2} \sim \mathrm{e}^{4x}, \tag{4.12}$$

Eq. (4.11) are estimated and the detailed balance approximately holds as

$$\frac{\Gamma_{\vec{p}\to\vec{p}+\vec{k}}}{\Gamma_{\vec{p}+\vec{k}\to\vec{p}}} \simeq \exp\left(\frac{E_{\vec{p}}-E_{\vec{p}+\vec{k}}}{T}\right) \tag{4.13}$$

with the kinetic energy defined by $E_{\vec{p}} \equiv \vec{p}^2/2M$ with momentum $\vec{p}$. Equilibration expect to lead to the Boltzmann distribution and the next-to-leading-order gradient expansion is essential to satisfying the detail balance. If we neglect the next-to-leading-order term, the rate for the process is equal to the rate for the inverse process. The leading-order and the next-to-leading-order terms in the Lindblad operator (4.10) derived by the gradient expansion can be interpreted as thermal fluctuating effects by random forces and dissipative effects by frictional forces during collisions with surrounding medium particles, as will be seen from the classical limit of the master equation.

Relation to Caldeira Leggett Model

Caldeira Leggett model[81] is the prototype of a colorless Brownian particle and the corresponding master equation is

$$\begin{aligned}\frac{\partial}{\partial t}\rho_Q(t,\vec{x},\vec{y}) =& i\frac{\nabla_x^2-\nabla_y^2}{2M}\rho_Q(t,\vec{x},\vec{y}) \\ &+\frac{\nabla^2 D(0)}{6}\left[(\vec{x}-\vec{y})^2+\frac{\vec{x}-\vec{y}}{2MT}\cdot(\vec{\nabla}_x-\vec{\nabla}_y)\right]\rho_Q(t,\vec{x},\vec{y}).\end{aligned} \tag{4.14}$$

It is known that Caldeira Leggett model is not in the Lindblad form and that, however, by introducing the additional term

$$+\frac{\nabla^2 D(0)}{6}\left[-\frac{1}{16M^2T^2}(\vec{\nabla}_x+\vec{\nabla}_y)^2\right]\rho_Q(t,\vec{x},\vec{y}) \tag{4.15}$$

to the right hand side of Eq. (4.14), it can be transformed into the Lindblad form with the corresponding Lindblad operator up to its coefficient

$$L = \left(\vec{x}_Q+\frac{i\vec{p}_Q}{4MT}\right). \tag{4.16}$$

On the other hand, after tracing over the internal color degrees of freedom in Eq. (4.9) with $C_F = \frac{N_c^2-1}{2N_c}$, the density matrix $\bar{\rho}_Q = \mathrm{Tr}_{\mathrm{color}}\rho_{\mathrm{Q}}$ satisfies

$$\begin{aligned}\frac{\partial}{\partial t}\bar{\rho}_Q(t,\vec{x},\vec{y}) = i\frac{\nabla_x^2-\nabla_y^2}{2M}\bar{\rho}_Q(t,\vec{x},\vec{y}) - C_F\left[F_1(\vec{0}) - F_1(\vec{x}-\vec{y})\right]\bar{\rho}_Q(t,\vec{x},\vec{y}) \\ + C_F\left[\vec{F}_2(\vec{x}-\vec{y})\cdot(\vec{\nabla}_x - \vec{\nabla}_y)\right]\bar{\rho}_Q(t,\vec{x},\vec{y}) \\ + C_F\left[F_3^{ij}(\vec{x}-\vec{y})\partial_x^i\partial_y^j + F_3^{ii}(\vec{0})\frac{\nabla_x^2+\nabla_y^2}{6}\right]\bar{\rho}_Q(t,\vec{x},\vec{y}),\end{aligned} \tag{4.17}$$

$$F_1(\vec{r}) \equiv D(\vec{r}) + \frac{\nabla^2 D(\vec{r})}{4MT} + \frac{\nabla^4 D(\vec{r})}{64M^2T^2}, \quad \vec{F}_2(\vec{r}) \equiv \vec{\nabla}\left(\frac{D(\vec{r})}{4MT} + \frac{\nabla^2 D(\vec{r})}{32M^2T^2}\right), \tag{4.18}$$

$$F_3^{ij}(\vec{r}) \equiv -\frac{\partial_i\partial_j D(\vec{r})}{16M^2T^2}. \tag{4.19}$$

Eq. (4.17) with $C_F = 1$ can be reduced to the Caldeira Leggett model master equation plus Eq. (4.15) by taking the semi classical limit $|\vec{x}-\vec{y}| \to 0$ and expanding $D(\vec{x}-\vec{y})$ up to the second order. This can be compensated for the expansion of small $\vec{x}_Q$ in Eq. (4.10) up to the leading order. In this regard, the Caldeira Leggett model is expected just for the localized state. In Ref. [84], it may be considered to lack the typical coherent length scale of the thermal environment. Thus, the simple application of the Caldeira Leggett model to the in-medium quarkonium relative motion is questionable, since the quarkonium spatial size in particular for the deeply bound ground state can be the same order of the typical environmental correlation length. The relative motion has the same number of dimensions of degrees of freedom as the Caldeira Leggett model, though.

Here, we consider the Wigner transformation of the master equation for Caldeira Leggett model, which is defined by

$$f(t,\vec{r},\vec{p}) \equiv \int d^3s\, e^{-i\vec{p}\cdot\vec{s}}\rho_Q\left(t,\vec{r}+\frac{\vec{s}}{2},\vec{r}-\frac{\vec{s}}{2}\right), \quad \vec{x} = \vec{r}+\frac{\vec{s}}{2}, \quad \vec{y} = \vec{r}-\frac{\vec{s}}{2}. \tag{4.20}$$

We note $f(t,\vec{r},\vec{p})$ is can be regarded as the phase space distribution except for the fact that it can be negative at some points. In this respect, the evolution of the density matrix can be seen as the Fokker Planck equation which has the corresponding Langevin equation. Here, we assume, for simplicity,

$$F_1(\vec{r}) \simeq D(\vec{r}) + \frac{\nabla^2 D(\vec{r})}{4MT}, \quad \vec{F}_2(\vec{r}) \simeq \vec{\nabla}F_1(\vec{r}), \quad F_3^{ij}(\vec{r}) = 0 \tag{4.21}$$

in the order of the gradient expansions and the time evolution of $f(t,\vec{r},\vec{p})$ in the semi classical limit $|\vec{r}| \to 0$ with $\kappa \equiv -\frac{\nabla^2 D(\vec{0})}{3}$ is

$$\frac{\partial f(t,\vec{r},\vec{p})}{\partial t} = -\frac{\vec{p}\cdot\vec{\nabla}_r}{M}f(t,\vec{r},\vec{p}) + \frac{\partial}{\partial\vec{p}}\cdot\left[\frac{\kappa}{2MT}\vec{p}f(t,\vec{r},\vec{p})\right] + \frac{\kappa}{2}\frac{\partial}{\partial\vec{p}}\cdot\frac{\partial f(t,\vec{r},\vec{p})}{\partial\vec{p}}. \tag{4.22}$$

We note Eq. (4.22) is in the same form of Kramers equation for the distribution function

$W(\vec{x},\vec{v},t)$ in the position-velocity space

$$\frac{\partial W(\vec{x},\vec{v},t)}{\partial t}=\sum_{i=1}^{3}\left[-\frac{\partial}{\partial x_i}v_i+\frac{\partial}{\partial v_i}\left(\Gamma v_i\right)+\Gamma v_{\rm th}^2\frac{\partial^2}{\partial v_i\partial v_i}\right]W(\vec{x},\vec{v},t), \tag{4.23}$$

where $v_{\rm th}=\sqrt{\frac{T}{M}}$ is the thermal velocity[85]. This can be described by the equivalent Langevin equation. In the Langevin equation, the stochastic force and drag force are included as

$$\dot{\vec{x}}=\vec{v},\quad \dot{\vec{v}}=-\Gamma\vec{v}+\vec{\Xi}(t),\quad \langle\Xi^i(t)\Xi^j(t')\rangle_\Xi=\frac{2\Gamma T}{M}\delta(t-t')\delta^{ij}, \tag{4.24}$$

the last equation of which represents the relation with the statistical average of the stochastic force $\Xi(t)$[85]. The correspondence between Eq. (4.22) and Eq. (4.23) is given by $\Gamma=\frac{\kappa}{2MT}$.

4.1.2 Extension to Quarkonium Case

We next move onto the case of a quarkonium in the quark-gluon plasma. As in the case of a single heavy quark case, the discussions start form the Hamiltonian (4.2). The differences from the discussions for a single heavy quark in Sec. 4.1.1 are the expression of $S^a(x)$ and the existence of the correction to the Hamiltonian ΔH_{QQ_c} in the gradient expansions. The expressions for $S^a(x)$ and $\dot{S}^a(x)$ are

$$S^a(\vec{x})=\delta\left(\vec{x}-\vec{x}_Q\right)\left(t_Q^a\otimes 1\right)-\delta\left(\vec{x}-\vec{x}_{Qc}\right)\left(1\otimes t_{Qc}^{a*}\right) \tag{4.25}$$

$$\dot{S}^a(\vec{x})=\left[-\frac{i}{2M}\nabla_x^2\delta\left(\vec{x}-\vec{x}_Q\right)-\frac{1}{M}\vec{\nabla}_x\delta\left(\vec{x}-\vec{x}_Q\right)\cdot\vec{p}_Q\right]\left(t_Q^a\otimes 1\right) \tag{4.26}$$

$$-\left[-\frac{i}{2M}\nabla_x^2\delta\left(\vec{x}-\vec{x}_{Q_c}\right)-\frac{1}{M}\vec{\nabla}_x\delta\left(\vec{x}-\vec{x}_{Q_c}\right)\cdot\vec{p}_{Q_c}\right]\left(1\otimes t_{Qc}^{a*}\right) \tag{4.27}$$

And the correction to the Hamiltonian is calculated as

$$\Delta H_S=\left[-2\mathcal{V}\left(\vec{x}_Q-\vec{x}_{Q_c}\right)-\frac{1}{8MT}\left\{\vec{p}_Q-\vec{p}_{Q_c},\vec{\nabla}D\left(\vec{x}_Q-\vec{x}_{Q_c}\right)\right\}\right]\left(t_Q^a\otimes t_{Q_c}^{a*}\right). \tag{4.28}$$

We note that ΔH_S is composed of the leading and the next-to-leading order terms in the gradient expansions. The leading term is from the gluon interactions and included in the Hamiltonian term as the quarkonium potential $V\left(\vec{x}_Q-\vec{x}_{Qc}\right)=-2\mathcal{V}\left(\vec{x}_Q-\vec{x}_{Qc}\right)$. The induced potential term here can improve the $\dot{S}^a(\vec{x})$ and accordingly the Lindblad operator. Following the same steps as in a single heavy quark case, the resultant effective Hamiltonian is

$$H_{\rm eff}\equiv\frac{p_Q^2+p_{Q_c}^2}{2M}+\left[V\left(\vec{x}_Q-\vec{x}_{Qc}\right)-\frac{1}{8MT}\left\{\vec{p}_Q-\vec{p}_{Q_c},\vec{\nabla}D\left(\vec{x}_Q-\vec{x}_{Qc}\right)\right\}\right]\left(t_Q^a\otimes t_{Qc}^{a*}\right). \tag{4.29}$$

The Lindblad master equation for a quarkonium in the quark-gluon plasma is derived after some algebra, as follows

$$\frac{d}{dt}\rho_{QQ_c}(t) = -\,i\,[H_{\rm eff},\rho_{QQ_c}] + \sum_a \int_k \left[2L^a(\vec{k})\rho_{QQ_c}L^{a\dagger}(\vec{k}) - \left\{L^{a\dagger}(\vec{k})L^a(\vec{k}),\rho_{QQ_c}\right\}\right], \tag{4.30}$$

$$\begin{aligned} L^a(\vec{k}) =& \sqrt{\frac{D(\vec{k})}{2}}\left[e^{i\vec{k}\cdot\vec{x}_Q/2}\left(1-\frac{\vec{k}\cdot\vec{p}_Q}{4MT}\right)e^{i\vec{k}\cdot\vec{x}_Q/2}\left(t_Q^a\otimes 1\right)\right. \\ & - e^{i\vec{k}\cdot\vec{x}_{Q_c}/2}\left(1-\frac{\vec{k}\cdot\vec{p}_{Q_c}}{4MT}\right)e^{i\vec{k}\cdot\vec{x}_{Q_c}/2}\left(1\otimes t_{Q_c}^{a*}\right) \\ & \left. -\frac{V\left(\vec{x}_Q-\vec{x}_{Q_c}\right)}{4T}\left(e^{i\vec{k}\cdot\vec{x}_Q}-e^{i\vec{k}\cdot\vec{x}_{Q_c}}\right)if^{abc}\left(t_Q^a\otimes t_{Q_c}^{a*}\right)\right]. \end{aligned} \tag{4.31}$$

The first two terms of the Lindblad operator are similar to U(1) case. Similarly, they can be interpreted as thermal fluctuating effects by random forces and dissipative effects by frictional forces during collisions with surrounding medium particles. The operator $e^{i\vec{k}\cdot\vec{x}_Q}t_Q^a$ acting on such states represents the momentum transfer of the heavy quark Q by $\vec{k}$ and changes the heavy quark color state and also the corresponding operator for the antiquark Q_c exists. Including the next-to-leading-order term can be interpreted as the modification of the rate, resulting in the momentum dependent rate as in Eq. (4.11).

Reduction to Relative Motion

Since quarkonium is a two-body system, its dynamics is composed of the two dynamics, the center of mass motion and the relative motion. In the role of quarkonia in heavy ion collisions, the dissociation of a quarkonium bound state, charmonium or bottomonium in the quark-gluon plasma is closely related to the relative distance between the two heavy quarks in the quarkonium potential. We hereafter are motivated to focus on the relative motion by tracing out the center of mass motion.

The procedure of tracing out the center of mass motion from the explicit Lindblad equation (4.30) can be directly performed by

$$\begin{aligned} \rho^r_{QQ_c}(\vec{r},\vec{s}) =& \int d\vec{R}d\vec{S}\,\rho_{QQ_c}(\vec{x}_Q,\vec{x}_{Q_c},\vec{y}_Q,\vec{y}_{Q_c})\delta(\vec{R}-\vec{S}) \\ \equiv& {\rm Tr}_R[\rho_{QQ_c}], \end{aligned} \tag{4.32}$$

where the center of mass coordinates of $\vec{R}$ and $\vec{S}$, and the relative coordinates of $\vec{r}$ and $\vec{s}$ are defined by

$$\vec{R}=\frac{\vec{x}_Q+\vec{x}_{Qc}}{2},\quad \vec{r}=\vec{x}_Q-\vec{x}_{Qc},\quad \vec{S}=\frac{\vec{y}_Q+\vec{y}_{Qc}}{2},\quad \vec{s}=\vec{y}_Q-\vec{y}_{Qc}. \tag{4.33}$$

Accordingly we introduce the center of mass momentum and the relative momentum as

$$\vec{P}=\vec{p}_Q+\vec{p}_{Q_c},\quad \vec{p}=\frac{\vec{p}_Q-\vec{p}_{Q_c}}{2}. \tag{4.34}$$

This procedure results in the master equation for the relative motion, which shows that

the relative motion is coupled to the center of mass motion and that they are not able to be completely decoupled at all. In the following, we take the specific assumption and derive the Lindblad operator for the relative motion. In these coordinates, the Hamiltonian and the Lindblad operators are

$$\begin{aligned} H_{\text{eff}} =& \frac{\vec{P}^2}{4M} + \frac{\vec{p}^2}{M} + \left[V\left(\vec{r}\right) - \frac{1}{4MT} \left\{ \vec{p}, \vec{\nabla} D\left(\vec{r}\right) \right\} \right] \left(t_Q^a \otimes t_{Qc}^{a*} \right) \\ \equiv& H_R + H_r, \end{aligned} \tag{4.35}$$

$$\begin{aligned} L^a(\vec{k}) =& \sqrt{\frac{D(\vec{k})}{2}} \left[e^{i\vec{k}\cdot\vec{R}} \left\{ 1 - \frac{\vec{k}}{4MT} \cdot \left(\frac{1}{2}\vec{P} + \vec{p} \right) \right\} e^{i\vec{k}\cdot\vec{r}/2} \left(t_Q^a \otimes 1 \right) \right. \\ & - e^{i\vec{k}\cdot\vec{R}} \left\{ 1 - \frac{\vec{k}}{4MT} \cdot \left(\frac{1}{2}\vec{P} - \vec{p} \right) \right\} e^{-i\vec{k}\cdot\vec{r}/2} \left(1 \otimes t_{Qc}^{a*} \right) \\ & \left. - e^{i\vec{k}\cdot\vec{R}} \frac{V\left(\vec{r}\right)}{4T} \left(e^{i\vec{k}\cdot\vec{r}/2} - e^{-i\vec{k}\cdot\vec{r}/2} \right) i f^{abc} \left(t_Q^a \otimes t_{Qc}^{a*} \right) \right] \\ \equiv& e^{i\vec{k}\cdot\vec{R}} C^a(\vec{k}, O_r, \vec{P}), \end{aligned} \tag{4.36}$$

where the operators H_r and $O_r \in \{\vec{r}, \vec{p}, t^a \otimes 1, 1 \otimes t^{a*}\}$ are only for the relative coordinate and the color space. The operator $C^a(\vec{k}, O_r, \vec{P})$ is defined like the above. To proceed further, we assume that the center of mass time scale is longer than that of the relative motion because the potential bends the trajectories of the relative motion [1] [2]. This assumption allows us to fix the center-of-mass momentum $\vec{P} = \vec{P}_{\text{CM}}$ in the equation and represent the quarkonium density matrix by

$$\rho_{QQ_c} = |\vec{P}_{\text{CM}}\rangle \langle \vec{P}_{\text{CM}}| \otimes \rho^r_{QQ_c}, \tag{4.37}$$

and express the Lindblad master equation for the relative motion by $\rho^r_{QQ_c}$ with the Lindblad operator $C^a(\vec{k}, O_r, \vec{P}_{\text{CM}})$ as below. We then can calculate

$$\text{Tr}_R \left(L^a(\vec{k}) \rho_{QQ_c} L^a(\vec{k}) \right) = C^a(\vec{k}, O_r, \vec{P}_{\text{CM}}) \rho^r_{QQ_c} C^{a\dagger}(\vec{k}, O_r, \vec{P}_{\text{CM}}), \tag{4.38}$$

$$\text{Tr}_R \left(L^{a\dagger}(\vec{k}) L^a(\vec{k}) \rho_{QQ_c} \right) = C^{a\dagger}(\vec{k}, O_r, \vec{P}_{\text{CM}}) C^a(\vec{k}, O_r, \vec{P}_{\text{CM}}) \rho^r_{QQ_c}, \tag{4.39}$$

$$\text{Tr}_R \left(\rho_{QQ_c} L^{a\dagger}(\vec{k}) L^a(\vec{k}) \right) = \rho^r_{QQ_c} C^{a\dagger}(\vec{k}, O_r, \vec{P}_{\text{CM}}) C^a(\vec{k}, O_r, \vec{P}_{\text{CM}}). \tag{4.40}$$

The last thing to be calculated is $\text{Tr}_R[H_{\text{eff}}, \rho_{QQ_c}]$ and its calculation can be done noting

$$\text{Tr}_R(O^1 O^2) = \text{Tr}_R(O^2 O^1) \tag{4.41}$$

for any operator $O^1 = {O^1}_R \otimes 1$ and O^2. This relation is derived as follows. For the eigenstates in the Hilbert space for the center of mass motion $\mathcal{H}_R$ indexed by the integers

[1] As in Ref. [86], with pNRQCD construction where $M \gg Mv \gg Mv^2, T$, the virial theorem tells $\vec{p}^2/M$ is in the same scale as the potential $\sim Mv^2$. The center of mass momentum is $\vec{P}_{\text{CM}} \ll Mv$ since the momentum $\sim Mv$ is already integrated out, and thus the center of mass kinetic energy is neglected by power counting. Ref. [87] also includes the center of mass motion, but neglects it in the case of $\vec{P}_{\text{CM}} < T$.

[2] We note that Eq. (4.30) are formulated in the position and momenta of the individual heavy quarks, where both the physics of relative and center of mass coordinates is present, and simulating them might expect to support this assumption if it shows their different time scales.

i_R and those in the Hilbert space for the relative motion $\mathcal{H}_r$ indexed by the integers i_r, we calculate

$$\left[\mathrm{Tr}_R(O^1O^2)\right]_{i_rj_r} = [(O^1O^2)^{k_Rk_R}]_{i_rj_r} = \left(O^1{}_R\right)^{k_Rl_R}\delta_{i_rm_r}(O^2)^{l_Rk_R}_{m_rj_r} = \left(O^1{}_R\right)^{k_Rl_R}(O^2)^{l_Rk_R}_{i_rj_r}, \tag{4.42}$$

$$\begin{aligned}\left[\mathrm{Tr}_R(O^2O^1)\right]_{i_rj_r} &= [(O^2O^1)^{k_Rk_R}]_{i_rj_r} = (O^2)^{k_Rl_R}_{i_rm_r}\left(O^1{}_R\right)^{l_Rk_R}\delta_{m_rj_r} = (O^2)^{k_Rl_R}_{i_rj_r}\left(O^1{}_R\right)^{l_Rk_R} \\ &= \left(O^1{}_R\right)^{l_Rk_R}(O^2)^{k_Rl_R}_{i_rj_r} = \left(\mathrm{Tr}_R(O^1O^2)\right)_{i_rj_r}.\end{aligned} \tag{4.43}$$

We then obtain

$$\mathrm{Tr}_R\left[H_R,\rho_{QQ_c}\right]=0, \quad \mathrm{Tr}_R\left[H_r,\rho_{QQ_c}\right]=\left[H_r,\rho^r_{QQ_c}\right]. \tag{4.44}$$

After these steps, the Lindblad equation for the relative motion of a quarkonium in the quark-gluon plasma is thus finally reduced to

$$\frac{d}{dt}\rho^r_{QQ_c}(t) = -i\left[H_r,\rho^r_{QQ_c}\right]+\sum_a\int_k\left[2L^a(\vec{k})\rho^r_{QQ_c}L^{a\dagger}(\vec{k})-\left\{L^{a\dagger}(\vec{k})L^a(\vec{k}),\rho^r_{QQ_c}\right\}\right], \tag{4.45}$$

$$L^a(\vec{k}) \equiv A_Q\left(t^a_Q\otimes 1\right)-B_{Q_c}\left(1\otimes t^{a*}_{Q_c}\right)+C_{QQ_c}\,if^{abc}\left(t^a_Q\otimes t^{a*}_{Q_c}\right). \tag{4.46}$$

$$A_Q = \sqrt{\frac{D(\vec{k})}{2}}\left\{1-\frac{\vec{k}}{4MT}\cdot\left(\frac{1}{2}\vec{P}_{\mathrm{CM}}+\vec{p}\right)\right\}e^{i\vec{k}\cdot\vec{r}/2} \tag{4.47}$$

$$B_{Q_c} = \sqrt{\frac{D(\vec{k})}{2}}\left\{1-\frac{\vec{k}}{4MT}\cdot\left(\frac{1}{2}\vec{P}_{\mathrm{CM}}-\vec{p}\right)\right\}e^{-i\vec{k}\cdot\vec{r}/2} \tag{4.48}$$

$$C_{QQ_c} = \sqrt{\frac{D(\vec{k})}{2}}\left\{-\frac{V(\vec{r})}{4T}\left(e^{i\vec{k}\cdot\vec{r}/2}-e^{-i\vec{k}\cdot\vec{r}/2}\right)\right\} \tag{4.49}$$

The constituents of the Lindblad operator A_Q, B_{Q_c}, and C_{QQ_c} are defined like the above. As the constituents of the Lindblad equation, the functions of the potential $V(\vec{x})$ and the medium correlations $D(\vec{x})$ determine the in-medium dynamics of a quarkonium. We note the shifted momentum form these operators is $\pm\vec{k}/2$ since we here consider the relative motion and that the transferred momentum for a heavy quark and antiquark is $\vec{k}$ as in Eq. (4.31) and Eq. (4.34). We will later find C_{QQ_c} in Eq. (4.46) is related only to the different color transitions as in Eq. (4.53).

Here we remark the relation to the stochastic potential model[68, 69, 88] in this thesis. The stochastic potential model describes the decoherence phenomenon of the quarkonium wave function. The Hamiltonian is composed of the kinetic term, the potential term, and the stochastic noise term. This stochastic description can be shown to be transformed into the Lindblad master equation by gradient expansion just up to the leading order. In this respect, the leading-order gradient expansion shows the fluctuating forces from the medium since the spatial derivative of the stochastic noise term in the Hamiltonian of the stochastic potential model represents stochastic forces to a quarkonium. Thus, the next-to-leading order term gives the dissipative effects on the in-medium quarkonium dynamics, so that the detailed balance relation does not hold just up to the leading-order gradient expansion in the recoilless limit. The two cases with and without dissipation differ in

whether or not recoils of a heavy quark are considered in that the momentum operator can change the heavy quark position. Recoils can translate the heavy quarks and contribute more to a localized wave function than to an extended wave function, which we will come back to the phenomenological case with the more realistic setup in Sec. 5.5.

We note that in U(1) case we can ignore the terms stemming from color factors such as t_Q^a and $t_{Q_c}^{a*}$ in the Lindblad operator. In these derivations for both U(1) and SU(N_c) color cases, the center of mass momentum $\vec{P}_{\rm CM}$ is an external parameter given by hand and can depend on time. This explicit dependence in the Lindblad operator (4.46) can provide one of the ways of describing a traversing quarkonium in the quark-gluon plasma medium with the quarkonium small velocity $\vec{P}_{\rm CM}/2M$. As discussed in Appendix B, we find that this effect on the quarkonium relative motion is mild and we then fix $\vec{P}_{\rm CM} = 0$ in all of the following simulations in Sec. 5.4 and Sec. 5.5.

Eq. (4.45) can also be represented in the singlet-octet bases [3]. The resultant Lindblad equation for the density matrix

$$\rho^r_{QQ_c} = \begin{pmatrix} \rho^r_s & 0 \\ 0 & \rho^r_o \end{pmatrix}, \quad \rho^r_o = \sum_i \rho^r_{o^i}. \tag{4.50}$$

with the four different Lindblad operators in the singlet-octet bases and $\vec{P}_{\rm CM} = 0$,

$$\frac{d}{dt}\rho^r_{QQ_c} = -i\left[H_r, \rho^r_{QQ_c}\right] + \sum_{i=1}^{4}\int_k \left[2L^i(\vec{k})\rho^r_{QQ_c}L^{i\dagger}(\vec{k}) - \left\{L^{i\dagger}(\vec{k})L^{a\dagger}(\vec{k})L^i(\vec{k}), \rho^r_{QQ_c}\right\}\right], \tag{4.51}$$

$$H_r = \begin{pmatrix} \frac{p^2}{M} & 0 \\ 0 & \frac{p^2}{M} \end{pmatrix} + \left[V(\vec{r}) - \frac{1}{4MT}\left\{\vec{p}, \vec{\nabla}D(\vec{r})\right\}\right]\begin{pmatrix} C_F & 0 \\ 0 & -\frac{1}{2N_C} \end{pmatrix}, \tag{4.52}$$

$$\begin{aligned} L^1(\vec{k}) &= \frac{1}{\sqrt{2N_c}}\left[A_Q - B_{Q_c} + \frac{N_c}{2}C_{QQ_c}\right]\begin{pmatrix} 0 & 1 \\ 0 & 0 \end{pmatrix}, \\ L^2(\vec{k}) &= \sqrt{C_F}\left[A_Q - B_{Q_c} - \frac{N_c}{2}C_{QQ_c}\right]\begin{pmatrix} 0 & 0 \\ 1 & 0 \end{pmatrix}, \\ L^3(\vec{k}) &= \sqrt{\frac{N_c^2-4}{4N_c}}\left[A_Q - B_{Q_c}\right]\begin{pmatrix} 0 & 0 \\ 0 & 1 \end{pmatrix}, L^4(\vec{k}) = \sqrt{\frac{N_c}{4}}\left[A_Q + B_{Q_c}\right]\begin{pmatrix} 0 & 0 \\ 0 & 1 \end{pmatrix}. \end{aligned} \tag{4.53}$$

In a single heavy quark case, we have seen the detailed balance approximately holds. In a quarkonium case, similarly, the detailed balance is expected to hold. We here consider color singlet-octet transitions caused by $L^1(\vec{k})$ and $L^2(\vec{k})$. In the Lindblad operator (4.53), the terms containing the factors M and $V(r)$ stem from the next-to-leading-order gradient expansion. Though it is difficult to find the analytic solutions of the steady-states, the information of the distribution of the steady-states as a solution of the Lindblad equation may be classically or qualitatively inferred.

In the Lindblad operators, the momentum operator $\vec{p}$ mixes the color singlet and octet states at different spatial points. When we extract only the dynamics in the color spaces, it is an easy approximation to take the static limit of the infinite heavy quark mass. Sup-

[3] We suppose SU(3) color case later in the numerical simulations.

posing that $L^1(\vec{k})$ and $L^2(\vec{k})$ in this limit act on the spatial eigenstate $|\vec{x}\rangle$, we obtain

$$L^1(\vec{k})\,|\vec{x}\rangle = \sqrt{\frac{D(\vec{k})}{2}}\sqrt{\frac{1}{2N_c}}\left[\left(e^{i\vec{k}\cdot\vec{x}/2}-e^{-i\vec{k}\cdot\vec{x}/2}\right)\left\{1-\frac{N_cV(\vec{x})}{8T}\right\}\right]|\vec{x}\rangle\,, \tag{4.54}$$

$$L^2(\vec{k})\,|\vec{x}\rangle = \sqrt{\frac{D(\vec{k})}{2}}\sqrt{C_F}\left[\left(e^{i\vec{k}\cdot\vec{x}/2}-e^{-i\vec{k}\cdot\vec{x}/2}\right)\left\{1+\frac{N_cV(\vec{x})}{8T}\right\}\right]|\vec{x}\rangle\,. \tag{4.55}$$

By sandwiching $\langle\vec{x}|$ in Eqs. (4.54) and (4.55), the ratio of the transition rate between the color singlet and octet states caused by $L^1(\vec{k})$ and $L^2(\vec{k})$ is thus represented by

$$\frac{\Gamma^2_{s\to o}}{\Gamma^1_{o\to s}} \propto \frac{\left[1-\frac{N_cV(\vec{x})}{8T}\right]^2}{\left[1+\frac{N_cV(\vec{x})}{8T}\right]^2}. \tag{4.56}$$

When the energy gap between the singlet and the octet state, the difference of the potential $V_o(\vec{x})-V_s(\vec{x})$ is smaller than the temperature, Eq. (4.56) can be approximated by

$$\frac{\Gamma^2_{s\to o}}{\Gamma^1_{o\to s}} \propto \mathrm{e}^{-\frac{1}{T}[V_o(\vec{x})-V_s(\vec{x})]}, \quad V_s(\vec{x}) \equiv \frac{N_c^2-1}{2N_c}V(\vec{x}), \quad V_o(\vec{x}) \equiv -\frac{1}{2N_c}V(\vec{x}). \tag{4.57}$$

In Eq. (4.57), $V_s(\vec{x})$ and $V_o(\vec{x})$ respectively represent the singlet attractive and octet repulsive potential. Eq. (4.57) implies that the energy difference in a singlet-octet transition appears in the exponent and that the detailed balance in the color space is approximately satisfied in the late time limit. These discussions imply that the leading-order gradient expansion cannot lead the detailed balance form and that including the next-to-leading-order gradient expansion can play a partial role in satisfying the detailed balance relation.

4.2 Comparison to Related Studies

More attention has been paid to the in-medium quarkonium dynamics with the Lindblad master equation in the open quantum systems framework recently. The two major schemes of the non-relativistic QCD (NRQCD) and the potential non-relativistic QCD (pNRQCD) effective theories in Sec. 2.2.1 have been often applied. These effective theories are established with some specific hierarchies of energy scales in the heavy quark system of interest. The essential difference between them is whether or not they are in the dipole limit of quarkonium states and the applicability of pNRQCD is limited in terms of the sizes of quarkonium states. However, as the excited states of a quarkonium have the more spread wave functions than the ground state, the question whether the whole interactions in the quarkonium dynamics in the quark-gluon plasma can be approximated by the dipole interactions or not is not clear.

We in turn mention recent developments in several studies based on either NRQCD or pNRQCD as in Fig. 4.1. Along the first branch in NRQCD scheme, with the help of the Lindblad master equation obtained after tracing out the medium degrees of freedom, the in-medium dynamics of quarkonia has been discussed. Now it is possible to discuss it with quantum dissipative effects by systematically deriving the Lindblad master equation with a set of approximations of time hierarchies. This is also based on the calculations

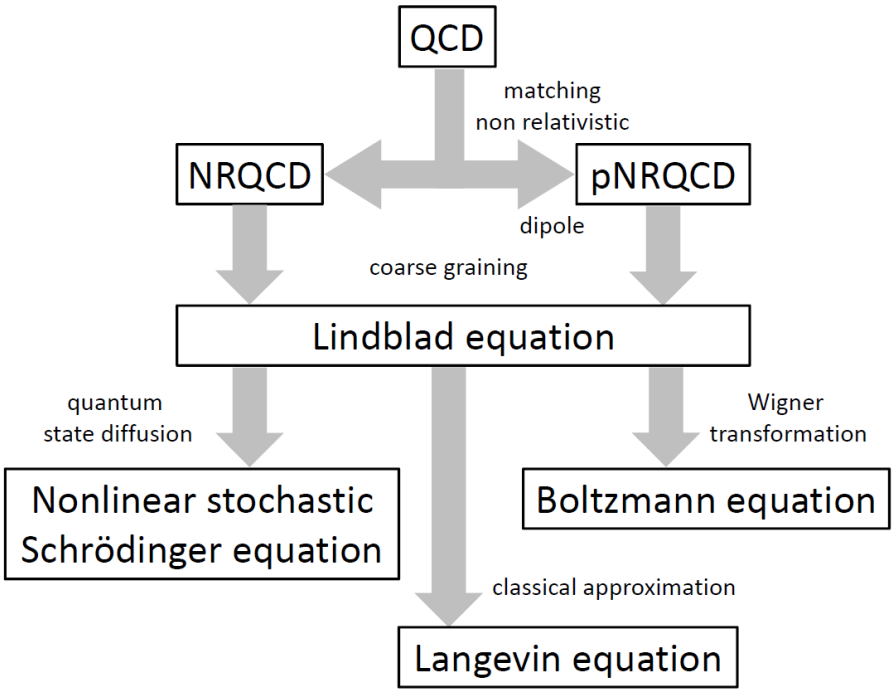

Fig. 4.1: Different approaches based on open quantum systems to in-medium quarkonium dynamics. Our work is via nonlinear stochastic Schrödinger equation, or quantum state diffusion method (Sec. 5).

in the small couplings. The first simulation of quantum dissipation is done in Ref. [89], where the discussion, however, is not complete in that the additional term is needed for quarkonium Lindbladian dynamics. The Lindbladian dynamics can be cast into the nonlinear stochastic Schrödinger equation by quantum state diffusion method[90], which can connect some phenomenological models in this form with a theoretical basis. By taking the classical limit, quarkonium dynamics can be effectively described by generalized Langevin equation with a stochastic force with the degrees of freedom of heavy quark colors, where the drag coefficient depends on the relative distance and the interference inside the heavy quark pair is introduced[71, 72]. In the context of classicalization, it was pointed out that in the single quark case it is questionable whether or not the superposition state is neglected in the time scale of interest even after the decoherence processes to the classical dynamics[91].

In the second branch, that is, pNRQCD scheme, with the help of the time scale separations, for a weakly coupled medium, the Lindblad master equation reduces to the Boltzmann equation of the distribution function of quarkonia after the Wigner transformation[75]. The improvement of this study is discussed in Ref. [83]. Going towards the non-perturbative regime, for a strongly coupled medium, the in-medium quarkonium dynamics is described by the Lindblad master equation with the heavy quark diffusion constant, the transport coefficient. This factor has been now estimated from the chromoelectric field correlator form perturbative lattice QCD results[92, 93].

In the summary of the characteristics of our work[44, 45, 46] among these studies, our analysis focuses on its Lindbladian dynamics affected by both the medium fluctuations and the dissipative effects in addition to the potential screening effect, and expects to deal with more excited quarkonium states.

Chapter 5

Numerical Simulations

In this Chap. 5, we discuss the quarkonium dynamics in the quark-gluon plasma from the Lindblad master equation derived in Sec. 4.1.2. In our study, the quantum dissipation and also the color transitions of quarkonium states are focused on. To discuss and interpret them, we need to numerically solve the Lindblad master equation, which demands a high numerical cost because the density matrix is in a matrix form. With the spatial coordinate discretized into $\mathcal{O}(N_x)$, the cost becomes proportional to $\mathcal{O}(N_x^2)$. We first explain how to reduce the cost via one of the stochastic unraveling methods, which is called the quantum state diffusion in Sec. 5.1. In Sec. 5.2, we next show the equation to be simulated instead of the Lindblad master equation, via the quantum state diffusion method. Then we show the numerical setups in the one-dimensional case in Sec. 5.3 and the numerical results both in U(1) and in SU(3) cases. We take two kinds of the simulation conditions: fixed temperature and time-dependent temperature. In the fixed temperature case, we confirm the equilibration of an in-medium quarkonium and show how the dissipation affects the quarkonium states in Sec. 5.4. In the phenomenological application to quarkonia in heavy ion collisions, we consider the decreasing temperature in time and simulate how different charmonium states and bottomonium states evolve in the presence of the dissipation is Sec. 5.5. From these simulations, we emphasize the dissipative effects on the in-medium quarkonium dynamics.

5.1 Quantum State Diffusion Method

Even though we could directly solve the Lindblad master equation (4.51) to analyze the relative motion of a quarkonium in the quark-gluon plasma, the time cost in the numerical calculations for unraveling its dynamics with the Lindblad master equation is expected to be high. The method of the quantum state diffusion is good for the reduction of the cost time by transforming the deterministic Lindblad master equation for a density matrix to the stochastic equation for a state vector as follows[94]. In this respect, the method of quantum state diffusion is one of the stochastic unravellings.

We here consider the stochastic differential equation in the Ito form

$$|d\psi\rangle \equiv |\psi(t+dt)\rangle - |\psi(t)\rangle = |v\rangle\, dt + \sum_k |f_k\rangle\, d\xi_k \tag{5.1}$$

for the state vector $|\psi\rangle$. With ensemble average over completely infinite set of the wave

functions, the density matrix is defined by

$$\rho = \mathbf{M}\left[|\psi\rangle\langle\psi|\right], \tag{5.2}$$

and it evolves according to the Lindblad master equation

$$\frac{d}{dt}\rho = -i\left[H,\rho\right] + \sum_k \left[2L_k\rho L_k^\dagger - \left\{L_k^\dagger L_k,\rho\right\}\right]. \tag{5.3}$$

$\mathbf{M}\left[\mathcal{O}\right]$ here expresses a mean over a distribution of $\mathcal{O}$, or an expectation value of $\mathcal{O}$.

The terms $|v\rangle\, dt$ and $\sum_k |f_k\rangle\, d\xi_k$ in Eq. (5.1) respectively represent the drift and fluctuation term. The differential stochastic complex fluctuations $d\xi_k$ satisfy

$$\mathbf{M}\left[\mathrm{Re}\left(d\xi_i\right)\mathrm{Re}\left(d\xi_j\right)\right] = \mathbf{M}\left[\mathrm{Im}\left(d\xi_i\right)\mathrm{Im}\left(d\xi_j\right)\right] = \delta_{ij}dt, \tag{5.4}$$

$$\mathbf{M}\left[\mathrm{Re}\left(d\xi_i\right)\mathrm{Im}\left(d\xi_j\right)\right] = 0, \tag{5.5}$$

$$\mathbf{M}\left[\mathrm{d}\xi_i\right] = 0. \tag{5.6}$$

The fluctuations at the different time are independent and Eq. (5.1) represents Markovian property.

To keep the norm of the state vector $|\psi\rangle$, the differential change in the state vector from the fluctuations in the infinitesimal time is orthogonal to the state

$$\langle\psi\,|f_k\rangle = 0. \tag{5.7}$$

Taking the means over $|d\psi\rangle$ and $|d\psi\rangle\langle d\psi|$ leads to

$$\mathbf{M}[|d\psi\rangle] = |v\rangle\, dt, \tag{5.8}$$

$$\mathbf{M}[|d\psi\rangle\langle d\psi|] = 2\sum_k |f_k\rangle\langle f_k|\, dt. \tag{5.9}$$

With these properties above, the change of the density matrix is

$$\mathrm{d}\rho \equiv \rho(t+dt) - \rho(t) = \mathbf{M}\left[|\psi\rangle\langle d\psi| + |d\psi\rangle\langle\psi| + |d\psi\rangle\langle d\psi|\right], \tag{5.10}$$

$$\dot{\rho} = |\psi\rangle\langle v| + |v\rangle\langle\psi| + 2\sum_k |f_k\rangle\langle f_k|. \tag{5.11}$$

By the projection onto the density matrix $\rho_\psi = |\psi\rangle\langle\psi|$ at the initial time, the stochastic terms $|f_k\rangle$ are calculated by the component of $\dot{\rho}$ which is orthogonal to the state $|\psi\rangle$

$$2\sum_k |f_k\rangle\langle f_k| = (\mathrm{I}-\rho_\psi)\dot{\rho}(\mathrm{I}-\rho_\psi). \tag{5.12}$$

It turns clearly with the help of the Lindblad master equation,

$$2\sum_k |f_k\rangle\langle f_k| = (\mathrm{I}-\rho_\psi)\dot{\rho}(\mathrm{I}-\rho_\psi) = \sum_k 2(\mathrm{I}-\rho_\psi)L_k\rho_\psi L_k^\dagger(\mathrm{I}-\rho_\psi) \tag{5.13}$$

$$\equiv \sum_k 2\,|L_{k,\Delta}\psi\rangle\langle L_{k,\Delta}\psi|, \tag{5.14}$$

where $L_{k,\Delta}$ is defibed by $L_{k,\Delta} \equiv L - \langle L\rangle_\psi$ and $\langle\mathcal{O}\rangle_\psi$ represents the expectation value of

$\mathcal{O}$ with respect to the state $|\psi\rangle$. On the other hand, the drift term is given by

$$|v\rangle = \dot{\rho}\,|\psi\rangle - |\psi\rangle\,\langle v|\psi\rangle\,, \tag{5.15}$$

from which

$$\langle v|\psi\rangle = \frac{1}{2}\,\langle\psi|\,\dot{\rho}\,|\psi\rangle + i\eta \tag{5.16}$$

is followed and $\eta \in \mathbb{R}$. Since η is just some non-physical phase change of the state, we can set $\eta = 0$ and thus derive

$$|v\rangle = -iH\,|\psi\rangle + \sum_k \left(2\,\langle L_k^\dagger\rangle_\psi\,L_k - L_k^\dagger L_k - \langle L_k^\dagger\rangle_\psi\,\langle L_k\rangle_\psi\right)|\psi\rangle\,. \tag{5.17}$$

The equation via the quantum state diffusion method, which is in the form of the nonlinear stochastic Schrödinger equation, is finally formulated by

$$\begin{aligned}|d\psi\rangle &\equiv |\psi(t+dt)\rangle - |\psi(t)\rangle \\ &= -iH\,|\psi(t)\rangle\,dt + \sum_k \left(2\,\langle L_k^\dagger\rangle_\psi\,L_k - L_k^\dagger L_k - \langle L_k^\dagger\rangle_\psi\,\langle L_k\rangle_\psi\right)|\psi(t)\rangle\,dt \\ &\quad + \sum_k \left(L_k - \langle L_k\rangle_\psi\right)|\psi(t)\rangle\,d\xi_k.\end{aligned} \tag{5.18}$$

The nonlinearity stems form the expectation values of the Lindblad operator $\langle L_k\rangle_\psi$ and $\langle L_k^\dagger\rangle_\psi$. As is shown above, the ensemble average of the solution of Eq. (5.18) for the wave functions ψ provides the approximate solution for the Lindblad master equation (5.3) for the density matrix. As a remark, the direct solution may be considered more reliable as it does not require any additional approximations which are needed for the stochastic unraveling.

In a practical numerical simulation, the "simplified" nonlinear stochastic Schrödinger equation

$$\begin{aligned}|d\psi\rangle &\equiv |\psi(t+dt)\rangle - |\psi(t)\rangle \\ &= -iH\,|\psi(t)\rangle\,dt + \sum_k \left(2\,\langle L_k^\dagger\rangle_\psi\,L_k - L_k^\dagger L_k\right)|\psi(t)\rangle\,dt + \sum_k L_k\,|\psi(t)\rangle\,d\xi_k\end{aligned} \tag{5.19}$$

was proposed[90]. This is derived by dropping from Eq. (5.18) the scalar terms, $\langle L_k^\dagger\rangle_\psi\,\langle L_k\rangle_\psi\,dt$ and $\langle L_k\rangle_\psi\,d\xi_k$, which are constant with respect to the spatial variable $\vec{x}$ in $\psi(\vec{x})$, since they just contributes the state norm, not the spatial structure of the wave function. This modification to Eq. (5.19), however, does not preserve the norm of the wave function and it is compensated by introducing the density matrix composed of the normalized wave functions for different samplings

$$\rho(t) \equiv \mathrm{M}\left[\frac{|\psi(t)\rangle\,\langle\psi(t)|}{\langle\psi(t)|\psi(t)\rangle}\right]. \tag{5.20}$$

This simplified version has been recently applied for the discussions on the equilibration of a single heavy quark in the quark-gluon plasma[80].

5.2 Nonlinear Stochastic Schrödinger Equation

Let us introduce our simulation prescription by applying the quantum state diffusion method to our case of the relative motion of a quarkonium in the quark-gluon plasma in Eq. (4.45). In SU(3) case, we instead solve Eq. (4.51), which has the quarkonium state vector or wave function with two color components of singlet and octet. The evolution equation for the wave function via the quantum state diffusion method consists of three parts: the effective Hamiltonian term, as well as the additional terms related to the Lindblad operators and the stochastic terms. They represent a stochastic integrodifferential equation, that is, the nonlinear stochastic Schrödinger equation, whose explicit form will be shown in Eq. (5.21) for U(1) case and Eq. (5.33) for SU(3) color case.

5.2.1 U(1) Case

For U(1) case, the nonlinear stochastic Schrödinger equation is

$$\begin{aligned} d\psi(\vec{x}) = \; & dt\Big[i\frac{\vec{\nabla}^2}{M}\psi(\vec{x}) - iV(\vec{x})\psi(\vec{x})\Big] \\ & + \frac{2dt}{\langle\psi|\,\psi\rangle}\Big\{\int d\vec{y}\,\Big(\tilde{G}_1(\vec{x},\vec{y})N(\vec{y})\psi(\vec{x}) + \vec{\tilde{H}}_1(\vec{x},\vec{y})\cdot N(\vec{y})\;\vec{\nabla}_x\psi(\vec{x}) \\ & \qquad + \vec{\tilde{G}}_2(\vec{x},\vec{y})\cdot\vec{J}(\vec{y})\;\psi(\vec{x}) + \tilde{H}_2^{ij}(\vec{x},\vec{y})\,J^j(\vec{y})\,\nabla_x^i\psi(\vec{x})\Big)\Big\} \\ & - dt\Big[\,I_1(\vec{x})\psi(\vec{x}) + \vec{I}_2(\vec{x})\cdot\vec{\nabla}\psi(\vec{x}) + I_3^{ij}(\vec{x})\nabla^i\nabla^j\psi(\vec{x})\Big] \\ & + \Big[\zeta_1\Big(\frac{\vec{x}}{2}\Big)\psi(\vec{x}) - \vec{\zeta}_2\Big(\frac{\vec{x}}{2}\Big)\cdot\vec{\nabla}\psi(\vec{x})\Big]\,, \end{aligned} \tag{5.21}$$

with

$$G_1(\vec{x}) = D(\vec{x}) + \frac{\vec{\nabla}^2}{8MT}D(\vec{x}), \quad \vec{G}_2(\vec{x}) = \vec{\nabla}D(\vec{x}) + \frac{\vec{\nabla}\vec{\nabla}^2}{8MT}D(\vec{x})\,, \tag{5.22}$$

$$\tilde{G}_1(\vec{x},\vec{y}) = G_1\Big(\frac{\vec{x}-\vec{y}}{2}\Big) - G_1\Big(\frac{\vec{x}+\vec{y}}{2}\Big)\,, \tag{5.23}$$

$$\vec{\tilde{G}}_2(\vec{x},\vec{y}) = \frac{1}{4MT}\Big[\vec{G}_2\Big(\frac{\vec{x}-\vec{y}}{2}\Big) + \vec{G}_2\Big(\frac{\vec{x}+\vec{y}}{2}\Big)\Big]\,, \tag{5.24}$$

$$\vec{\tilde{H}}_1(\vec{x},\vec{y}) = \frac{1}{4MT}\Big[[\vec{\nabla}D]\Big(\frac{\vec{x}-\vec{y}}{2}\Big) - [\vec{\nabla}D]\Big(\frac{\vec{x}+\vec{y}}{2}\Big)\Big]\,, \tag{5.25}$$

$$\tilde{H}_2^{ij}(\vec{x},\vec{y}) = \frac{1}{16M^2T^2}\Big[[\nabla^i\nabla^j D]\Big(\frac{\vec{x}-\vec{y}}{2}\Big) + [\nabla^i\nabla^j D]\Big(\frac{\vec{x}+\vec{y}}{2}\Big)\Big]\,, \tag{5.26}$$

$$\begin{aligned} I_1(\vec{x}) = \; & D(\vec{0}) - D(\vec{x}) \\ & + \frac{\vec{\nabla}^2 D(\vec{0})}{4MT} + \frac{(\vec{\nabla}^2)^2 D(\vec{0})}{64M^2T^2} + \frac{(\vec{\nabla}^2)^2 D(\vec{x})}{64M^2T^2} + \frac{\vec{\nabla}^2 D(\vec{x})}{4MT}\,, \end{aligned} \tag{5.27}$$

$$\vec{I}_2(\vec{x}) = \frac{\vec{\nabla}\vec{\nabla}^2 D(\vec{x})}{16M^2T^2} - \frac{\vec{\nabla}D(\vec{x})}{2MT}\,, \quad I_3^{ij}(\vec{x}) = \frac{\nabla^i\nabla^j D(\vec{0})}{16M^2T^2} + \frac{\nabla^i\nabla^j D(\vec{x})}{16M^2T^2}\,, \tag{5.28}$$

$$N(\vec{x}) = \psi^\dagger(\vec{x})\psi(\vec{x})\,, \quad \vec{J}(\vec{x}) = \psi^\dagger(\vec{x})\vec{\nabla}\psi(\vec{x})\,, \tag{5.29}$$

$$\zeta_1(\vec{x}) = d\xi(\vec{x}) - d\xi(-\vec{x}) + \frac{\vec{\nabla}^2 d\xi(\vec{x})}{2MT} - \frac{\vec{\nabla}^2 d\xi(-\vec{x})}{2MT}\,, \tag{5.30}$$

$$\vec{\zeta}_2(\vec{x}) = \frac{\vec{\nabla} d\xi(\vec{x})}{2MT} - \frac{\vec{\nabla} d\xi(-\vec{x})}{2MT}\,. \tag{5.31}$$

5.2.2 SU(3) Color Case

For SU(3) color case, the nonlinear stochastic Schrödinger equation for the colored state with two components

$$|\psi\rangle_k = \begin{pmatrix} |\psi_s\rangle \\ |\psi_o\rangle \end{pmatrix}_k \tag{5.32}$$

in color singlet octet bases is

$$\begin{aligned}
&d\psi(\vec{x})_k \\
&= dt \begin{pmatrix} i\frac{\vec{\nabla}^2}{M}\psi_s(\vec{x}) + C_F\left[-iV(\vec{x})\psi_s(\vec{x}) + \frac{\vec{\nabla}D(\vec{x})}{2MT}\vec{\nabla}\psi_s(\vec{x}) + \frac{\vec{\nabla}^2 D(\vec{x})}{4MT}\psi_s(\vec{x})\right] \\ i\frac{\vec{\nabla}^2}{M}\psi_o(\vec{x}) - \frac{1}{2N_c}\left[-iV(\vec{x})\psi_o(\vec{x}) + \frac{\vec{\nabla}D(\vec{x})}{2MT}\vec{\nabla}\psi_o(\vec{x}) + \frac{\vec{\nabla}^2 D(\vec{x})}{4MT}\psi_o(\vec{x})\right] \end{pmatrix}_k \\
&+ \frac{2dt}{\langle\psi|\,\psi\rangle}\frac{1}{2N_c}\int dy\Big[\tilde{G}_1^1(\vec{x},\vec{y})\Big]N_1(\vec{y})\tilde{\psi}_1(\vec{x})_k \\
&\qquad + \Big[\vec{\tilde{H}}_1^1(\vec{x},\vec{y})\Big]N_1(\vec{y})\cdot\vec{\nabla}\psi_1(\vec{x})_k \\
&\qquad + \Big[\vec{\tilde{G}}_2^1(\vec{x},\vec{y})\Big]\cdot\vec{J}_1(\vec{y})\psi_1(\vec{x})_k + \Big[\tilde{H}_2^{1,ij}(\vec{x},\vec{y})\Big]J_1^j(\vec{y})\cdot\vec{\nabla}\psi_1(\vec{x})_k \\
&\qquad + \Big[N_c\frac{V(x)}{4T}K_S^1(\vec{x},\vec{y}) + N_c\frac{V(y)}{4T}\Big(1+\frac{\nabla^2}{8MT}\Big)K_S^1(\vec{x},\vec{y}) \\
&\qquad\qquad + \frac{N_c^2}{4}\frac{V(x)V(y)}{4T^2}K_S^1(\vec{x},\vec{y})\Big]N_1(\vec{y})\psi_1(\vec{x})_k \\
&\qquad + \Big[N_c\frac{V(y)}{4T}\frac{\vec{\nabla}}{4MT}K_S^1(\vec{x},\vec{y})\Big]N_1(\vec{y})\cdot\vec{\nabla}\psi_1(\vec{x})_k \\
&\qquad + \Big[N_c\frac{V(x)}{4T}\vec{K}_S^2(\vec{x},\vec{y})\Big]\cdot\vec{J}_1(\vec{y})\psi_1(\vec{x})_k \\
&+ \frac{2dt}{\langle\psi|\,\psi\rangle}C_F\int dy\Big[\tilde{G}_1^2(\vec{x},\vec{y})\Big]N_2(\vec{y})\psi_2(\vec{x})_k + \Big[\vec{\tilde{H}}_1^2(\vec{x},\vec{y})\Big]N_2(\vec{y})\cdot\vec{\nabla}\psi_2(\vec{x})_k \\
&\qquad + \Big[\vec{\tilde{G}}_2^2(\vec{x},\vec{y})\Big]\cdot\vec{J}_2(\vec{y})\psi_2(\vec{x})_k + \Big[\tilde{H}_2^{2,ij}(\vec{x},\vec{y})\Big]J_2^j(\vec{y})\nabla^i\psi_2(\vec{x})_k \\
&\qquad - \Big[N_c\frac{V(x)}{4T}K_S^1(\vec{x},\vec{y}) + N_c\frac{V(y)}{4T}\Big(1+\frac{\nabla^2}{8MT}\Big)K_S^1(\vec{x},\vec{y}) \\
&\qquad\qquad - \frac{N_c^2}{4}\frac{V(x)V(y)}{4T^2}K_S^1(\vec{x},\vec{y})\Big]N_2(\vec{y})\psi_2(\vec{x})_k \\
&\qquad - \Big[N_c\frac{V(y)}{4T}\frac{\vec{\nabla}}{4MT}K_S^1(\vec{x},\vec{y})\Big]N_2(\vec{y})\cdot\vec{\nabla}\psi_2(\vec{x})_k \\
&\qquad - \Big[N_c\frac{V(x)}{4T}\vec{K}_S^2(\vec{x},\vec{y})\Big]\cdot\vec{J}_2(\vec{y})\psi_2(\vec{x})_k \\
&+ \frac{2dt}{\langle\psi|\,\psi\rangle}\frac{N_c^2-4}{4N_c}\int dy\Big[\tilde{G}_1^3(\vec{x},\vec{y})\Big]N_3(\vec{y})\psi_3(\vec{x})_k + \Big[\vec{\tilde{H}}_1^3(\vec{x},\vec{y})\Big]N_3(\vec{y})\cdot\vec{\nabla}\psi_3(\vec{x})_k \\
&\qquad + \Big[\vec{\tilde{G}}_2^3(\vec{x},\vec{y})\Big]\cdot\vec{J}_3(\vec{y})\psi_3(\vec{x})_k + \Big[\tilde{H}_2^{3,ij}(\vec{x},\vec{y})\Big]J_3^j(\vec{y})\nabla^i\psi_3(\vec{x})_k
\end{aligned}$$

$$
\begin{aligned}
&+\frac{2dt}{\langle\psi|\,\psi\rangle}\frac{N_c}{4}\int dy\Big[\tilde{G}_1^4(\vec{x},\vec{y})\Big]N_4(\vec{y})\psi_4(\vec{x})_k+\Big[\vec{\tilde{H}}_1^4(\vec{x},\vec{y})\Big]N_4(\vec{y})\cdot\vec{\nabla}\psi_4(\vec{x})_k\\
&\qquad\qquad+\Big[\vec{\tilde{G}}_2^4(\vec{x},\vec{y})\Big]\vec{J}_4(\vec{y})\psi_4(\vec{x})_k+\Big[\tilde{H}_2^{4,ij}(\vec{x},\vec{y})\Big]J_4^j(\vec{y})\cdot\vec{\nabla}\psi_4(\vec{x})_k\\
&-\frac{dt}{\langle\psi|\,\psi\rangle}\frac{1}{2N_c}\Big[I_1(\vec{x})+\vec{I}_2(\vec{x})\cdot\vec{\nabla}+I_3^{ij}(\vec{x})\nabla^i\nabla^j\\
&\qquad\qquad+\frac{N_c}{2}\frac{V(\vec{x})}{2T}L_1(\vec{x})+\frac{N_c}{2}\frac{\nabla^iV(\vec{x})}{2T}L_2^i(\vec{x})+\frac{N_c^2}{4}\frac{V(\vec{x})^2}{4T^2}L_3(\vec{x})\Big]\check{\psi}_1(\vec{x})_k\\
&-\frac{dt}{\langle\psi|\,\psi\rangle}C_F\Big[I_1(\vec{x})+\vec{I}_2(\vec{x})\cdot\vec{\nabla}+I_3^{ij}(\vec{x})\nabla^i\nabla^j\\
&\qquad\qquad-\frac{N_c}{2}\frac{V(r)}{2T}L_1(\vec{x})-\frac{N_c}{2}\frac{\nabla^iV(\vec{x})}{2T}L_2^i(\vec{x})+\frac{N_c^2}{4}\frac{V(x)^2}{4T^2}L_3(\vec{x})\Big]\check{\psi}_2(\vec{x})_k\\
&-\frac{dt}{\langle\psi|\,\psi\rangle}\frac{N_c^2-4}{4N_c}\Big[I_1(\vec{x})+\vec{I}_2(\vec{x})\cdot\vec{\nabla}+I_3^{ij}(\vec{x})\nabla^i\nabla^j\Big]\check{\psi}_3(\vec{x})_k\\
&-\frac{dt}{\langle\psi|\,\psi\rangle}\frac{N_c}{4}\Big[I_1^4(\vec{x})+\vec{I}_2^4(\vec{x})\cdot\vec{\nabla}+I_3^{4,ij}(\vec{x})\nabla^i\nabla^j\Big]\check{\psi}_4(\vec{x})_k\\
&+\frac{1}{\sqrt{2N_c}}\Big[\Big(1+\frac{\vec{\nabla}^2}{2MT}\Big)\zeta_1^1\Big(\frac{\vec{x}}{2}\Big)+\vec{\zeta}_2^1\Big(\frac{\vec{x}}{2}\Big)\cdot\vec{\nabla}+\frac{N_c}{2}\frac{S(x)}{2T}\zeta_1^1\Big(\frac{\vec{x}}{2}\Big)\Big]\tilde{\psi}_1(\vec{x})_k\\
&+\sqrt{C_F}\Big[\Big(1+\frac{\vec{\nabla}^2}{2MT}\Big)\zeta_1^2\Big(\frac{\vec{x}}{2}\Big)+\vec{\zeta}_2^2\Big(\frac{\vec{x}}{2}\Big)\cdot\vec{\nabla}-\frac{N_c}{2}\frac{S(x)}{2T}\zeta_1^2\Big(\frac{\vec{x}}{2}\Big)\Big]\tilde{\psi}_2(\vec{x})_k\\
&+\sqrt{\frac{N_c^2-4}{4N_c}}\Big[\Big(1+\frac{\vec{\nabla}^2}{2MT}\Big)\zeta_1^3\Big(\frac{\vec{x}}{2}\Big)+\vec{\zeta}_2^3\Big(\frac{\vec{x}}{2}\Big)\cdot\vec{\nabla}\Big]\tilde{\psi}_3(\vec{x})_k\\
&+\sqrt{\frac{N_c}{4}}\Big[\Big(1+\frac{\vec{\nabla}^2}{2MT}\Big)\zeta_1^4\Big(\frac{\vec{x}}{2}\Big)+\vec{\zeta}_2^4\Big(\frac{\vec{x}}{2}\Big)\cdot\vec{\nabla}\Big]\tilde{\psi}_4(\vec{x})_k\,,
\end{aligned}
\tag{5.33}
$$

with

$$G_1(\vec{x})=D(\vec{x})+\frac{\vec{\nabla}^2}{8MT}D(\vec{x}),\quad \vec{G}_2(\vec{x})=\vec{\nabla}D(\vec{x})+\frac{\vec{\nabla}\vec{\nabla}^2}{8MT}D(\vec{x}),\tag{5.34}$$

$$\tilde{G}_1^1(\vec{x},\vec{y})=\tilde{G}_1^2(\vec{x},\vec{y})=\tilde{G}_1^3(\vec{x},\vec{y})=G_1\Big(\frac{\vec{x}-\vec{y}}{2}\Big)-G_1\Big(\frac{\vec{x}+\vec{y}}{2}\Big)\,,\tag{5.35}$$

$$\tilde{G}_1^4(\vec{x},\vec{y})=G_1\Big(\frac{\vec{x}-\vec{y}}{2}\Big)+G_1\Big(\frac{\vec{x}+\vec{y}}{2}\Big)\,,\tag{5.36}$$

$$\vec{\tilde{G}}_2^1(\vec{x},\vec{y})=\vec{\tilde{G}}_2^2(\vec{x},\vec{y})=\vec{\tilde{G}}_2^3(\vec{x},\vec{y})=\frac{1}{4MT}\Big[\vec{G}_2\Big(\frac{\vec{x}-\vec{y}}{2}\Big)+\vec{G}_2\Big(\frac{\vec{x}+\vec{y}}{2}\Big)\Big]\,,\tag{5.37}$$

$$\vec{\tilde{G}}_2^4(\vec{x},\vec{y})=\frac{1}{4MT}\Big[\vec{G}_2\Big(\frac{\vec{x}-\vec{y}}{2}\Big)-\vec{G}_2\Big(\frac{\vec{x}+\vec{y}}{2}\Big)\Big]\,,\tag{5.38}$$

$$
\begin{aligned}
\vec{\tilde{H}}_1^1(\vec{x},\vec{y})&=\vec{\tilde{H}}_1^2(\vec{x},\vec{y})=\vec{\tilde{H}}_1^3(\vec{x},\vec{y})\\
&=\frac{1}{4MT}\Big[[\vec{\nabla}D]\Big(\frac{\vec{x}-\vec{y}}{2}\Big)-[\vec{\nabla}D]\Big(\frac{\vec{x}+\vec{y}}{2}\Big)\Big]\,,
\end{aligned}
\tag{5.39}
$$

$$\vec{\tilde{H}}_1^4(\vec{x},\vec{y})=\frac{1}{4MT}\Big[[\vec{\nabla}D]\Big(\frac{\vec{x}-\vec{y}}{2}\Big)+[\vec{\nabla}D]\Big(\frac{\vec{x}+\vec{y}}{2}\Big)\Big]\,,\tag{5.40}$$

$$
\begin{aligned}
\tilde{H}_2^{1,ij}(\vec{x},\vec{y})&=\tilde{H}_2^{2,ij}(\vec{x},\vec{y})=\tilde{H}_2^{3,ij}(\vec{x},\vec{y})\\
&=\frac{1}{16M^2T^2}\Big[[\nabla^i\nabla^jD]\Big(\frac{\vec{x}-\vec{y}}{2}\Big)+[\nabla^i\nabla^jD]\Big(\frac{\vec{x}+\vec{y}}{2}\Big)\Big]\,,
\end{aligned}
\tag{5.41}
$$

$$\tilde{H}_2^{4,ij}(\vec{x},\vec{y}) = \frac{1}{16M^2T^2}\Big[[\nabla^i\nabla^j D]\Big(\frac{\vec{x}-\vec{y}}{2}\Big) - [\nabla^i\nabla^j D]\Big(\frac{\vec{x}+\vec{y}}{2}\Big)\Big]\,, \tag{5.42}$$

$$\begin{aligned} I_1^1(\vec{x}) &= I_1^2(\vec{x}) = I_1^3(\vec{x}) \\ &= D(\vec{0}) - D(\vec{x}) + \frac{\vec{\nabla}^2 D(\vec{0})}{4MT} + \frac{(\vec{\nabla}^2)^2 D(\vec{0})}{64M^2T^2} + \frac{(\vec{\nabla}^2)^2 D(\vec{x})}{64M^2T^2}\,, \end{aligned} \tag{5.43}$$

$$I_1^4(\vec{x}) = D(\vec{0}) + D(\vec{x}) + \frac{\vec{\nabla}^2 D(\vec{0})}{4MT} + \frac{(\vec{\nabla}^2)^2 D(\vec{0})}{64M^2T^2} - \frac{(\vec{\nabla}^2)^2 D(\vec{x})}{64M^2T^2}\,, \tag{5.44}$$

$$\vec{I}_2^1(\vec{x}) = \vec{I}_2^2(\vec{x}) = \vec{I}_2^3(\vec{x}) = \frac{\vec{\nabla}\vec{\nabla}^2 D(\vec{x})}{16M^2T^2}, \quad \vec{I}_2^4(\vec{x}) = -\frac{\vec{\nabla}\vec{\nabla}^2 D(\vec{x})}{16M^2T^2}\,, \tag{5.45}$$

$$I_3^{1,ij}(\vec{x}) = I_3^{2,ij}(\vec{x}) = I_3^{3,ij}(\vec{x}) = \frac{\nabla^i\nabla^j D(\vec{0})}{16M^2T^2} + \frac{\nabla^i\nabla^j D(\vec{x})}{16M^2T^2}\,, \tag{5.46}$$

$$I_3^{4,ij}(\vec{x}) = \frac{\nabla^i\nabla^j D(\vec{0})}{16M^2T^2} - \frac{\nabla^i\nabla^j D(\vec{x})}{16M^2T^2}\,, \tag{5.47}$$

$$\psi_1(\vec{x}) = \begin{pmatrix} 0 & 1 \\ 0 & 0 \end{pmatrix}\psi(\vec{x}), \quad \psi_2(\vec{x}) = \begin{pmatrix} 0 & 0 \\ 1 & 0 \end{pmatrix}\psi(\vec{x}), \tag{5.48}$$

$$\psi_3(\vec{x}) = \psi_4(\vec{x}) = \begin{pmatrix} 0 & 0 \\ 0 & 1 \end{pmatrix}\psi(\vec{x}), \tag{5.49}$$

$$\check{\psi}_1(\vec{x}) = \begin{pmatrix} 0 & 0 \\ 0 & 1 \end{pmatrix}\psi(\vec{x}), \quad \check{\psi}_2(\vec{x}) = \begin{pmatrix} 1 & 0 \\ 0 & 0 \end{pmatrix}\psi(\vec{x}), \tag{5.50}$$

$$\check{\psi}_3(\vec{x}) = \check{\psi}_4(\vec{x}) = \begin{pmatrix} 0 & 0 \\ 0 & 1 \end{pmatrix}\psi(\vec{x}), \tag{5.51}$$

$$\tilde{\psi}_1(\vec{x}) = \begin{pmatrix} 0 & 0 \\ 1 & 0 \end{pmatrix}\psi(\vec{x}), \quad \tilde{\psi}_2(\vec{x}) = \begin{pmatrix} 0 & 1 \\ 0 & 0 \end{pmatrix}\psi(\vec{x}), \tag{5.52}$$

$$\tilde{\psi}_3(\vec{x}) = \tilde{\psi}_4(\vec{x}) = \begin{pmatrix} 0 & 0 \\ 0 & 1 \end{pmatrix}\psi(\vec{x}), \tag{5.53}$$

$$N_1(\vec{x}) = \psi^\dagger(\vec{x})\tilde{\psi}_1(\vec{x}), \quad \vec{J}_1(\vec{x}) = \psi^\dagger(\vec{x})\vec{\nabla}_x\tilde{\psi}_1(\vec{x}), \tag{5.54}$$

$$N_2(\vec{x}) = \psi^\dagger(y)\tilde{\psi}_2(\vec{x}), \quad \vec{J}_2(\vec{x}) = \psi^\dagger(\vec{x})\vec{\nabla}_x\tilde{\psi}_1(\vec{x}), \tag{5.55}$$

$$N_3(\vec{x}) = N_4(\vec{x}) = \psi^\dagger(y)\tilde{\psi}_3(\vec{x}), \quad \vec{J}_3(\vec{x}) = \vec{J}_4(\vec{x}) = \psi^\dagger(\vec{x})\vec{\nabla}_x\tilde{\psi}_3(\vec{x}), \tag{5.56}$$

$$K_S^1(\vec{x},\vec{y}) = D\Big(\frac{\vec{x}-\vec{y}}{2}\Big) - D\Big(\frac{\vec{x}+\vec{y}}{2}\Big)\,, \tag{5.57}$$

$$\vec{K}_S^2(\vec{x},\vec{y}) = \frac{1}{4MT}\Big[[\vec{\nabla}D]\Big(\frac{\vec{x}-\vec{y}}{2}\Big) + [\vec{\nabla}D]\Big(\frac{\vec{x}-\vec{y}}{2}\Big)\Big]\,, \tag{5.58}$$

$$L_1(\vec{x}) = 2D(\vec{0}) - 2D(\vec{x}) + \frac{\vec{\nabla}^2 D(\vec{0})}{4MT}, \quad \vec{L}_2(\vec{x}) = \frac{\vec{\nabla}D(\vec{x})}{4MT}, \tag{5.59}$$

$$L_3(\vec{x}) = D(\vec{0}) - D(\vec{x})\,, \tag{5.60}$$

$$\zeta_1^1(\vec{x}) = \zeta_1^2(\vec{x}) = \zeta_1^3(\vec{x}) = d\xi(\vec{x}) - d\xi(-\vec{x}), \quad \zeta_1^4(\vec{x}) = d\xi(\vec{x}) + d\xi(-\vec{x})\,, \tag{5.61}$$

$$\vec{\zeta}_2^1(\vec{x}) = \vec{\zeta}_2^2(\vec{x}) = \vec{\zeta}_2^3(\vec{x}) = \frac{\vec{\nabla}d\xi(\vec{x})}{2MT} - \frac{\vec{\nabla}d\xi(-\vec{x})}{2MT}, \tag{5.62}$$

$$\vec{\zeta}_2^4(\vec{x}) = \frac{\vec{\nabla}d\xi(\vec{x})}{2MT} + \frac{\vec{\nabla}d\xi(-\vec{x})}{2MT}\,. \tag{5.63}$$

5.3 Simulation Setups

We perform numerical simulations for the relative motion of an in-medium quarkonium with the fixed center of mass momentum $P_{\mathrm{CM}} = 0$ via the quantum state diffusion method, ignoring the heavy quark colors for U(1) case while including them for SU(3) case. We numerically solve the Hamiltonian term via the 4th-order Runge-Kutta method and the Lindblad terms via a simple forward Euler time step. We introduce the singlet potential with C_F,[1]

$$V_{\mathrm{Debye}}(x) = C_F V(x) = -\frac{C_F\alpha}{\sqrt{x^2 + {x_{\mathrm{c}}}^2}}\mathrm{e}^{-m_{\mathrm{D}}|x|}. \tag{5.64}$$

as the regularized Debye screening potential with the cutoff parameter x_{c} at the origin in the denominator, which behaves as $\propto -\frac{1}{|x|}$ near the origin and exhibits screening effect in the long distance. This is motivated by the phenomenological implications to the three dimensional case, since we do not consider to solve the rigorous one dimensional case, in which the potential is linear in the relative distance. We chose the cutoff length as the inverse of a heavy quark mass, which is needed because the non relativistic description $|p| < M$ breaks down at this scale[95]. We here also approximate the correlation function

$$D(x) = \gamma \exp\left(-\frac{x^2}{l_{\mathrm{corr}}^2}\right) \tag{5.65}$$

and then noise correlation function $M[d\xi(x)d\xi(y)^*]$ is accordingly $M[d\xi(x)d\xi(y)^*] = D(x-y)dt$, while other noise correlation functions are zero. The parametrization for these functions is chosen in the following, referring to Eqs. (A.7) and (A.8) and also the references[69, 80, 88],

$$C_F\alpha = 0.3, \quad m_{\mathrm{D}} = 2l_{\mathrm{corr}}^{-1} = 2T, \quad \gamma = \frac{T}{\pi}, \tag{5.66}$$

which does not break the scale hierarchy assumptions. The setting $m_{\mathrm{D}} = 2/\ell_{\mathrm{corr}}$ in Eq. (5.66) is estimated by equating the full width half maximum of $D(r)$ in Eq. (A.7) and that in Eq. (5.65).

By numerically solving the nonlinear stochastic Schrödinger equation for the relative motion of an in-medium quarkonium in the quark-gluon plasma in U(1) and SU(3) color cases with these settings, we analyze and discuss the full dissipative dynamics. We note that the simulation by the stochastic potential model is equivalent to that by the stochastic evolution obtained after discarding all terms stemming from the next-to-leading gradient expansions in the quantum state diffusion equation, even though the former is linear while the latter is nonlinear in the quarkonium wave function. The discarded terms are negligible in the $T/M \to 0$ limit except for the kinetic energy. To show how the dissipation influences the evolution of quarkonium states, we compare to the simulations in the stochastic potential model without the dissipative effects[69, 88], which is the motivation of our work.

In the simulations in the following section, the temperature of the quark-gluon plasma is chosen to be the fixed temperature $T/M = 0.1$ or 0.3 in Sec. 5.4 and $T(t) = T_0 \cdot [t_0/(t_0+t)]^{1/3}$ with $t_0 = 0.84$ fm and $T_0 = 0.47$ GeV for the case of the Bjorken expand-

[1] We interpret $C_F = 1$ and $C_F\alpha = \alpha$ for U(1) case while $C_F = \frac{N_c^2-1}{2N_c}$ for SU(N_c) case.

ing quark-gluon plasma in Sec. 5.5. In these simulations, the center of mass momentum of a quarkonium is set to $P_{\rm CM} = 0$ as the dependence of the quarkonium dynamics on the center of mass momentum is found to be small, which is shown in Appendix B. In the numerical simulations of the quarkonium dynamics, we have to discretize the space and time by $\Delta x = 1/M$ and $\Delta t = 0.1M(\Delta x)^2$. We set the spatial discretization Δx much finer than the typical medium length scales $m_{\rm D}^{-1} \sim l_{\rm corr}/2 \sim 1/2T$. We also take the volume of the system $L = N_x \Delta x$ much larger than such medium length scales. Then, these parameters and numerical setups are summarized in Table 5.1.

Table 5.1: Numerical setups, the parametrization of the potential $V(x)$ and the correlations $D(x)$, and the center-of-mass momentum.

Δx	Δt	N_x	γ	$l_{\rm corr}$	$C_F\alpha$	$m_{\rm D}$	$x_{\rm c}$	$P_{\rm CM}$
$1/M$	$0.1M(\Delta x)^2$	254	T/π	$1/T$	0.3	$2T$	$1/M$	0

Finally, let us remark on the boundary conditions used for the wave function $\psi(x)$ and the noise field $d\xi(x)$. In the simulations with a finite volume $[-L/2, L/2]$ for both U(1) and SU(3) cases, we impose the periodic boundary conditions on the wave function $\psi(x)$,

$$\psi\left(\frac{L}{2}, t\right) = \psi\left(-\frac{L}{2}, t\right). \tag{5.67}$$

Then we are careful to the boundary condition for the noise field appearing in the stochastic evolution in the quantum state diffusion approach. Considering the wave function evolution only due to the noise field $d\xi(x)$ at the boundary $x = L/2$. The stochastic evolution in $\psi\left(\frac{L}{2}, t+dt\right) - \psi\left(\frac{L}{2}, t\right)$ is typically

$$\left[d\xi\left(\frac{L}{4}\right) \pm d\xi\left(-\frac{L}{4}\right)\right]\psi\left(\frac{L}{2}\right). \tag{5.68}$$

On the other hand, at the boundary $x = -L/2$, the wave function evolution only due to the noise field is

$$\left[d\xi\left(-\frac{L}{4}\right) \pm d\xi\left(\frac{L}{4}\right)\right]\psi\left(-\frac{L}{2}\right). \tag{5.69}$$

The boundary condition on wave function (5.67) requires the boundary condition for the noise field

$$d\xi\left(-\frac{L}{4}\right) = d\xi\left(\frac{L}{4}\right), \tag{5.70}$$

which means that the noise field $d\xi(x)$ obeys a periodicity of $L/2$. Thus we take the volume size to be doubled, comparing to the previous study of a single heavy quark in quark gluon plasma[80] as in Table 5.1. Thus we take the volume size to be doubled, comparing to the previous study of a single heavy quark in quark gluon plasma[80] as in Table 5.1. Correspondingly, as in [80], the correlation function $D(r)$ for the noise field

$d\xi(x)$ for $x, y \in [-L/4, L/4]$ should be interpreted as $D(r_{xy})$ with

$$\mathrm{M}[d\xi(x)d\xi^*(y)] = D(r_{xy})dt, \quad r_{xy} \equiv \min\left\{|x-y|, \frac{L}{2} - |x-y|\right\}, \tag{5.71}$$

which is all that is needed for solving the quantum state diffusion equation.

5.4 Simulations at Fixed Temperature

5.4.1 U(1) case

Here consider U(1) case in this Sec. 5.4.1. Through the simulations of Eq. (5.21) or Eq. (4.45), we study how quantum dissipation affect the dynamical evolution of quarkonium relative motion by neglecting the dissipative parts form the full dissipative dynamics. We can also simulate the effects of the center of mass motion of a quarkonium on its dynamical evolution of the relative motion, which are, however, found to be mild and shown in Appendix B.

We first show how the quantum dissipation influences the dynamics of the relative motion. From our numerical results, we confirm that the quarkonium system approaches a steady-state at late times due to the quantum dissipation. The steady-state is found to be independent of the initial conditions with which the numerical simulations are performed. Furthermore, we also find that the distribution of the steady-states appearing at late times is close to the Boltzmann distribution, in which the temperature is at least within 10% of the simulation input of the temperature of the thermal quark-gluon plasma medium by the fitting. Therefore, the quarkonium system appears to approach the genuine thermal equilibrium state at late times, which is assisted by the interplay of both quantum fluctuations and dissipation.

We next show how the dynamical evolution depends on the temperature and the heavy quark mass by comparing with simulations of the two temperature cases $T/M = 0.1$ and $T/M = 0.3$. By rescaling the evolution time t by the heavy quark relaxation time τ_{eq}, we find that a similar relaxation behavior shows up in both of the cases.

Equilibration with Quantum Dissipation

We first prepare either the ground state or the first excited state of the Hamiltonian

$$H_{\mathrm{Debye}} = \frac{p^2}{M} - \frac{\alpha}{\sqrt{x^2 + x_{\mathrm{c}}^2}} \mathrm{e}^{-m_{\mathrm{D}}|x|} \tag{5.72}$$

as the two initial conditions of the simulations. We note that this Hamiltonian H_{Debye} is different from the effective Hamiltonian H_{eff} in the Lindblad master equation (4.45) for U(1) case. With these two initial conditions, we simulate the dynamics and calculate the occupation numbers of the ground state and the excited states in the two temperature setups $T/M = 0.1$ and $T/M = 0.3$.

In Fig. 5.1, we plot the occupation numbers $N_i(Mt)$ of the i-th eigenstates for the ground state ($i = 0$), the first excited state ($i = 1$) of the Hamiltonian H_{Debye} as a function of (nondimensional) time Mt. The occupation numbers of the ground state and the first excited state are respectively represented by the red and blue lines. The difference

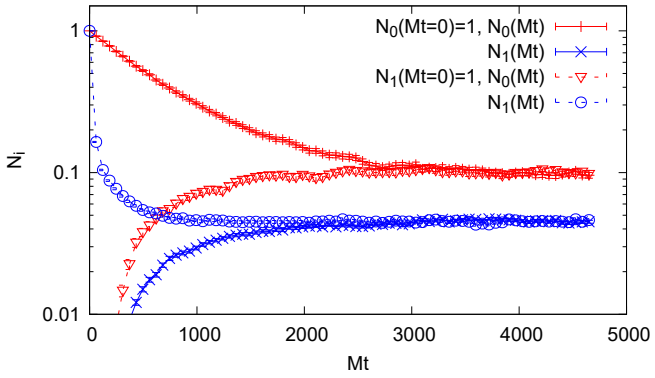

Fig. 5.1: Time evolution of the occupation numbers of the ground state N_0 (red line), the first excited state N_1 (blue line) with respect to (nondimensional) time Mt. The system reaches a steady-state at late times, which is independent of the initial conditions. Error bars represent the statistical errors within the ensemble average.

between the *solid* lines and the *dashed* lines is their initial conditions. Specifically, for the *solid* lines, the initial condition is the ground state while for the *dashed* lines, it is the first excited state. From these results, we find that as (nondimensional) time Mt increases, each of the occupation numbers respectively takes some constant value which is irrespective of the initial condition within the statistical error bars. This behavior of the time evolution of the occupation numbers tells that the dynamics of quarkonium relative motion relaxes and becomes equilibrated in the thermal quark-gluon plasma with the dissipative effects. If we calculate the partition function Z with the Hamiltonian $H_{\rm Debye}$ and the (nondimensional) eigenenergy E_i/M, then $\mathrm{e}^{-E_0/T}/Z \simeq 0.107$ and $\mathrm{e}^{-E_1/T}/Z \simeq 0.040$. These are almost within the 10% level to the values $N_0^{eq} \simeq 0.096 \pm 0.005$ and $N_1^{eq} \simeq 0.044 \pm 0.001$ at $Mt = 4650$ in the simulations in Fig. 5.1.

We in turn plot in Fig. 5.2, as a function of the (nondimensional) eigenenergy E_i/M of the Hamiltonian $H_{\rm Debye}$, the occupation numbers of the lowest twenty one levels at $Mt = 4650$ for $T/M = 0.1$, which is well within the steady state regime. By fitting

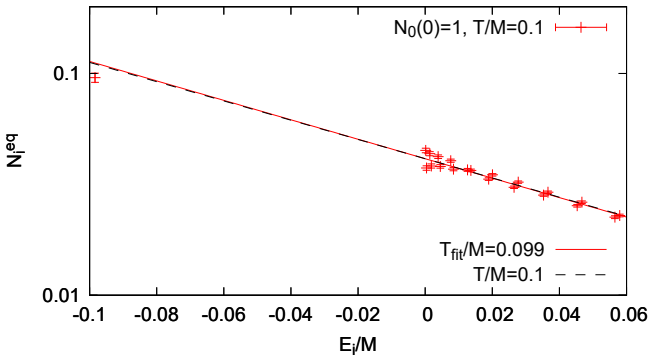

Fig. 5.2: Steady state distributions of the eigenstates in $-0.10 \leq E_i/M \leq 0.06$ at $Mt = 4650$ for $T/M = 0.1$. The data is fitted by the Boltzmann distribution $\propto \exp[-E_i/T_{\rm fit}]$ for levels with the relative velocity less than 0.5 (lowest twenty-one levels). The fitted temperatures are $T_{\rm fit}/M = 0.099 \pm 0.004$.

the data with the Boltzmann distribution $\propto \exp(-E_i/T_{\rm fit})$, the fitted temperature $T_{\rm fit}$ reads $T_{\rm fit}/M = 0.099 \pm 0.004$, which is approximately the same as the setup temperature $T/M = 0.1$. We limit the fitting range to the eigenstates ϕ_i with the velocity $\frac{\sqrt{\langle p^2 \rangle_{\phi_i}}}{M/2} < 0.5$, which leads to the fitting of the lowest twenty-one levels. We expect the deviation of the ground state from the fitting line to come from its binding energy which is near the boundary of the applicability $\tau_E \ll \tau_S$. We also show the results for the same analysis with $T/M = 0.3$ at time $Mt = 900$ in Fig. 5.3. The fitting range corresponds to the

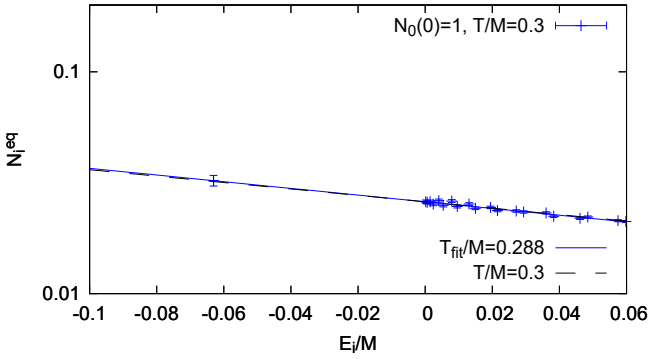

Fig. 5.3: Steady state distributions of the eigenstates in $-0.10 \leq E_i/M \leq 0.06$ at $Mt = 900$ for $T/M = 0.3$. The data is fitted by the Boltzmann distribution $\propto \exp[-E_i/T_{\rm fit}]$ for levels with the relative velocity less than 0.5 (lowest twenty-one levels). The fitted temperatures are $T_{\rm fit}/M = 0.288 \pm 0.013$.

lowest twenty-one levels also in this case. Fitting the distribution data by the Boltzmann distribution $\propto \exp(-E_i/T_{\rm fit})$ results in the fitted temperature $T_{\rm fit}/M = 0.288 \pm 0.013$. In the steady-states, the distribution of the eigenstates approaches the black dotted lines, which shows the Boltzmann distribution with the setup temperatures $T/M = 0.1$ and $T/M = 0.3$. Even though we approximately solve the Lindblad master equation and do not find the exact analytic solution, we find that the distribution in the presence of quantum dissipation approaches the thermally equilibrated one which is independent of the initial states and that it is approximately in the Boltzmann distribution.

We hereafter focus on the quantum dissipative effects on the relative motion as stated in Sec. 4.2. In order to discuss the effects of the dissipation and its importance, by dropping the $\mathcal{O}(T/M)$ terms in Eq. (5.21), we can compare the simulations of the full dissipative dynamics and those without dissipation. We show this comparison performed at $T/M = 0.1$ in Fig. 5.4. We can see the clear differences from dissipation not only in the asymptotic behavior on long time scales but also in the initial behavior. The red and blue lines represent the time evolution of the occupation numbers of the ground and the first excited state, respectively, in the case with dissipation, while the dark-green and green lines do in the case without dissipation. Fig. 5.4 tells that when the dissipation is switched off, the initial decay rate of the ground state becomes larger and the production rate of the first excited states accordingly becomes larger. Furthermore, the occupation numbers of the ground and the first excited state decrease and approach the smaller value equally after enough time, which is underestimated comparing the case with dissipation. This can be interpreted in terms of the Lindblad operator (4.46). This can be physically interpreted as follows. The dissipation or equivalently drag force plays a role in preventing the heavy quark pair of a quarkonium from dissociating in the quark-gluon plasma and

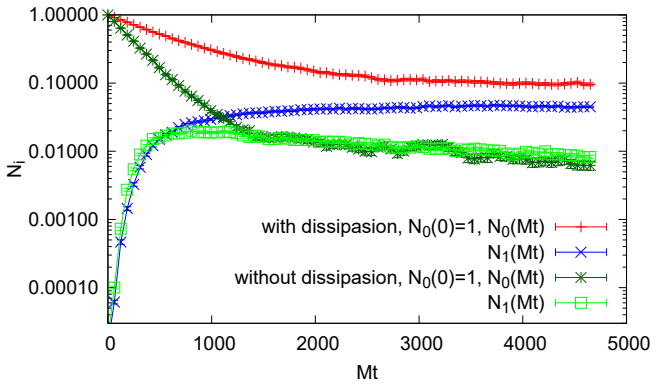

Fig. 5.4: Effect of the dissipation on the occupation numbers. Shown is the time evolution of the occupation numbers of the ground state N_0, the first excited state N_1 with dissipation (red and blue lines) and without dissipation (dark-green and green lines). The bars represent statistical errors.

also balancing itself with the thermal fluctuations to maintain the system in equilibrium. Since the momentum operator is not included in the Lindblad operator without dissipation as in Eq. (4.46), the transition rate does not depend on the states. Even in the initial evolution, we can see the clear effects of the dissipation, and therefore, we conclude that the dissipative effects cannot be neglected even in the short time scale. As an example of such a short time scale, we later consider the typical finite lifetime scale $\sim$10 fm of the quark-gluon plasma. In our setups, for a bottomonium particle, 10 fm corresponds to about (nondimensional) time $Mt \sim 480$ and we will come back to this phenomenological case of the more realistic setup in Sec. 5.5. In this short time scale, as we can see in Fig. 5.4, it is suggested that the dissipative effects on the quarkonium dynamics in the quark-gluon plasma are important and that considering dissipative effects in theoretical discussions on quarkonium dynamics is also important, even though the above simulations do not consider the temperature change in the experiments.

Dependence of Temperature and Heavy Quark Mass

We here study how the time evolution of the occupation numbers depends on the temperature at the fixed heavy quark mass, where we can also see the dependence on the heavy quark mass at the fixed temperature. We prepare the initial state of the ground state of the Hamiltonian H_{Debye}. We then simulate the evolution at $T/M = 0.1$ and $T/M = 0.3$ and show the results in Fig. 5.5 (a). For bottomonium case, these settings correspond to comparing $T \simeq 0.47$ GeV and $T \simeq 1.41$ GeV, respectively. In Fig. 5.5 (a), the red and green lines represent the time evolution of the occupation numbers of the ground and the first excited state respectively in the case of $T/M = 0.1$, while the blue and pink lines do in the case of $T/M = 0.3$. Fig. 5.5 (a) tells that the relaxation to the equilibrium takes place much faster in higher temperature case $T/M = 0.3$ than in $T/M = 0.1$ case. The following physical effects contribute this behavior. First, the heavy quark damping rate γ becomes larger in higher temperatures. Second, the spatial extent of the wave function of the ground state becomes more extended, which receives the decoherence effect more easily. In order to cancel out the first effect, we scale the (nondimensional) time by the unit of heavy quark damping timescale $\tau_{\text{eq}} \equiv MTl_{\text{corr}}^2/\gamma = \pi M/T^2$ estimated in the classical

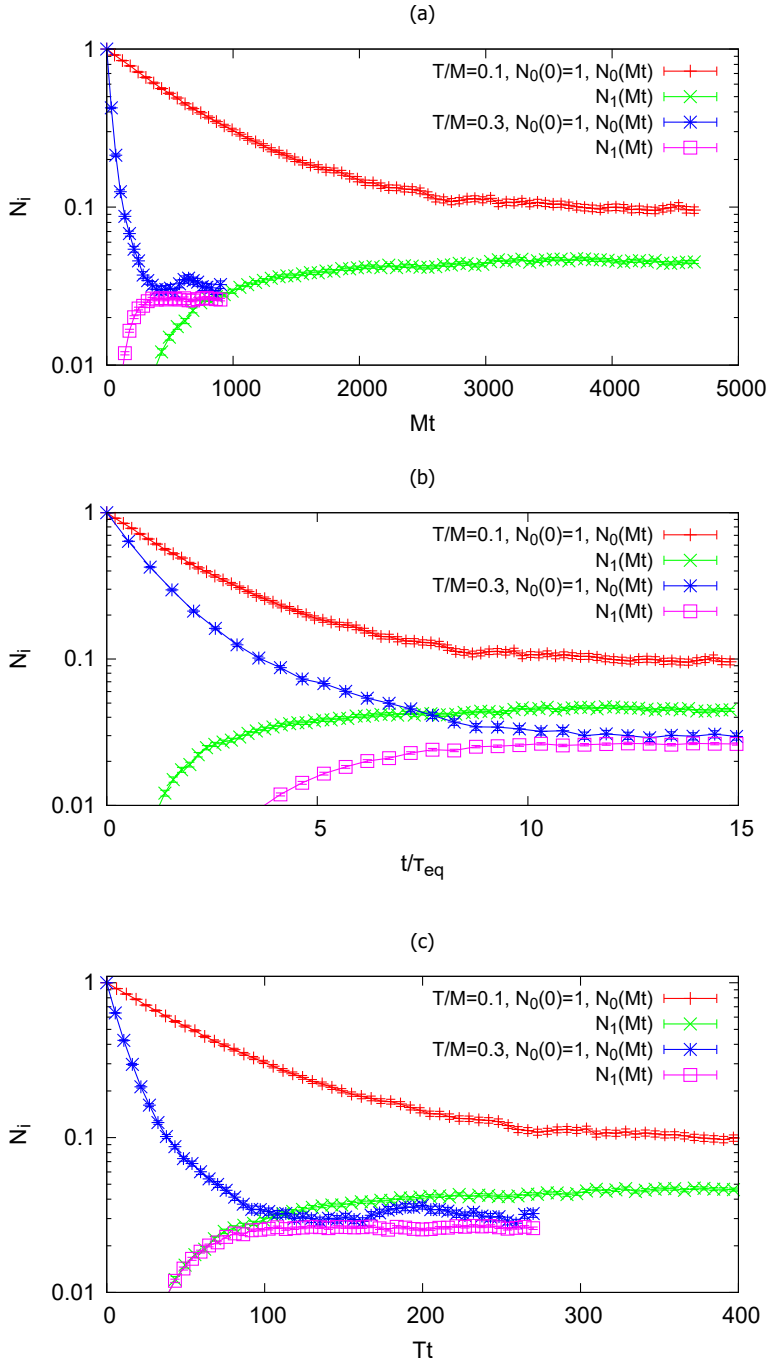

Fig. 5.5: (a) Time evolution of the occupation numbers of the lowest two levels, for $T/M = 0.1$, N_0 (red line) and N_1 (green line), and for $T/M = 0.3$, N_0 (blue line) and N_1 (pink line). (b) Time evolution of the occupation numbers of the lowest two levels as a function of rescaled time by heavy quark damping rate $\tau_{\rm eq}$. (c) Time evolution of the occupation numbers of the lowest two levels as a function of rescaled time by the temperature. In the above figures, we show the results for $T/M = 0.3$ only until the system reaches a steady-state. The bars represent the statistical errors.

limit and plot the rescaled (nondimensional) time in Fig. 5.5 (b). There is still a difference between $T/M = 0.1$ and $T/M = 0.3$ cases, which we expect it to stem from the effect of the decoherence to the ground state wave function as follows. The decoherence rate for a wave function of size $\ell_\psi \equiv \sqrt{\langle x^2 \rangle_\psi}$ is estimated from stochastic potential model as $\tau_{\rm dec}^{-1} = D(0) - D(\ell_\psi)$, which amounts to $\tau_{\rm dec} \simeq 456/M$ and $19/M$ for the ground state at $T/M = 0.1$ and 0.3, respectively. By rescaling it with $\tau_{\rm eq}$, we estimate $\tau_{\rm dec}/\tau_{\rm eq} = 1.45$ for $T/M = 0.1$ and $\tau_{\rm dec}/\tau_{\rm eq} = 0.55$ for $T/M = 0.3$, respectively. This can qualitatively, but roughly,[2] show the reason why the initial decay for $T/M = 0.3$ case is faster than $T/M = 0.1$ case even after the rescaling.

As mentioned above, the settings $T/M = 0.1$ and $T/M = 0.3$ are respectively interpreted as a bottomonium and a charmonium at the fixed temperature $T = 0.47$ GeV. We, in turn, find that as shown in Fig. 5.5 (c), the relaxation of a bottomonium to the equilibrium proceeds more slowly than that of a charmonium again with the same two physical effects as above.

5.4.2 SU(3) Color Case

In the previous Sec. 5.4.1, we have numerically solved the colorless quantum state diffusion equation or the Lindblad master equation for colorless quarkonium relative motion. We have there shown that the dissipation has non-negligible effects for the description of the in-medium quarkonium dynamics. However, these simulations lack the color degrees of freedom of a quarkonium, and we next consider its dynamics including SU(3) color states. In this section, we then in SU(3) color case simulate how dissipative effects appear in the dynamics as well as the color transition effects in the fixed temperature case. In the following simulations of Eq. (5.33) or Eq. (4.51) for SU(3) color case with the setups in Sec. 5.3, we fix the center of mass momentum $P_{\rm CM} = 0$ as taken in U(1) case. The different points are the following. Two kinds of the potential appear, specifically the attractive potential for the singlet states and the repulsive potential for the octet states. The singlet potential is strengthened and the octet potential is weakened in its strength, The state vector in the quantum state diffusion evolution, which is affected by these potentials, has the two components of the color singlet and the color octet. In these setups, the mixing of the different color states is induced by the Lindblad operators (4.53).

Equilibration with Quantum Dissipation

First, we simulate how the color transitions and the quantum dissipation influences the dynamics of the quarkonium relative motion. We prepare either the singlet ground state or the singlet first excited state of the Hamiltonian

$$H_{\rm Singlet,\,Debye} = \frac{p^2}{M} - \frac{C_F \alpha}{\sqrt{x^2 + x_{\rm c}^2}} {\rm e}^{-m_{\rm D}|x|} \tag{5.73}$$

as the two initial conditions of the following simulations. With these two initial conditions, the wave functions are evolved by nonlinear stochastic Schrödinger equation (5.33). From the ensemble average of the wave functions, we then numerically construct the density matrix and calculate the occupation probabilities of the several singlet and octet states

[2] To be strict, the inclusion of the dissipation changes the initial decay rate from the estimate by the decoherence rate as we saw in the previous section.

in the temperature setup $T/M = 0.1$.

The results of the time evolution of occupation probabilities are shown in Fig. 5.6. We

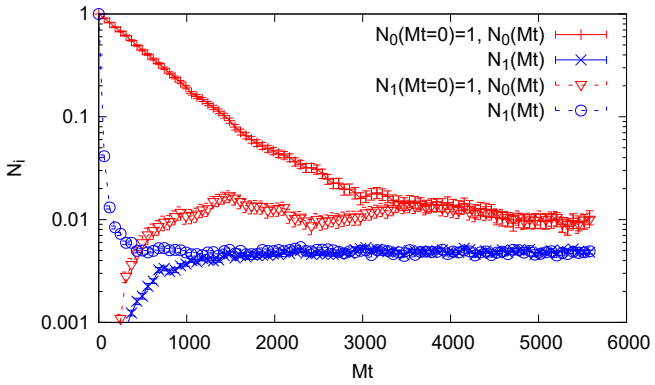

Fig. 5.6: Time evolution of the occupation numbers of the ground state N_0 (red line), the first excited state N_1 (blue line) with respect to (nondimensional) time Mt. The system reaches a steady-state at late times, which is independent of the initial conditions. Error bars represent the statistical errors within the ensemble average.

there plot the occupations $N_i(Mt)$ of the i-th eigenstates for the ground state ($i = 0$), the first excited state ($i = 1$) of the Hamiltonian $H_{\text{Singlet, Debye}}$ as a function of (nondimensional) time Mt. The occupation probabilities of the ground state and the first excited state are respectively represented by the red and blue lines. The difference between *solid* lines and the *dashed* lines is their initial conditions. As in U(1) case, specifically, for the *solid* lines, the initial conditions are the ground state while for the *dashed* lines, the initial conditions are the first excited state. From Fig. 5.6, we find that as (nondimensional) time Mt increases, each of the occupation probabilities respectively relaxes to some static constant value which is independent of the initial conditions within the statistical error bars. This indicates that quarkonium relative motion in the quark-gluon plasma goes to equilibrium and that it approaches a steady-state in the presence of the dissipation. If we calculate the partition function Z in SU(3) case with the (nondimensional) eigenenergy E_i/M of the Hamiltonian $H_{\text{Singlet, Debye}}$, then $\mathrm{e}^{-E_0/T}/Z \simeq 0.0128$ and $\mathrm{e}^{-E_1/T}/Z \simeq 0.005$. These are almost within the 20% level to the values $N_0^{eq} \simeq 0.0105 \pm 0.0020$ and $N_1^{eq} \simeq 0.0048 \pm 0.0002$ at $Mt = 5580$ in the simulations in Fig. 5.6. We note that the dotted red line in Fig. 5.6 seems to show the oscillating behavior which might reflect the singlet octet transitions.

Comparing Fig. 5.6 with the results for U(1) case, the equilibration becomes delayed and the occupation probabilities $N_i(Mt)$ becomes smaller. These differences are expected to appear partially from the fact that quarkonia experience color excitations of the singlet and the octet in SU(3) case. Quarkonia thus take more various colorful states than in the U(1) case, which can decrease the occupation probabilities of every singlet state in the thermal states, compared to the U(1) case. If a singlet wave function transit into an octet wave function, it is difficult for this wave function to return the original singlet state since the wave function can be extended by the repulsive octet potential after the transition. This seemingly leads to the more delayed and slower equilibration. However, this can be compensated by the decay factor of the singlet sector in SU(3) case which becomes C_F times as large as in U(1) case and thus the time to take for the equilibration appear approximately similar to that in U(1) case.

We also plot the time evolution of the occupations of the total singlet and octet color states in Fig. 5.7. Fig. 5.7 shows that the singlet and octet states occupation probabilities

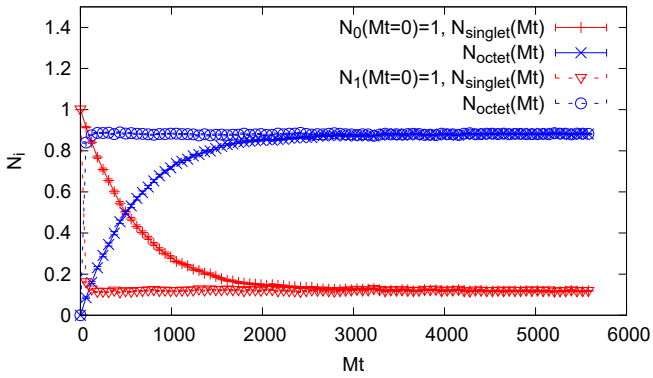

Fig. 5.7: Time evolution of the occupations of the singlet (red line) and octet (blue line) color states with respect to (nondimensional) time Mt. The color states reach a steady state which is independent of the initial conditions. Error bars represent the statistical errors within the ensemble average.

relax to the respective constant value independent of the initial conditions within the statistical error bars. We also show the spatial distribution in the singlet and octet sectors in Fig. 5.8 and Fig. 5.9. The singlet first excited state is more unstable to the interactions

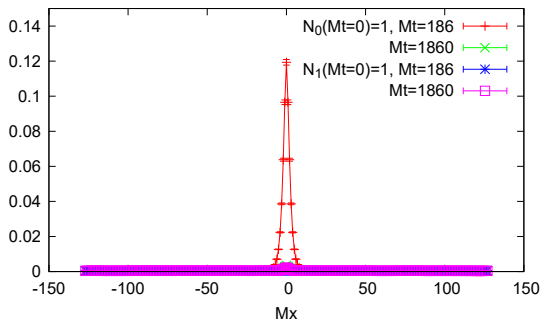

Fig. 5.8: The spatial distribution of the singlet at $Mt = 186, 1860$ from the two initial conditions.

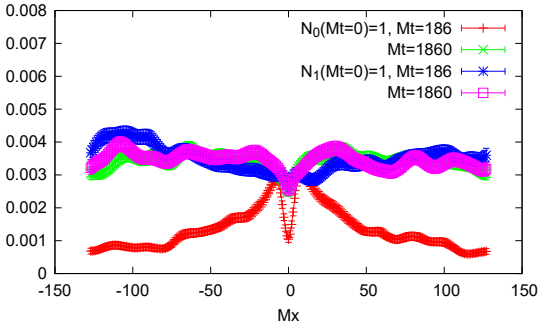

Fig. 5.9: The spatial distribution of the octet at $Mt = 186, 1860$ from the two initial conditions.

with the medium than the singlet ground state and the behavior of the equilibration of the color space is different in two initial conditions. It also implies that the equilibration of the singlet and octet states is achieved faster than the quarkonium equilibration of each singlet state is achieved.

We in turn show in Fig. 5.10, the steady distribution of the eigenstates of the Hamiltonian $H_{\text{Singlet, Debye}}$. We there plot, as a function of the (nondimensional) eigenenergy E_i/M of the Hamiltonian $H_{\text{Singlet, Debye}}$ with $T/M = 0.1$, the occupations probabilities of the lowest twenty one levels at $Mt = 5580$ when the distribution approaches the steady state regime. By fitting the data with the Boltzmann distribution $\propto \exp(-E_i/T_{\text{fit}})$, the fitting temperature T_{fit} is found $T_{\text{fit}}/M = 0.101 \pm 0.026$, which is almost the same as the setup temperature $T/M = 0.1$. We set the fitting range to the eigenstates ϕ_i which

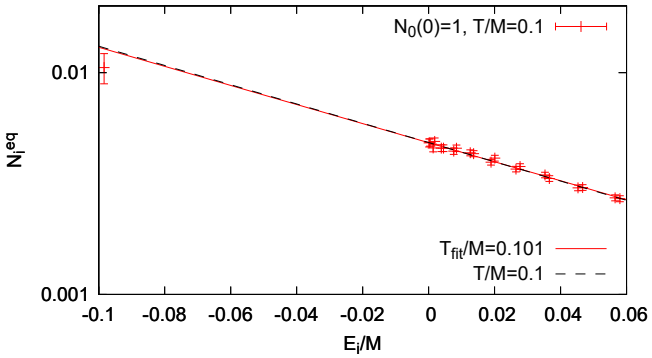

Fig. 5.10: Steady state distributions of the eigenstates in $-0.10 \leq E_i/M \leq 0.06$ at Mt=5580 for $T/M = 0.1$. The data is fitted by the Boltzmann distribution $\propto \exp[-E_i/T_{\rm fit}]$ for levels with relative velocity less than 0.5 (lowest twenty-one levels) The fitted temperatures are $T_{\rm fit}/M = 0.101 \pm 0.026$. The dotted black line represents the Boltzmann distribution $N_i^{\rm eq} \propto \exp[-E_i/T]$ with $T/M = 0.1$ satisfying $N_0^{\rm eq} = 0.0128$.

have the velocity $\frac{\sqrt{\langle p^2 \rangle_{\phi_i}}}{M/2} < 0.5$. From these results, we therefore find that the steady distribution at late times is close to the Boltzmann distribution and that quarkonium system becomes genuinely thermalized at late times in the presence of the dissipation and colors.

5.5 Simulations in the Bjorken expanding quark-gluon plasma

5.5.1 U(1) case

In this Sec. 5.5.1, in turn, we take in U(1) case into account the time-dependent background, that is, the Bjorken expanding quark-gluon plasma medium with the temperature $T(t)$ in order to relate our these simulations to quarkonia, specifically charmonia or bottomonia, in heavy ion collision experiments. This can be achieved by solving the quantum state diffusion equation for the environment undergoing Bjorken expansion with the time-dependent temperature. We take

$$T(t) = T_0 \Big(\frac{t_0}{t_0 + t} \Big)^{\frac{1}{3}}, \quad T_0 = 0.47 \text{ GeV}, \quad t_0 = 0.84 \text{ fm}, \tag{5.74}$$

in our numerical parameter for the temperature. To relate the observable of quarkonium yields in heavy ion collisions, we define occupation numbers by projecting the wave functions onto the eigenstates of the Hamiltonian with the vacuum Cornell potential

$$H_{\rm Cornell} = \frac{p^2}{M} - \frac{\alpha}{\sqrt{x^2 + x_{\rm c}^2}} + \sigma x, \tag{5.75}$$

$$\alpha = 0.3, \quad \sigma = 1.12 \text{ GeV/fm}, \quad M = \begin{cases} 4.7 \text{ GeV} & \text{(bottom)}, \\ 1.6 \text{ GeV} & \text{(charm)}, \end{cases}$$

and numerically evaluate them. We can thus relate the quarkonium yield with these occupation numbers at kinetic freezeout and this effective description is based on the following assumptions. The first one is that the quarkonium wave function at the hadronization is the same as the vacuum eigenstate. The second one is that the quarkonium does not interact significantly with other hadronic matter. Then the probability to find a quarkonium state at the final stage can be obtained by projecting the bound state in the vacuum Cornell potential onto the density matrix at the temperature when the quark-gluon plasma medium is vanishing. In our simulations, even though the projection is performed during the whole evolution of in-medium quarkonia, the occupation numbers at that temperature as mentioned above are meaningful for phenomenological implications. In the numerical simulations, though the initial quarkonium state in heavy ion collisions is not well understood and it is still an open question, we prepare the eigenstate of $H_{\rm Cornell}$ as an initial quarkonium wave function for the simplification. We note that during the evolution by quantum state diffusion equation, we employ the Debye screening potential $V_{\rm Debye}(x)$ as a potential $V(x)$. We simulate the time evolution of the occupation number of the bottomonium states and the charmonium states up to the physical time around 18 fm when the medium temperature is about 170 MeV in our setups.[3] To see the effect of quantum dissipation, we also simulate quarkonium dynamics dropping the dissipative terms as in Fig. 5.4 in Sec. 5.4.1. We plot the results in Fig. 5.11, in which the *solid* lines represent bottomonium case and the *dashed* lines represent charmonium case. For bottomonium

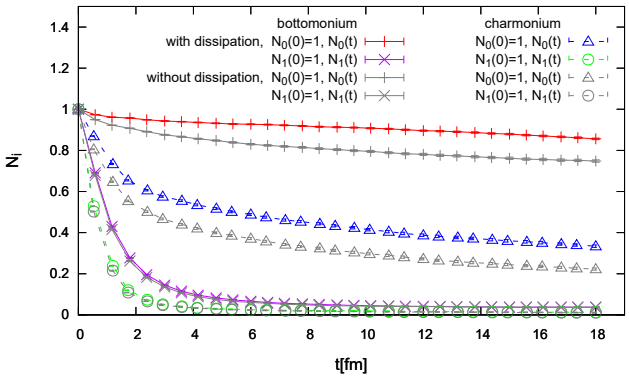

Fig. 5.11: Time evolution of the occupation numbers of the ground state and the first excited state in Cornell potential both for bottomonium and for charmonium. We plot the simulation with dissipation and without dissipation. The bars represent statistical errors.

case with dissipation, the red line represents the time evolution of the occupation number of the ground state with the initial condition of the ground state while the purple line represents that of the first excited state with the initial condition of the first excited state. The gray lines represent the simulations without dissipation, and the different plot marks on them correspond to the simulations with dissipation from the different initial conditions. For the charmonium case with dissipation, the blue line represents that of the ground state with the initial condition of the ground state while the green line represents that of the first excited state with the initial condition of the first excited state. Each kind of the plot marks on the gray lines represents the corresponding initial conditions from which our

[3] The typical lifetime of the quark-gluon plasma is $\sim$ 10 fm in full three-dimensional hydrodynamic simulations.

simulations without dissipation are performed. From Fig. 5.11, we find that the occupation numbers of the first excited states decay faster and more than those of the ground states both for bottomonium state and for charmonium state. This behavior supports the phenomenological idea of sequential melting, which represents the more suppression of the yields of the higher excited states. This thus qualitatively agrees to the behavior of the nuclear modification factor R_{AA} in heavy ion collisions in Sec. 1.2.2. We also see that the ground state and the first excited state of the charmonium states decay faster than those of the bottomonium states. From the point of view of the decoherence, the decoherence of the wave function affects charmonium states more than bottomonium states because bottomonium is more localized.

As shown by the gray lines in Fig. 5.11, the dissipative effects seem to be milder and less important than in the case of the fixed temperature in Fig. 5.4 because the decoherence and damping proceed much slower at lower temperatures. We find that the dissipative effects on the relative motion of a quarkonium in the quark-gluon plasma are non-negligible for the ground states while they are marginally effective for the first excited state. The reason why dissipation affects the ground state more is that the wave function decoherence is effective more for widely spread states such as excited states and that the relative importance of the dissipation on the ground state accordingly enhances as found in the single heavy quark case[80].

5.5.2 SU(3) color case

In this Sec. 5.5.2, we consider the Bjorken expanding quark-gluon plasma medium mainly in SU(3) color case and make a closer look at charmonia or bottomonia in heavy ion collision experiments. Thus we are motivated to simulate the dynamics in the quark-gluon plasma medium with the time-dependent temperature as we did in U(1) case. We take, as an initial quarkonium wave function, the ground state and the first excited state of the vacuum Hamiltonian $H_{\rm Cornell}$ [4]. We then simulate, with and without dissipation, how the occupation numbers of the bottomonium states and the charmonium states evolve up to the physical time around 18 fm when the medium is vanishing. We in Fig. 5.12 plot the results and show the dissipative effects on the quarkonium dynamics. The *solid* lines represent bottomonium case and the *dashed* lines represent charmonium case. For bottomonium case with dissipation, the red line represents the time evolution of the occupation numbers of the ground state with the initial condition of the ground state while the purple line represents that of the first excited state with the initial condition of the first excited state. For charmonium case with dissipation, the blue line represents that of the ground state with the initial condition of the ground state while the green line represents that of the first excited state with the initial condition of the first excited state. The gray lines represent the simulations without dissipation, and the different plot marks on them are for the simulations with dissipation from the different initial conditions for both bottomonium and charmonium. From Fig. 5.12, as sequential melting phenomena seen in nuclear modification factor R_{AA} in heavy ion collisions in Sec. 1.2.2, we find that the occupation numbers of the first excited states decay faster and more than those of the deeply bound ground states both for bottomonium state and for charmonium state.

[4]Several quarkonium production models exists and among them, the color singlet model and color octet model have been developed and discussed[39]. As as initial state of the simulations, in Ref. [73] the authors take the spatially localized state reflecting that quarkonia are produced by hard collisions in the experiments.

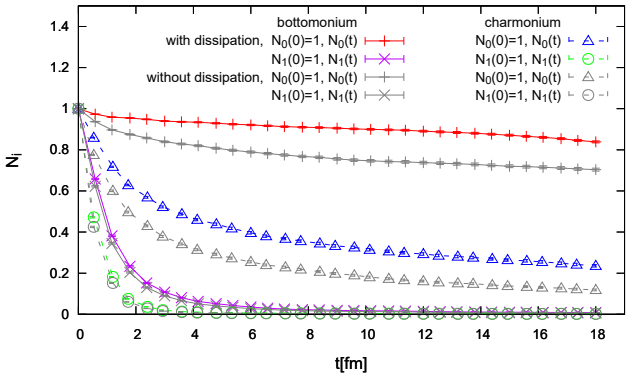

Fig. 5.12: Time evolution of the occupation numbers of the ground state and the first excited state in Cornell potential both for bottomonium and for charmonium. We plot the simulation with dissipation and without dissipation. The bars represent statistical errors.

Even though the one-dimensional simulations of the stochastic potential model show the results similar to that of the complex potential model[88], the dissipation leads the difference in theoretically evaluating quarkonium yields. Thus, the preceding discussions on quarkonium dissociation without dissipation such as some approaches based on complex potential, stochastic potential model, and potential non-relativistic QCD are not adequate and theoretical discussions including dissipation will provide some more promising implications on the experimental interpretations. If we prepare and find more realistic initial conditions for the simulation from the theoretical and experimental researches, we expect more reliable simulations and interpret quarkonium dynamics more precisely.

We, at last, show the density matrix and discuss the spatial distribution of the wave function in the octet sector. In Fig. 5.13 and Fig. 5.14, we show the density matrix in the octet sector $|\rho_{\rm o}(x,y)|^2$ at the final time of the simulations $\sim$ 18 fm when the initial condition is the Cornell ground state. From the initial states in the singlet sector, the

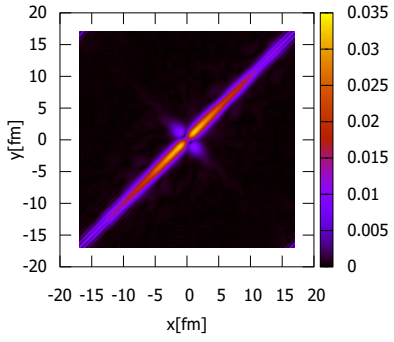

Fig. 5.13: The octet density matrix of charmonium states at the last simulation time.

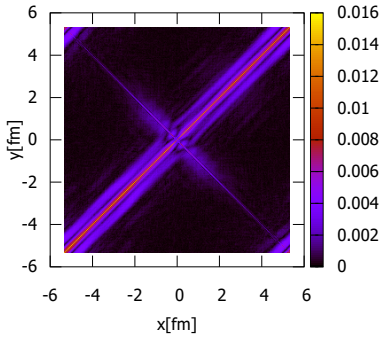

Fig. 5.14: The octet density matrix of bottomonium states at the last simulation time.

density matrix of the octet experiences the decoherence and begin to take the diagonal form along the line of $y = x$. The singlet bottomonium states are more deeply bound than the singlet charmonium states, and the smaller occupancies around the diagonal line $y = x$ are expected to be found for the bottomonium case. The diagonal lines in Fig. 5.13

and Fig. 5.14 represent the spatial distributions in the octet sector and the time evolution of the corresponding distributions is shown in Fig. 5.15 and Fig. 5.16. The time evolution of the spatial distributions in the singlet sector is also shown in Fig. 5.17 and Fig. 5.18. The

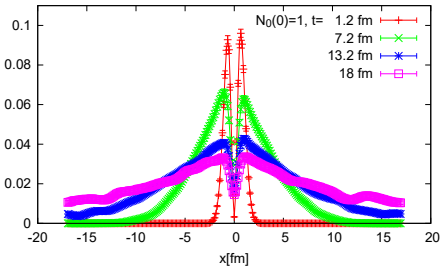

Fig. 5.15: Spatial distributions of charmonium states in the octet sector.

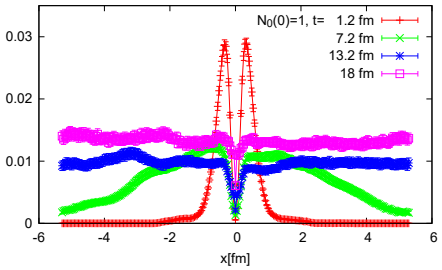

Fig. 5.16: Spatial distributions of bottomonium states in the octet sector.

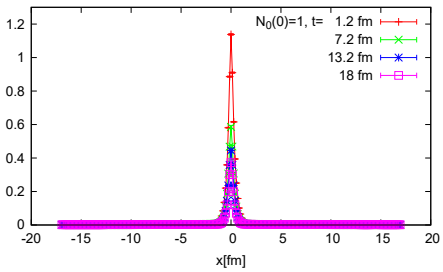

Fig. 5.17: Spatial distributions of charmonium states in the singlet sector.

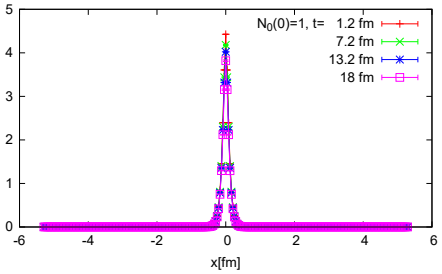

Fig. 5.18: Spatial distributions of bottomonium states in the singlet sector.

charmonium states in the singlet can be more excited than the bottomonium states. For charmonia, the occupancy near the origin is higher and for bottomonia, the occupancies are distributed spatially in the repulsive octet potential.

Other than SU(3) color case, when we consider SU(2) color case, we face the peculiar property in the evolution of the density matrix or the wave function in the nonlinear stochastic Schrödinger equation, which is shown in Appendix D. It is that the density matrix in the triplet sector $|\rho_{\rm t}(x,y)|^2$ even at the final time of the simulations remains finite both in the diagonal line of $y = x$ and in the non-diagonal line of $y = -x$, which tells quantum long-range correlations of the states in the thermal bath from the SU(2) theoretical simulations.

Chapter 6

Summary

In this thesis, we study the dynamics of quarkonium in the quark-gluon plasma. We regard the quarkonium system as an open quantum system in a thermal bath. Based on the framework of the open quantum system and quantum chromodynamics, we derive the Lindblad equation for the relative motion of the quantum Brownian heavy quark pair.

The Lindblad equation ensures the basic physical properties of positivity, hermiticity, and unitarity of the reduced density matrix. In this Lindblad equation for the quarkonium relative motion, three kinds of forces, Debye screened potential force, stochastic force, and drag force govern the time evolution of an in-medium quarkonium. The information of the interactions is embedded in the Lindblad operators. The effects of the stochastic force and the drag force are represented by the momentum shift in collisions and the change of the collision rate with the recoil of heavy quarks during collisions, respectively. Although the Lindblad operator for the relative motion of the heavy quark pair depends on the center of mass momentum, we just considered the static case ($P_{\rm CM} = 0$) in the simulations since its dependence is found to be small. Thus a full quantum mechanical and Lindbladian simulation with dissipation was performed for heavy quarks in the quark-gluon plasma.

We solved the Lindblad equation by a stochastic unravelling method called the quantum state diffusion. Applying this method, any Lindblad master equation is shown to be equivalent to a nonlinear stochastic Schrödinger equation by which we can correctly produce a mixed state ensemble for the density matrix. In our numerical simulation in one dimension, we first checked the basic properties of the master equation for both U(1) and SU(3) color cases. The occupation number of eigenstates relaxes toward a value independent of the initial condition, and the steady state distribution is consistent with the Boltzmann distribution. We also studied the effects of quantum dissipation and color transitions by comparing a simulation without them. The quantum dissipation delays the relaxation toward equilibrium, which is consistent with our intuitive classical picture that the drag force prevents a heavy quark pair from dissociating. We then simulated the temperature and heavy quark mass dependences on the time evolution. The time evolution strongly depends on these quantities but is found to scale to a considerable extent with the heavy quark damping time. The color transitions in SU(3) case may delay the relaxation comparing with U(1) case, since the octet states have more difficulty in transiting into the singlet states than the singlet do into the octet.

We finally considered the Bjorken expanding quark-gluon plasma in relativistic heavy ion collisions and solved the master equation with a time-dependent temperature. By simulating the bottomonium and charmonium yields, we found that charmonium dissociates

faster than bottomonium and that the excited states decay faster than the ground states. We also found that the quantum dissipation delays the ground state dissociation compared to the case without dissipation while the excited state dissociation is insensitive to it. Therefore the dissipation can affect the yields of quarkonia in heavy ion collision experiments. This difference comes from the fact that the decoherence due to thermal fluctuation drives the dissociation for an extended state while it is ineffective for a localized state such as the ground state. The dissipation thus becomes as important as the decoherence for a localized state. In this regard, our simulations suggest that, when discussing the in-medium quarkonium dynamics, it is not adequate that one refers to and relies on the theoretical approaches without dissipation which are based on the complex potential model, the stochastic potential model and potential non-relativistic QCD effective theory.

To proceed further to future comprehensive discussions with more realistic simulations, we need to extend our discussions to a three-dimensional simulation and couple it with a three-dimensional hydrodynamic background. In the three-dimensional simulation, our simulations will contain the degrees of freedom of the radial direction, which is included in the potential non-relativistic QCD approach, where the dissipative effects on the quarkonium dynamics have not been simulated. By comparing such simulations with our simulations, it may be then made clear whether or not the dipole approximation of quarkonium state is appropriate in the dynamics.

Appendix A

Environmental Correlation Functions

The explicit forms of the physical quantities $D(\vec{x})$ and $V(\vec{x})$ are evaluated in the thermal quantum field theory. First, the two point retarded correlator in momentum space for soft scale momentum $Q^\mu = (\omega, \vec{q})$ is calculated in Coulomb gauge:

$$G^{R,\mu\nu}(Q) = \int d^4x \mathrm{e}^{iQx}\, i\theta(t)\langle[A^\mu(t,\vec{x}), A^\nu(0,\vec{0})]\rangle = \frac{-P_T^{\mu\nu}}{Q^2-\Pi_T} + \frac{Q^2}{q^2}\frac{-\delta^{\mu 0}\delta^{\nu 0}}{Q^2-\Pi_L}, \quad \text{(A.1)}$$

where P_T represents the transverse projection

$$P_T^{ij} = \delta^{ij} - \frac{q^i q^j}{q^2}, \quad P_T^{00} = P_T^{0j} = P_T^{i0} = 0. \quad \text{(A.2)}$$

Here we define two kinds of self energies

$$\Pi_L(Q) = -m_D^2\frac{Q^2}{q^2}(1-F(\omega/q)), \quad \Pi_T(Q) = \frac{m_D^2}{2}\left[1+\frac{Q^2}{q^2}(1-F(\omega/q))\right] \quad \text{(A.3)}$$

$$F(x) \equiv \frac{x}{2}\left[\ln\left|\frac{x+1}{x-1}\right| - i\pi\theta(1-|x|)\right], \quad m_D^2 = \frac{1}{3}g^2T^2\left(N_c + \frac{1}{2}N_f\right), \quad \text{(A.4)}$$

which are approximated by hard thermal loop scheme with N_c and N_f respectively representing the numbers of the color degrees of freedom and the numbers of the flavors of quarks. In the region of small ω, the longitudinal self energy and accordingly the retarded correlator are obtained:

$$\Pi_L(\omega,\vec{q}) = -m_D^2\frac{Q^2}{q^2}\left(1-\frac{\omega}{2q}\log\frac{q+\omega}{q-\omega} + i\pi\frac{\omega}{2q}\right) \simeq m_D^2\left(1+i\pi\frac{\omega}{2q}\right), \quad \text{(A.5)}$$

$$G_{00}^R(\omega,\vec{x}) \simeq \int \frac{d^3q}{(2\pi)^3}e^{i\vec{q}\cdot\vec{x}}\frac{-1}{q^2+m_D^2+i\frac{\pi m_D^2\omega}{2q}}. \quad \text{(A.6)}$$

Thus from Kramers Kronig relation, we can evaluate the following functions in Sec.4:

$$\begin{aligned} D(\vec{x}) &= T\,\frac{d}{d\omega}\sigma(\omega,\vec{x})\bigg|_{\omega=0} = 2g^2T\frac{\partial}{\partial\omega}\operatorname{Im}G_{00}^R(\omega,\vec{x})\bigg|_{\omega=0} \\ &= g^2T\int\frac{d^3q}{(2\pi)^3}e^{i\vec{q}\cdot\vec{x}}\frac{\pi m_D^2}{q\left(q^2+m_D^2\right)^2}, \quad \text{(A.7)} \\ V(\vec{x}) &= -2\mathcal{V}(\vec{x}) \end{aligned}$$

$$= \int_{-\infty}^{\infty} \frac{d\omega}{2\pi} \frac{\sigma(\omega,\vec{x})}{\omega} = g^2 \int_{-\infty}^{\infty} \frac{d\omega}{2\pi} \frac{2\,\mathrm{Im}\, G^R_{00}(\omega,\vec{x})}{\omega} = g^2\, \mathrm{Re}\, G^R_{00}(\omega,\vec{x})\big|_{\omega=0}$$
$$= -\frac{g^2}{4\pi|\vec{x}|} e^{-m_D|\vec{x}|} \tag{A.8}$$

Since these results are obtained by hard thermal loop approximation, the applicability of these expressions is for $|\vec{x}| \gtrsim m_D^{-1}$.

Appendix B

Dependence of the Center of Mass Motion

Here in U(1) case, we test the effects of the center-of-mass motion on the relative motion of a quarkonium at $T/M = 0.1$. We set the center-of-mass momentum at different values $P_{\rm CM}/M = 0, 0.4, 0.6, 0.8, 1.0$ equivalent to the velocity $v_{\rm CM} = 0, 0.2, 0.3, 0.4, 0.5$. In Fig. B.1, shown are the time evolution of the ground state occupations and also the occupation for each eigenstate at late times $Mt = 4650$ when the system has reached a non-equilibrium steady state. The results are quite insensitive to the values of $P_{\rm CM}$.

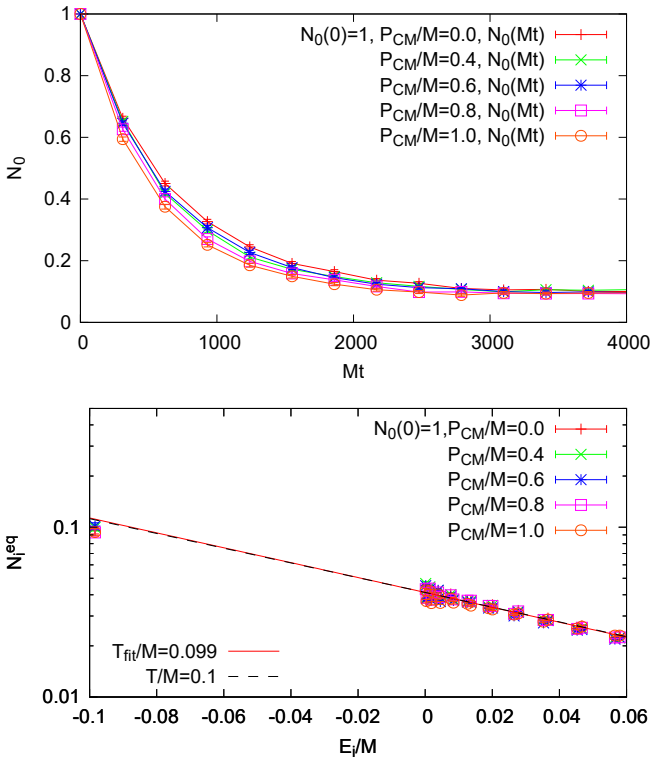

Fig. B.1: (Top) Effects of the center-of-mass motion on the ground state occupation number. (Bottom) Effects of the center-of-mass momentum on the eigenstate occupation numbers at late enough time $Mt = 4650$. The center-of-mass momentum is $P_{\rm CM}/M = 0, 0.4, 0.6, 0.8, 1.0$. The bars represent statistical errors.

Appendix C

Dependence of Heavy Quark Diffusion Constant

In our analysis and simulations, quarkonia can probe fundamental length scales of the quark-gluon plasma, the screening length ${m_{\rm D}}^{-1}$ and the correlation length $l_{\rm corr}$. The screening length has been evaluated via the real-part of the heavy quark potential and the heavy quark free energies in various lattice QCD simulations[96, 97]. The real part of the potential in which the screening length appears has been studied by lattice QCD calculations.

Through our simulations, we relate the correlation length to debye mass, respecting the fitting the correlation function (A.7) by Gaussian from. While it is related ideally in the high-temperature region, in other regions the relation might be different. Considering this context, the correlation length could be regarded as a parameter independent of other parameters.

The correlation length is related to the imaginary part of the potential, or in particular, the correlation function D function. However, the non-perturbative lattice QCD results on complex potential have larger error bars in the imaginary part than in the real part. Precise determination of the correlation length is now difficult from these results. Some studies by lattice QCD may provide improvement in the future.

We then test whether or not we read it from the experimental results with our simulations in U(1) case. First, we relate the results from other studies to the correlation length and obtain the information of the correlation length. We here constrain the form of the environmental correlation function by employing the heavy quark diffusion constant obtained from other studies such as lattice QCD and hydrodynamics[98], in which the Fig. C.1 are shown.

We define the heavy quark diffusion constant with drag coefficient η as

$$D = \frac{T}{M\eta}. \tag{C.1}$$

From the Fig. C.1, we estimate $D \sim \frac{4}{2\pi T}$, which is within the common range where the preceding studies shows the similar results. On the other hand, from the classical limit of the master equation which is typically described by

$$\frac{d}{dt}p = -\frac{\gamma}{MTl_{\rm corr}^2}p\,, \tag{C.2}$$

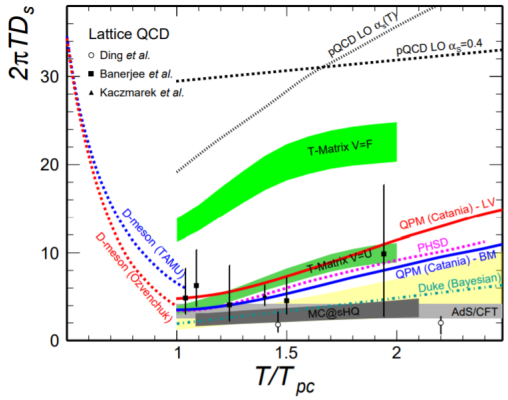

Fig. C.1: Heavy quark diffusion constant from several studies. This figure is taken from Ref. [98].

as discussed in Ref. [80]. We can deduce the heavy quark diffusion constant by comparing the drag coefficient in Eq. (C.2) and thus constrain γ with a parameter $l_{\rm corr}$ as

$$D = \frac{T^2 l_{\rm corr}^2}{\gamma}, \qquad \frac{\gamma}{l_{\rm corr}^2} = \frac{\pi}{2} T^3 \tag{C.3}$$

We then simulate the time evolution of the occupations of the quarkonium state when varying the correlation length $l_{\rm corr} = \frac{c}{T}$ with $c = 0.25, 0.5, 1.0, 1.25, 1.5$. The simulation setups are listed in Table C.1 in case $2\pi TD = 4$.

Table C.1: Numerical setups

Δx	Δt	N_x	T	γ	$l_{\rm corr}$	α	m_D	$r_{\rm c}$
$1/M$	$0.1M(\Delta x)^2$	508	$0.1M, 0.3M$	$\frac{\pi}{2} l_{\rm corr}^2 T^3$		0.3	$2T$	$1/M$

We show the results of the time evolution of the occupation number of the vacuum Cornell eigenstates for charmonium and bottomonium in the top of Fig. C.2. We also simulate as the above, varying the heavy quark diffusion constant $2\pi TD = 2, 8$ and accordingly, γ being changed. The results are also shown in the middle and bottom of Fig. C.2.

From these results, we can see, when the diffusion constant is fixed and change the time evolution of the correlation length, the survival probability of the Cornell ground state is sensitive to the correlation length. We also may find whether or not the diffusion constant is large does not affect the charmonium ground state almost up to the lifetime of the quark-gluon plasma. On the other hand, the bottomonium counterpart is sensitive to how large the diffusion constant is. It does give a non-negligible contribution to the experimental observables. It may imply that the observables such as nuclear modification factor should have information on the correlation length of the quark-gluon plasma with the interplay to heavy quark diffusion constant. Therefore, the yields of quarkonia can work as measures of the correlation length. The former is one of the dynamical properties and has not yet been precisely analyzed by the lattice QCD approach. If the experimental instruments have the above resolution, we might extract its information and its measurement, which might become the value of the reference length for the hydrodynamical description of the quark-gluon plasma.

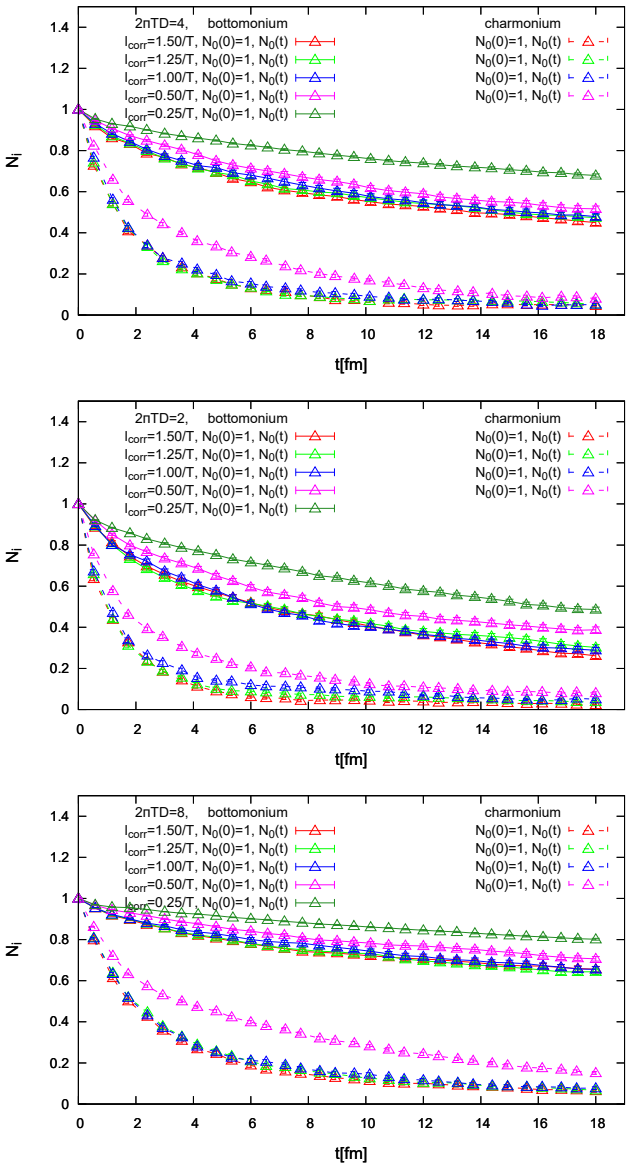

Fig. C.2: Time evolution of the occupation of the charmonium or bottomonium ground state with different correlation lengths. The bars represent the statistical errors. (top) $2\pi TD = 4$ case. (middle) $2\pi TD = 2$ case. (bottom) $2\pi TD = 8$ case.

Appendix D

SU(2) symmetry of the Lindblad equation

Here we prove the Lindblad master equation in SU(2) case to satisfy the following symmetry by the transformation

$$\rho^{S}_{AB,kl}\left(\vec{r},\vec{r}',t\right)=-\epsilon_{Aj}\epsilon_{Bi}\rho_{ij,kl}\left(-\vec{r},\vec{r}',t\right), \tag{D.1}$$

$$\rho^{S*}_{kl,AB}\left(\vec{r},\vec{r}',t\right)=-\rho_{kl,ij}\left(\vec{r},-\vec{r}',t\right)\epsilon_{Aj}\epsilon_{Bi}, \tag{D.2}$$

$$\rho^{SS^*}_{ij,kl}\left(\vec{r},\vec{r}',t\right)=\epsilon_{in}\epsilon_{jm}\rho_{mn,pq}\left(-\vec{r},-\vec{r}',t\right)\epsilon_{kq}\epsilon_{lp}. \tag{D.3}$$

If we can show the symmetry on Eq. (D.1), accordingly we show the symmetry on Eq. (D.2) and Eq. (D.3) since they are regarded as the conjugate. The transformation can be considered as the parity transformation and the exchanges of color indexes, which here we call *S transformation*. The Lindblad operator (4.46) is

$$L^{a}(\vec{k})=A_{Q}(\vec{p},\vec{r})\left(t^{a}_{Q}\otimes 1\right)-B_{Q_c}(\vec{p},\vec{r})\left(1\otimes t^{a*}_{Q_c}\right)+C_{QQ_c}(\vec{r})\,if^{abc}\left(t^{a}_{Q}\otimes t^{a*}_{Q_c}\right), \tag{D.4}$$

and the Lindblad master equation (4.45) with the Hamiltonian $H\equiv H_{ijkl}(\vec{p},\vec{r})$ is

$$\frac{d}{dt}\rho(t)=-i\left[H,\rho\right]+\int_{k}\sum_{a}\left[2L^{a}(\vec{k})\rho L^{a\dagger}(\vec{k})-\left\{L^{a\dagger}(\vec{k})L^{a}(\vec{k}),\rho\right\}\right], \tag{D.5}$$

$$H_{ijkl}(\vec{p},\vec{r})=\frac{\vec{p}^{2}}{M}\left(1\otimes 1\right)_{ijkl}+\left[V\left(\vec{r}\right)-\frac{\vec{p}\cdot\vec{\nabla}D\left(\vec{r}\right)+\vec{\nabla}D\left(\vec{r}\right)\cdot\vec{p}}{4MT}\right]\left(t^{a}_{Q}\otimes t^{a*}_{Q_c}\right)_{ijkl}. \tag{D.6}$$

With $\sigma^{ab}_{2}=-i\epsilon^{ab}$ and $-\epsilon^{ab}t^{\alpha be}=t^{\alpha da}\epsilon^{de}$, we show the some useful relations in SU(2)

$$-\epsilon_{Aj}\epsilon_{Bi}\left(t^{a}_{Q}\otimes 1\right)_{ijab}=\left(1\otimes t^{a*}_{Qc}\right)_{ABij}\epsilon_{ib}\epsilon_{ja}, \tag{D.7}$$

$$-\epsilon_{Aj}\epsilon_{Bi}\left(1\otimes t^{a*}_{Qc}\right)_{ijab}=\left(t^{a}_{Q}\otimes 1\right)_{ABij}\epsilon_{ib}\epsilon_{ja}, \tag{D.8}$$

$$-\epsilon_{Aj}\epsilon_{Bi}if^{abc}\left(t^{b}_{Q}\otimes t^{c*}_{Qc}\right)_{ijkl}=if^{abc}\left(t^{b}_{Q}\otimes t^{c*}_{Qc}\right)_{ABij}\epsilon_{il}\epsilon_{jk}, \tag{D.9}$$

$$-\epsilon_{Aj}\epsilon_{Bi}\left(t^{a}_{Q}\otimes t^{a*}_{Qc}\right)_{ijkl}=\left(t^{a}_{Q}\otimes t^{a*}_{Qc}\right)_{ABji}\epsilon_{jb}\epsilon_{ia}, \tag{D.10}$$

where we note

$$\left(t^{a}\otimes t^{a*}\right)_{ij,kl}=\left(t^{a}\right)_{ik}\left(t^{a*}\right)_{jl}=\left(t^{a}\right)_{ik}\left(t^{a}\right)_{lj}, \tag{D.11}$$

$$(t^a \otimes 1)_{ij,kl} = (t^a)_{ik}\,\delta_{jl}, \tag{D.12}$$
$$(1 \otimes t^{a*})_{ij,kl} = \delta_{ik}\,(t^{a*})_{jl} = \delta_{ik}\,(t^a)_{lj}\,. \tag{D.13}$$

Thus, the S transformation on the Lindblad operator correspond to the representation of the operators

$$-\epsilon_{Aj}\epsilon_{Bi}A_Q(-\vec{p},-\vec{r})\left(t^a_Q\otimes 1\right)_{ijkl} = B_{Q_c}(\vec{p},\vec{r})\left(1\otimes t^{a*}_{Qc}\right)_{ABij}\epsilon_{il}\epsilon_{jk}, \tag{D.14}$$
$$-\epsilon_{Aj}\epsilon_{Bi}B_{Q_c}(-\vec{p},-\vec{r})\left(1\otimes t^{a*}_{Qc}\right)_{ijkl} = -A_Q(\vec{p},\vec{r})\left(t^a_Q\otimes 1\right)_{ABij}\epsilon_{il}\epsilon_{jk}, \tag{D.15}$$
$$-\epsilon_{Aj}\epsilon_{Bi}C_{QQ_c}(-\vec{r})\,if^{abc}\left(t^a_Q\otimes t^{a*}_{Qc}\right)_{ijkl} = -C_{QQ_c}(\vec{r})\,if^{abc}\left(t^a_Q\otimes t^{c*}_{Qc}\right)_{ABij}\epsilon_{il}\epsilon_{jk}. \tag{D.16}$$

The latter relations lead

$$-\epsilon_{Aj}\epsilon_{Bi}L^a(-\vec{p},-\vec{r},\vec{k})_{ijkl} = L^a(\vec{p},\vec{r},\vec{k})_{ABij}[-\epsilon_{il}\epsilon_{jk}], \tag{D.17}$$
$$-\epsilon_{Aj}\epsilon_{Bi}L^{\dagger a}(-\vec{p},-\vec{r},\vec{k})_{ijkl} = L^{\dagger a}(\vec{p},\vec{r},\vec{k})_{ABij}[-\epsilon_{il}\epsilon_{jk}]. \tag{D.18}$$

From the above relations, we show the S transformation on the Lindblad master equation as follows

$$-\epsilon_{Aj}\epsilon_{Bi}H_{ijkl}(-\vec{p},-\vec{r}) = H_{ABij}(\vec{p},\vec{r})[-\epsilon_{il}\epsilon_{jk}], \tag{D.19}$$
$$\begin{aligned}&-\epsilon_{Aj}\epsilon_{Bi}L^a(-\vec{p},-\vec{r},\vec{k})_{ijab}\rho_{abcd}\,(-\vec{r},\vec{r}',t)\,L^{\dagger a}(\vec{p},\vec{r},\vec{k})_{cdkl}\\ &\quad = L^a(\vec{p},\vec{r},\vec{k})_{ABij}[-\epsilon_{ib}\epsilon_{ja}]\rho_{abcd}\,(-\vec{r},\vec{r}',t)\,L^{\dagger a}(\vec{p},\vec{r},\vec{k})_{cdkl},\end{aligned} \tag{D.20}$$
$$\begin{aligned}&-\epsilon_{Aj}\epsilon_{Bi}L^{\dagger a}(-\vec{p},-\vec{r},\vec{k})_{ijab}L^a(-\vec{p},-\vec{r},\vec{k})_{abcd}\rho_{cdkl}\,(-\vec{r},\vec{r}',t)\\ &\quad = L^{\dagger a}(\vec{p},\vec{r},\vec{k})_{ABij}[-\epsilon_{ib}\epsilon_{ja}]L^a(-\vec{p},-\vec{r},\vec{k})_{abcd}\rho_{cdkl}\,(-\vec{r},\vec{r}',t)\\ &\quad = L^{\dagger a}(\vec{p},\vec{r},\vec{k})_{ABij}L^a(\vec{p},\vec{r},\vec{k})_{ijab}[-\epsilon_{ad}\epsilon_{bc}]\rho_{cdkl}\,(-\vec{r},\vec{r}',t)\,.\end{aligned} \tag{D.21}$$

Therefore the S transformed density matrix $-\epsilon_{Aj}\epsilon_{Bi}\rho_{ij,kl}\,(-\vec{r},\vec{r}',t)$ satisfy the same Lindblad master equation, which is the symmetry of the Lindblad master equation.

From this property, as shown in Fig. D.1 and Fig. D.2, the density matrix in the triplet sector $|\rho_{\rm t}(x,y)|^2$ even at the final time of the simulations remains finite both in the diagonal line of $y=x$ and in the non-diagonal line of $y=-x$, which tells quantum long-range correlations of the states in the thermal bath from the SU(2) theoretical simulations.

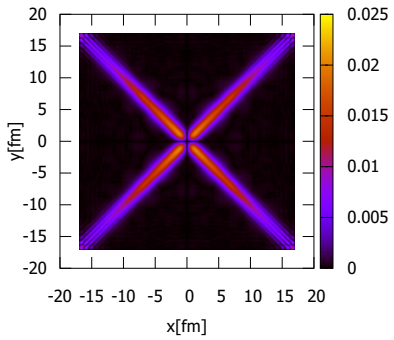

Fig. D.1: The triplet density matrix of charmonium states at the last simulation time.

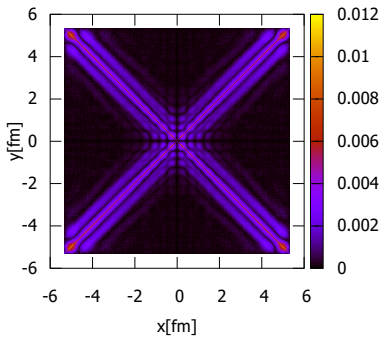

Fig. D.2: The triplet density matrix of bottomonium states at the last simulation time.

References

[1] David J. Gross and Frank Wilczek, Phys. Rev. Lett., **30**, 1343–1346 (1973).

[2] H.David Politzer, Phys. Rev. Lett., **30**, 1346–1349 (1973).

[3] Yoichiro Nambu and G. Jona-Lasinio, Phys. Rev., **122**, 345–358 (1961).

[4] H. Fukaya, S. Aoki, S. Hashimoto, T. Kaneko, J. Noaki, T. Onogi, and N. Yamada, Phys. Rev. Lett., **104**, 122002, [Erratum: Phys.Rev.Lett. 105, 159901 (2010)] (2010), arXiv:0911.5555.

[5] Kenneth G. Wilson, pages 45–59 (2 1974).

[6] John C. Collins and M.J. Perry, Phys. Rev. Lett., **34**, 1353 (1975).

[7] N. Cabibbo and G. Parisi, Phys. Lett. B, **59**, 67–69 (1975).

[8] Y. Aoki, G. Endrodi, Z. Fodor, S.D. Katz, and K.K. Szabo, Nature, **443**, 675–678 (2006), hep-lat/0611014.

[9] Szabolcs Borsanyi, Zoltan Fodor, Christian Hoelbling, Sandor D Katz, Stefan Krieg, Claudia Ratti, and Kalman K. Szabo, JHEP, **09**, 073 (2010), arXiv:1005.3508.

[10] A. Bazavov et al., Phys. Rev. D, **90**, 094503 (2014), arXiv:1407.6387.

[11] A. Bazavov et al., Phys. Lett. B, **795**, 15–21 (2019), arXiv:1812.08235.

[12] O. Scavenius, A. Mocsy, I.N. Mishustin, and D.H. Rischke, Phys. Rev. C, **64**, 045202 (2001), nucl-th/0007030.

[13] M. Asakawa and K. Yazaki, Nucl. Phys. A, **504**, 668–684 (1989).

[14] P. Braun-Munzinger and J. Wambach, Rev. Mod. Phys., **81**, 1031–1050 (2009), arXiv:0801.4256.

[15] A. Chodos, R.L. Jaffe, K. Johnson, Charles B. Thorn, and V.F. Weisskopf, Phys. Rev. D, **9**, 3471–3495 (1974).

[16] S. Ejiri, F. Karsch, and K. Redlich, Phys. Lett. B, **633**, 275–282 (2006), hep-ph/0509051.

[17] D. Ivanenko and D.F. Kurdgelaidze, Lett. Nuovo Cim., **2**, 13–16 (1969).

[18] Massimo Mannarelli, PoS, **CONFINEMENT8**, 010 (2008), arXiv:0812.2831.

[19] J.D. Bjorken, Phys. Rev. D, **27**, 140–151 (1983).

[20] Lokesh Kumar, Nucl. Phys. A, **904-905**, 256c–263c (2013), arXiv:1211.1350.

[21] Chi Yang, Nucl. Phys. A, **967**, 800–803 (2017).

[22] K Adcox, SS Adler, S Afanasiev, C Aidala, NN Ajitanand, Y Akiba, A Al-Jamel, J Alexander, R Amirikas, K Aoki, et al., Nuclear Physics A, **757**(1-2), 184–283 (2005).

[23] John Adams, MM Aggarwal, Z Ahammed, J Amonett, BD Anderson, D Arkhipkin, GS Averichev, SK Badyal, Y Bai, J Balewski, et al., Nuclear Physics A, **757**(1-2), 102–183 (2005).

[24] http://alice-j.org/ ().

[25] K. Yagi, T. Hatsuda, and Y. Miake, Quark-gluon plasma: From big bang to little bang, volume 23, (, 2005).

[26] G. Aarts et al., Eur. Phys. J. A, **53**(5), 93 (2017), arXiv:1612.08032.

[27] Serguei Chatrchyan et al., Phys. Rev. Lett., **107**, 052302 (2011), arXiv:1105.4894.

[28] A. Adare et al., Phys. Rev. C, **91**(2), 024913 (2015), arXiv:1404.2246.

[29] Vardan Khachatryan et al., Phys. Lett. B, **770**, 357–379 (2017), arXiv:1611.01510.

[30] Albert M Sirunyan et al., Phys. Lett. B, **790**, 270–293 (2019), arXiv:1805.09215.

[31] Serguei Chatrchyan et al., Phys. Rev. Lett., **109**, 222301, [Erratum: Phys.Rev.Lett. 120, 199903 (2018)] (2012), arXiv:1208.2826.

[32] Albert M Sirunyan et al., Phys. Rev. Lett., **120**(14), 142301 (2018), arXiv:1706.05984.

[33] ATLAS-CONF-2019-054 (11 2019).

[34] A. Adare et al., Phys. Rev. Lett., **98**, 232301 (2007), nucl-ex/0611020.

[35] A. Adare et al., Phys. Rev. C, **84**, 054912 (2011), arXiv:1103.6269.

[36] L. Adamczyk et al., Phys. Rev. C, **90**(2), 024906 (2014), arXiv:1310.3563.

[37] Rosi Reed, J. Phys. G, **38**, 124185 (2011), arXiv:1109.3891.

[38] Zaochen Ye, Nucl. Phys. A, **967**, 600–603 (2017).

[39] A. Andronic et al., Eur. Phys. J. C, **76**(3), 107 (2016), arXiv:1506.03981.

[40] Jaroslav Adam et al., Phys. Lett. B, **766**, 212–224 (2017), arXiv:1606.08197.

[41] Christopher Beresford Powell, PoS, **EPS-HEP2011**, 485 (2011), arXiv:1111.6944.

[42] Shreyasi Acharya et al., JHEP, **02**, 012 (2019), arXiv:1811.12727.

[43] Shreyasi Acharya et al., Phys. Rev. Lett., **123**(19), 192301 (2019), arXiv:1907.03169.

[44] Takahiro Miura, Yukinao Akamatsu, Masayuki Asakawa, and Alexander Rothkopf, Phys. Rev. D, **101**(3), 034011 (2020), arXiv:1908.06293.

[45] Takahiro Miura, Yukinao Akamatsu, Masayuki Asakawa, and Alexander Rothkopf, JPS Conf. Proc., **32**, 010084 (2020).

[46] Oskar Alund, Yukinao Akamatsu, Fredrik Laurén, Takahiro Miura, Jan Nordström, and Alexander Rothkopf, J. Comput. Phys., **425**, 109917 (2021), arXiv:2004.04406.

[47] T. Matsui and H. Satz, Phys. Lett. B, **178**, 416–422 (1986).

[48] Agnes Mocsy, Peter Petreczky, and Michael Strickland, Int. J. Mod. Phys. A, **28**, 1340012 (2013), arXiv:1302.2180.

[49] J.I. Kapusta and Charles Gale, Finite-temperature field theory: Principles and applications, Cambridge Monographs on Mathematical Physics. (Cambridge University Press, 2011).

[50] Michel Le Bellac, Thermal Field Theory, Cambridge Monographs on Mathematical Physics. (Cambridge University Press, 3 2011).

[51] Nora Brambilla, Antonio Pineda, Joan Soto, and Antonio Vairo, Rev. Mod. Phys., **77**, 1423 (2005), hep-ph/0410047.

[52] Alexey A. Petrov and Andrew E. Blechman, Effective Field Theories, (WSP, 2016).

[53] Leslie L. Foldy and Siegfried A. Wouthuysen, Phys. Rev., **78**, 29–36 (1950).

[54] E. Braaten, Introduction to the NRQCD factorization approach to heavy quarkonium (11 1996), hep-ph/9702225.

[55] H.J. Rothe, Lattice gauge theories: An Introduction, volume 43, 1992).

[56] M. Laine, O. Philipsen, P. Romatschke, and M. Tassler, JHEP, **03**, 054 (2007), hep-ph/0611300.

[57] A. Beraudo, J.-P. Blaizot, and C. Ratti, Nucl. Phys. A, **806**, 312–338 (2008), arXiv:0712.4394.

[58] Nora Brambilla, Jacopo Ghiglieri, Antonio Vairo, and Peter Petreczky, Phys. Rev. D, **78**, 014017 (2008), arXiv:0804.0993.

[59] Alexander Rothkopf, Tetsuo Hatsuda, and Shoichi Sasaki, Phys. Rev. Lett., **108**, 162001 (2012), arXiv:1108.1579.

[60] M. Asakawa, T. Hatsuda, and Y. Nakahara, Prog. Part. Nucl. Phys., **46**, 459–508 (2001), hep-lat/0011040.

[61] Yannis Burnier, Olaf Kaczmarek, and Alexander Rothkopf, Phys. Rev. Lett., **114**(8), 082001 (2015), arXiv:1410.2546.

[62] Peter Petreczky, Alexander Rothkopf, and Johannes Weber, Nucl. Phys. A, **982**, 735–738 (2019), arXiv:1810.02230.

[63] Brandon Krouppa, Radoslaw Ryblewski, and Michael Strickland, Phys. Rev. C, **92**(6), 061901 (2015), arXiv:1507.03951.

[64] Brandon Krouppa and Michael Strickland, Universe, **2**(3), 16 (2016), arXiv:1605.03561.

[65] Ajaharul Islam and Michael Strickland (10 2020), arXiv:2010.05457.

[66] M. Laine, JHEP, **05**, 028 (2007), arXiv:0704.1720.

[67] Peter Petreczky, Chuan Miao, and Agnes Mocsy, Nucl. Phys. A, **855**, 125–132 (2011), arXiv:1012.4433.

[68] Yukinao Akamatsu, Phys. Rev. D, **87**(4), 045016 (2013), arXiv:1209.5068.

[69] Shiori Kajimoto, Yukinao Akamatsu, Masayuki Asakawa, and Alexander Rothkopf, Phys. Rev. D, **97**(1), 014003 (2018), arXiv:1705.03365.

[70] Roland Katz and Pol Bernard Gossiaux, Annals Phys., **368**, 267–295 (2016), arXiv:1504.08087.

[71] Jean-Paul Blaizot, Davide De Boni, Pietro Faccioli, and Giovanni Garberoglio, Nucl. Phys. A, **946**, 49–88 (2016), arXiv:1503.03857.

[72] Jean-Paul Blaizot and Miguel Angel Escobedo, JHEP, **06**, 034 (2018), arXiv:1711.10812.

[73] Nora Brambilla, Miguel A. Escobedo, Joan Soto, and Antonio Vairo, Phys. Rev. D, **97**(7), 074009 (2018), arXiv:1711.04515.

[74] Nora Brambilla, Miguel Ángel Escobedo, Michael Strickland, Antonio Vairo, Peter Vander Griend, and Johannes Heinrich Weber (12 2020), arXiv:2012.01240.

[75] Xiaojun Yao and Thomas Mehen, Phys. Rev. D, **99**(9), 096028 (2019), arXiv:1811.07027.

[76] Miguel Angel Escobedo, Joan Soto, and Massimo Mannarelli, Phys. Rev. D, **84**, 016008 (2011), arXiv:1105.1249.

[77] H.P. Breuer and F. Petruccione, The theory of open quantum systems, 2002).

[78] Ulrich Weiss, Quantum dissipative systems, volume 13, (World scientific, 2012).

[79] Goran Lindblad, Commun. Math. Phys., **48**, 119 (1976).

[80] Yukinao Akamatsu, Masayuki Asakawa, Shiori Kajimoto, and Alexander Rothkopf, Journal of High Energy Physics, **2018**(7), 29 (2018).

[81] Amir O Caldeira and Anthony J Leggett, Physica A: Statistical mechanics and its Applications, **121**(3), 587–616 (1983).

[82] Yukinao Akamatsu, Phys. Rev. D, **91**(5), 056002 (2015), arXiv:1403.5783.

[83] Yukinao Akamatsu (9 2020), arXiv:2009.10559.

[84] Maximilian A Schlosshauer, Decoherence: and the quantum-to-classical transition, (Springer Science & Business Media, 2007).

[85] Hannes Risken and Till Frank, The Fokker-Planck Equation-Methods of Solution and Applications, (Springer, Berlin, Heidelberg, 1996).

[86] Xiaojun Yao and Berndt Müller, Phys. Rev. C, **97**(1), 014908, [Erratum: Phys.Rev.C 97, 049903 (2018)] (2018), arXiv:1709.03529.

[87] Jean-Paul Blaizot and Miguel Angel Escobedo, Phys. Rev. D, **98**(7), 074007 (2018), arXiv:1803.07996.

[88] Shiori Kajimoto, PhD thesis, Osaka U. (2020).

[89] Davide De Boni, JHEP, **08**, 064 (2017), arXiv:1705.03567.

[90] Nicolas Gisin and Ian C Percival, Journal of Physics A: Mathematical and General, **25**(21), 5677 (1992).

[91] Yukinao Akamatsu, Phys. Rev. C, **92**(4), 044911, [Erratum: Phys.Rev.C 101, 059901 (2020)] (2015), arXiv:1503.08110.

[92] Nora Brambilla, Miguel A. Escobedo, Antonio Vairo, and Peter Vander Griend, Phys. Rev. D, **100**(5), 054025 (2019), arXiv:1903.08063.

[93] Nora Brambilla, Viljami Leino, Peter Petreczky, and Antonio Vairo, Phys. Rev. D, **102**(7), 074503 (2020), arXiv:2007.10078.

[94] Ian Percival, Quantum state diffusion, (Cambridge University Press, 1998).

[95] Rodney Loudon, American journal of physics, **27**(9), 649–655 (1959).

[96] Yu Maezawa, Takashi Umeda, Sinya Aoki, Shinji Ejiri, Tetsuo Hatsuda, Kazuyuki Kanaya, and Hiroshi Ohno, Prog. Theor. Phys., **128**, 955–970 (2012), arXiv:1112.2756.

[97] Szabolcs Borsányi, Zoltán Fodor, Sándor D. Katz, Attila Pásztor, Kálmán K. Szabó, and Csaba Török, JHEP, **04**, 138 (2015), arXiv:1501.02173.

[98] Xin Dong, Yen-Jie Lee, and Ralf Rapp, Ann. Rev. Nucl. Part. Sci., **69**, 417–445 (2019), arXiv:1903.07709.